AD-A125 301 NUMERICAL SIMULATION OF THE INFLUENCE OF SMALL SCALE MOUNTAIN RANGES ON A BAROCLINC WAVE(U) NAVAL POSTGRADUATE SCHOOL MONTEREY CA J P WALKER DEC 82 1/2

UNCLASSIFIED F/G 4/2 NL

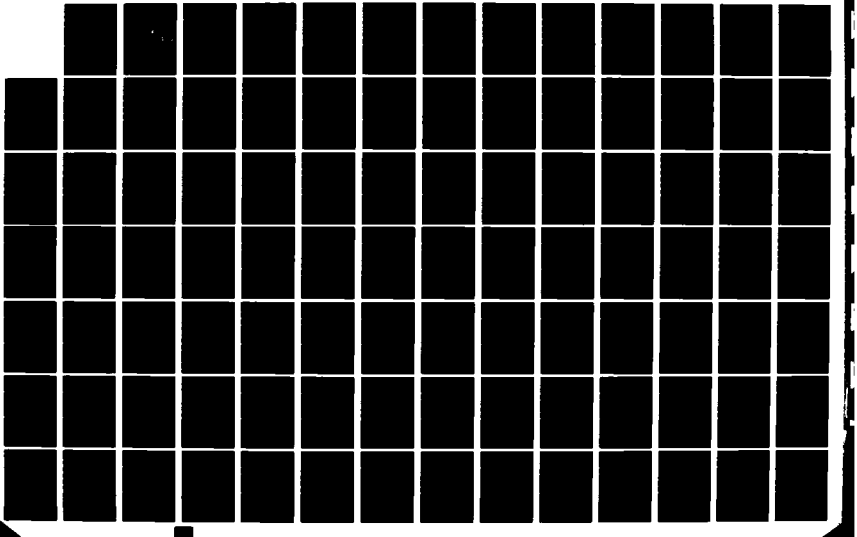

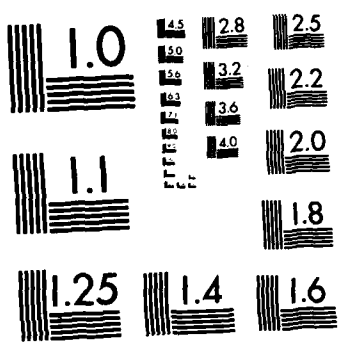

(2)

NAVAL POSTGRADUATE SCHOOL
Monterey, California

THESIS

B

NUMERICAL SIMULATION OF THE INFLUENCE OF SMALL SCALE MOUNTAIN RANGES ON A BAROCLINIC WAVE

by

Jeffrey Peter Walker

December 1982

Thesis Advisor: R. T. Williams

Approved for public release; distribution unlimited

UNCLASSIFIED

SECURITY CLASSIFICATION OF THIS PAGE (When Data Entered)

REPORT DOCUMENTATION PAGE	READ INSTRUCTIONS BEFORE COMPLETING FORM
1. REPORT NUMBER	2. GOVT ACCESSION NO. AD-A125301 / 3. RECIPIENT'S CATALOG NUMBER
(4) (6) TITLE (and Subtitle) Numerical Simulation of the Influence of Small Scale Mountain Ranges on a Baroclinic Wave	(9) TYPE OF REPORT & PERIOD COVERED Master's Thesis December 1982
	6. PERFORMING ORG. REPORT NUMBER
7. AUTHOR(s) (10) Jeffrey Peter Walker	8. CONTRACT OR GRANT NUMBER(s)
9. PERFORMING ORGANIZATION NAME AND ADDRESS Naval Postgraduate School Monterey, California 93940	10. PROGRAM ELEMENT, PROJECT, TASK AREA & WORK UNIT NUMBERS
11. CONTROLLING OFFICE NAME AND ADDRESS Naval Postgraduate School Monterey, California 93940	(11) REPORT DATE December 1982
	13. NUMBER OF PAGES (12) 159
14. MONITORING AGENCY NAME & ADDRESS(if different from Controlling Office)	15. SECURITY CLASS. (of this report)
	15a. DECLASSIFICATION/DOWNGRADING SCHEDULE

16. DISTRIBUTION STATEMENT (of this Report)

Approved for public release; distribution unlimited

17. DISTRIBUTION STATEMENT (of the abstract entered in Block 20, if different from Report)

18. SUPPLEMENTARY NOTES

19. KEY WORDS (Continue on reverse side if necessary and identify by block number)

Topographic Effects
Numerical Weather Prediction
Baroclinic Instability
Lee Cyclogenesis

20. ABSTRACT (Continue on reverse side if necessary and identify by block number)

A 6-level hemispheric primitive equation model was numerically integrated to examine the influence of various mountain ranges on a baroclinic flow. The objective was to simulate the apparent topographically-induced cyclogenesis that occurs over south central Alaska and isolate the mechanisms involved. It was found that the model simulates some of the characteristics of cyclogenesis in the lee of the Rockies, Alps, and Greenland. The topography

DD FORM 1 JAN 73 1473 EDITION OF 1 NOV 65 IS OBSOLETE
S/N 0102-014-6601

UNCLASSIFIED

SECURITY CLASSIFICATION OF THIS PAGE (When Data Entered)

20. Abstract (Continued)

appeared to cause a more local development in the lee at the expense of development over the whole domain of integration. The presence of a gap in the mountains was responsible for generating an eddy in the flow that moved eastward. This eddy became the primary development in cases with "horse-shoe-shaped" mountains that had a maximum elevation of 3000 m. The overall results suggest that a weak form of development in the lee of the Alaska Range is possible and that the resulting surface development would be weak but more clearly defined at the 850 mb level.

Approved for public release; distribution unlimited

Numerical Simulation of the Influence of Small Scale Mountain Ranges on a Baroclinic Wave

by

Jeffrey Peter Walker
B.S., Lowell Technological Institute, 1970

Submitted in partial fulfillment of the requirements
for the degree of

MASTER OF SCIENCE IN METEOROLOGY

from the

NAVAL POSTGRADUATE SCHOOL
December 1982

Author: Jeffrey P. Walker

Approved by: Roger T. Williams
Thesis Advisor

Russell L. Elsberry
Second Reader

Chairman, Department of Meteorology

Dean of Science and Engineering

ABSTRACT

A 6-level hemispheric primitive equation model was numerically integrated to examine the influence of various mountain ranges on a baroclinic flow. The objective was to simulate the apparent topographically-induced cyclogenesis that occurs over south central Alaska and isolate the mechanisms involved. It was found that the model simulates some of the characteristics of cyclogenesis in the lee of the Rockies, Alps, and Greenland. The topography appeared to cause a more local development in the lee at the expense of development over the whole domain of integration. The presence of a gap in the mountains was responsible for generating an eddy in the flow that moved eastward. This eddy became the primary development in cases with "horseshoe-shaped" mountains that had a maximum elevation of 3000 m. The overall results suggest that a weak form of development in the lee of the Alaska Range is possible and that the resulting surface development would be weak but more clearly defined at the 850 mb level.

TABLE OF CONTENTS

LIST OF TABLES

LIST OF FIGURES

ACKNOWLEDGEENT

The author wishes to thank Professor R. T. Williams for his invaluable guidance, support, and assistance throughout this project. His role has made the completion of this work possible. Much appreciation is due Professor Williams, Professor, R. L. Elsberry, and Captain J. L. Hayes for their thorough reviews of the manuscripts and their helpful comments and suggestions, and to Dr. F. J. Winninghoff and Mrs. O. Haney for their significant help in the numerical experiments. Much appreciation is also extended to the staff of the W. R. Church Computer Center for their assistance and support during the many hours of facility time needed to accomplish the numerical computations. The author would also like to thank Miss Nita Raichart for typing the thesis and Miss Kyong Lee for drafting the figures. A special loving thanks to my wife and children who have been incredibly patient and supportive during the academic courses and throughout the work on this thesis.

I. INTRODUCTION

A subject area still unresolved in meteorology is the role of orography and its interaction with the atmosphere. In particular, the investigation of the apparent link between orography and lee cyclogenesis has an immediate and direct application to operational meteorology.

Well known areas where cyclogenesis occurs are in the lee of the Rocky Mountains and the Alps and the lee of Greenland. Lee cyclogenesis near these mountain massifs has been studied extensively (e.g. Hess and Wagner, 1948; McClain, 1960; Bonner, 1961; Chung and Reinelt, 1973; Buzzi and Tibaldi, 1978; Radinovic, 1965; Trevison, 1976; Egger, 1972, 1974; and Buzzi, Malguzzi, and Tabaldi, 1980). These studies include observational, statistical, and numerical approaches. In general, results show that mountain massifs appear to have cyclogenetic mechanisms that are common to all and others which are unique to the particular mountain complex.

Approximately one-third of the significant snow events (>3 in) in Anchorage, Alaska, have been attributed to a weak form of lee cyclogenesis [Finch and Walker, 1979]. Figures 1a and 1b show composites of 11 cases depicting average conditions at the time of maximum snowfall at Anchorage, Alaska. Figure 2 is a schematic showing the major topographic features in Alaska and pertinent geographic names that will be referred to in the text. The 850 mb height minimum over the Kenai Peninsula south of Anchorage (Figure 1b) is believed to be a combination

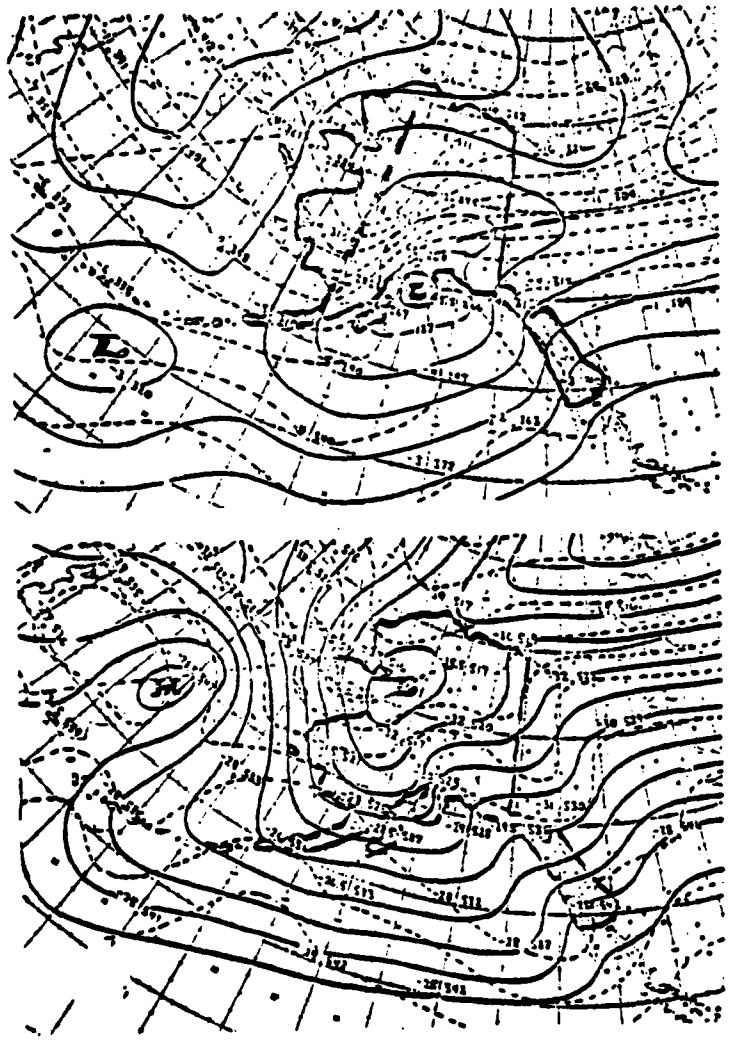

Figure 1. Composites of 11 Cases of Lee Cyclogenesis in Alaska at Time of Maximum Snowfall at Anchorage, Alaska, a) 500 mb Heights and Temperatures; b) 850 mb

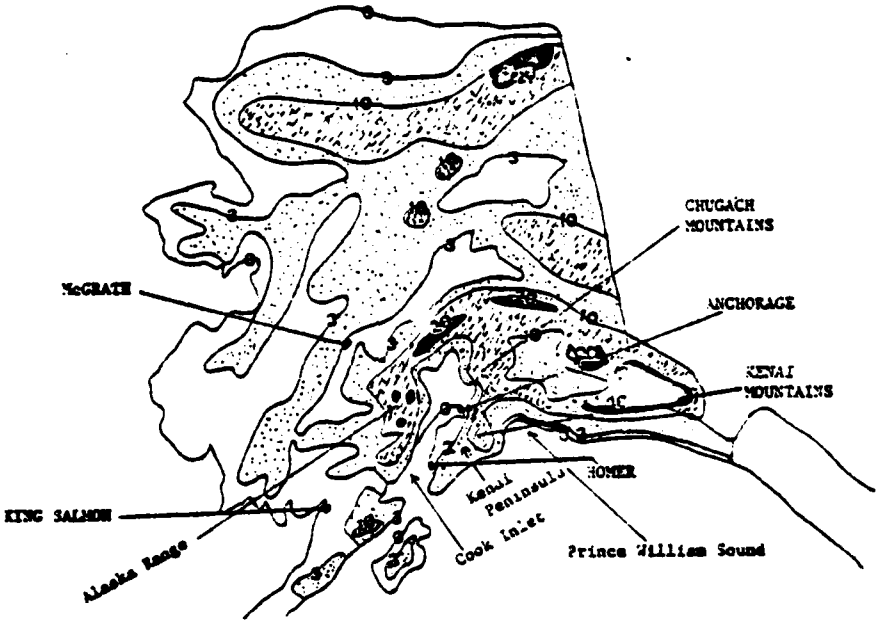

Figure 2. Terrain Elevations of Major Topographic Features in Alaska

of a weakening low pressure center over the northern Gulf of Alaska and a localized cyclone over Cook Inlet in the lee of the Alaska Range. From these composites, two events have been identified as preceding cyclogenesis in the lee of the Alaska Range:

(1) The blocking of cold air advection over southwest Alaska by the Alaska Range and subsequent strong cold air advection at low levels through a gap in the Alaska Range toward lower Cook Inlet; and

(2) Strong possitive vorticity advection over Cook Inlet at 500 mb.

The synoptic situation that results in significant precipitation at Anchorage is one in which a quasi-stationary (period of days) large amplitude wave over western Alaska at the 500 mb level exists coincidentally with a weak quasi-stationary depression in the lower levels over south central Alaska. A major contribution of this large amplitude wave aloft over western Alaska is to steer weakening cyclones from the southwest Gulf of Alaska toward Prince William Sound (see Figure 2). This causes warm moist air ahead of the cycline to flow northwestward toward the lee of the Alaska Range over Cook Inlet. A cold artic air mass over western and interior Alaska advances southeastward and is subsequently blocked and deformed by the Alaska Range. This cold air on the west side of the Alaska Range and the warm maritime air to the east form an increasingly strong low tropospheric baroclinic zone. As a positive vorticity maximum (short wave trough) aloft approaches Anchorage from the west, a low-level depression (detected at the 850 mb level either over the Alaska Range to the west of Anchorage or in the form of a weakening low moving northwestward from the northern Gulf of Alaska and Prince William Sound area) becomes coupled with cold air advection

through a gap in the Alaska Range near southern Cook Inlet in response to increasingly westerly flow in that area. At this point, the subsequent development becomes quite complex. It appears that there are several possible solutions depending upon the relative magnitudes of the contributions to development. For example, the degree and depth of the strong baroclinic zone, the strength of the positive vorticity advection aloft, the initial intensity of the incoming low or the intensity of the low present over the Alaska Range in the low-levels can all combine in various ways. This combination may be important since, as observed, precipitation amounts at Anchorage during these events can vary more than 7 inches. Of course, the amount of precipitable water also enters here.

Development of lee cyclones has been attributed to baroclinic instability, whereby a baroclinic conversion of available potential energy to kinetic energy is triggered by the perturbing action of the topography [Buzzi and Tibaldi, 1978; Tabaldi, Buzzi, and Malguzzi, 1980]. Huppert and Bryan (1976) mentioned that Robinson and McWilliams (1974) and Bretherton (1975) found that bottom topography in ocean models can force eddies in unstable currents with growth rates fast enough to be important in mesoscale dynamics.

Due to the strong degree of baroclinicity present in the Alaska case, it is likely that baroclinic instability occurs here also. However, the scale of the instability necessary for development is difficult to ascertain due to the various possible contributions of factors discussed above.

For example, the contribution from the cold air advection through the gap in the Alaska Range can vary considerable. These winds over southern Cook Inlet arrive via the Kamishak gap. They were investigated on the mesoscale by Macklin, et al. (1980). This paper contains a good description of the nature of the geography and the phenomenon. Shultz (1976) derived an empirical relationship whereby the eastward wind through the Kamishak gap is approximately given by 6.5 times the surface pressure difference between Homer and King Salmon, Alaska. The higher the pressure at King Salmon relative to Homer, the stronger the super-ageostrophic wind through the gap. Westerly ageostraphic velocities of greater than 30 $m\text{-}sec^{-1}$ are not uncommon over this area. This injection of cold air can vary from a low-level phenomenon driven primarily by the lower tropospheric pressure distribution, to a phenomenon spanning a deep layer when an upper level westerly jet is present. The intensity of this cold air injection should have a significant effect on releasing the baroclinic instability. However, the various scales of motion governing this injection make it difficult to draw any firm conclusions as to the nature of the mechanisms involved. If the injection occurs on large space scales, the weakening cyclone over the northern Gulf of Alaska can be indefinitely maintained or intensified, and thus prevent any development over Cook Inlet. The result is a delayed precipitation event at Anchorage, or possibly no precipitation. Strong, large-scale cold advection over western Alaska occasionally can intensify the 500 mb low to the point where it captures a weakening low over the northwest Gulf of Alaska and evolves into an extensive and deep cold low which lasts for a period of days. During this period, perturbations develop

in the cyclonic flow around this cold low, evidently in response to smaller-scale instabilities. These perturbations occasionally move northwest toward the Anchorage area and become coupled with an injection of cold air over southern Cook Inlet. Anchorage then receives significant snowfall. The low-level depression is apparent in the analyzed fields during this time and appears to be a result of a reintensification of the weakening low when it becomes coupled wth the cold air injection. In general, the horseshoe shape of the Alaska Range appears to be responsible for the maintenance of the baroclinic zone to the west of Anchorage and the quasi-stationary nature of the synoptic pattern, which allows the weak cyclogenesis to occur over Cook Inlet.

The presence of relatively warm maritime air in the lee of the Alaska Range, coupled with a cold air injection from the south, causes a negative Laplician of low-level thickness ($-\nabla^2 T$). This term is proportional to the increase in low-level cyclonic vorticity [Petterssen, 1956; Radinovic, 1965]. As the divergence aloft, associated with the approaching short wave trough, moves over the lee area, it appears possible that it becomes coupled with the low-level cyclonic vorticity and causes formation of a weak lee cyclone which may even remain in wave form near the surface. Analysis of 850 mb data suggest that, at this time, a closed low or trough is present over the area. Frequently, a mesoscale analysis of the Cook Inlet area also suggests the presence of a closed low in the surface pressure and wind fields. Snowfall at Anchorage normally occurs at this time.

A significant fall in surface pressure is not normally noted at Anchorage during these events. However, lee development may only be a localization of the depression. If inflow in the lower levels due to the cyclonic vorticity generation caused by the cold air injection is matched by outflow aloft, upward vertical motion would result. This vertical motion would provide the mechanism to precipitate the moisture from the maritime air. The maritime air appears to be a prerequisite for precipitation at Anchorage [Finch and Walker, 1979].

Once the lee depression is formed, it then moves in a generally north-easterly direction along the mean low-level thickness lines ahead of the short wave aloft, in a manner similar to the movement of a weak wave or shallow depression along a front. Although the 500 mb short wave is distinct, a closed circulation does not extend to that level because the main 500 mb trough usually remains over western Alaska (as long as artic air continues to flow southward). Further, the north-eastward movement of the depression is over mountainous terrain which serves to weaken it more rapidly and the upper-level short wave is weakening due to increasing Coriolis parameter and loss of available potential energy.

Other possible mechanisms for precipitation at Anchorage during these events are overrunning of cold air over Cook Inlet by the incoming maritime air, and/or convection due to relatively colder air aloft moving unimpeded over Cook Inlet ahead of the low-level cold air which is held back by the mountain. The latter mechanism was observed by Buzzi and Tabaldi (1978) in the case of Alpine lee cyclogenesis.

Cyclogenesis in the lee of the Alaska Range appears to have much in common with cyclogenesis in the lee of the Alps, the Rockies, and Greenland. However, the sequence of events leading to cyclogenesis in the lee of te Alaska Range more closely parallels the sequence that leads to cyclogenesis in the lee of the Alps, as would be expected from the strikingly similar topographic shape, orientation, and space scales of the two mountain complexes. The similarities to Alpine lee cyclogenesis include: 1) a cold air outbreak impinging on the mountain from the northwest; 2) warmer, maritime air in the lee; 3) deformation of the thermal pattern in the low levels by the mountain; 4) cold air advection through a gap in the mountain range to the southwest; and 5) the contribution to develop from the upper-level divergence ahead of the upper trough.

The features that distinguish Alaskan from Alpine lee cyclogeneis include the weaker intensity and smaller space scale from the Alaskan cyclone and the fact that Alaskan cyclones are not preceded by a "primary" cyclone at the surface moving northeast with a trailing cold front which interacts with the mountain.

The purpose of this study is to examine the influence of various mountain complexes on a baroclinic wave by numerically integrating a 6-level hemispheric primitive equation model. The objectives are to simulate the apparent topographically-induced cyclogenesis over south central Alaska and isolate the mechanisms involved.

Most operational numerical prediction models cannot simulate this effect because they have insufficient grid resolution and a poor mountain representation. Consequently, it was thought that numerical

simulations using more realistic terrain would reveal more information about the mechanisms involved in lee cyclogenesis over Cook Inlet, Alaska.

Numerical simulations of cyclogenesis in the lee of the Alps have been attempted [Egger, 1972; Trevisan, 1976; Bleck, 1977; and Tibaldi, Buzzi, and Malguzzi, 1980]. Since cyclogenesis in the lee of the Alaska Range appears to have mechanisms similar to those at work in Alpine lee cyclogenesis, a series of numerical experiments were designed similar to the experiments presented in Tabaldi, Buzzi, and Malguzzi (1980) to study cyclogenesis in the lee of the Alaska Range.

II. DESCRIPTION OF MODEL

The numerical model used in these experiments is a version of the UCLA general circulation model [Arakawa and Mintz, 1974]. Hayes and Williams (1977) used the model to investigate the interaction of atmospheric flow with a mountain range of finite length. The model was recently used to simulate flow around a finite length mountain [Williams, et al., 1981].

The basic configuration of the model was similar to that described by Monaco and Williams (1975) and Hayes and Williams (1977). Only a brief summary is presented here.

A. BASIC EQUATIONS

The model uses the primitive equation for a dry, adiabatic and frictionless atmosphere with no diffusion of heat or momentum and no sources or sinks. The prognostic variables are horizontal velocity (u, v), temperature (T), and pressure (π). Equations are given in Appendix A). A dry convective adjustment is included. Smoothing is not used except where explicitly stated.

B. HORIZONTAL GRID

The variables u, v, T, and π are staggered horizontally (Figure 3) according to Arakawa's scheme "C" [Arakaw and Mintz, 1974]. This scheme simulates well the geostrophic adjustment process. The horizontal domain is a 60° sector of the globe with cyclic continuity imposed on

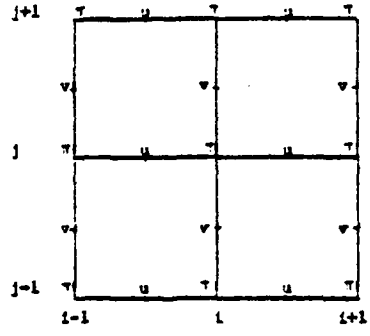

Figure 3. Distribution of Variables on Horizontal Grid

the longitudinal boundaries. The southern Boundary is a vertical wall along the equator. A 30 x 24 point spherical grid is superposed on the sector giving 2° east-west resolution and 4° north-south resolution. To save computer time, the east-west direction was given higher resolution (rather than the north-south direction) to better resolve wave phenomena and to maintain reasonable mountain widths without making them too steep. However, in an attempt to better resolve some specific features, other experiments were conducted with a 30 x 48 spherical grid. The results, in general, showed improvement over the 30 x 24 point grid. The horizontal difference equations used in this model are the same as those described by Arakawa, et al. (1974).

C. VERTICAL RESOLUTION

The primitive equations used in these experiments are written with the vertical σ-coordinate [Phillips, 1957]:

$$\sigma = \frac{p - p_T}{\pi} \qquad \text{where } \pi = p_s - p_T \qquad (2\text{-}1)$$

Here, p is the pressure at any level, p_T is the constant pressure used to define the top of the atmosphere, and p_s is the surface pressure. The bottom boundary is taken to be the surface of the earth and the upper boundary is defines as the 200 mb level. The upper and lower boundary conditions are $\dot{\sigma} = d\sigma/dt = 0$ since

$$\sigma \equiv 1 \quad \text{at} \quad p = p_s$$

and

$$\sigma \equiv 0 \quad \text{at} \quad p = p_T = 200 \text{ mb}$$

The atmosphere is divided into six equal σ-layers (Figure 4). The prognostic variables u, v, and T are computed at mid-layer while the geopotential ϕ and vertical velocity $\dot{\sigma}$ are computed diagnostically at σ-levels. The vertical difference equations are written following Arakawa and Suarez (1982).

D. TIME DIFFERENCING

The model uses the Euler-backward and leapfrog time differencing schemes. Integration is performed by repetitions of one Matsuno (Euler-backward) time step followed by four centered (leapfrog) time steps. The use of the Euler-backward scheme reduces solution separation caused by the leapfrog scheme and it also selectively damps high frequency waves. The time step in these experiments is 180 s (3 min).

E. POLAR PROBLEM

With a constant time step, computational instability in the model will result as a consequence of decreasing latitudinal grid distance associated with the convergence of meridians toward the poles. To maintain computational stability, a method of zonal smoothing developed by Arakawa and Mintz (1974) is used. This smoothing is also described in Haltinear and Williams (1980). The zonal smoothing as accomplished

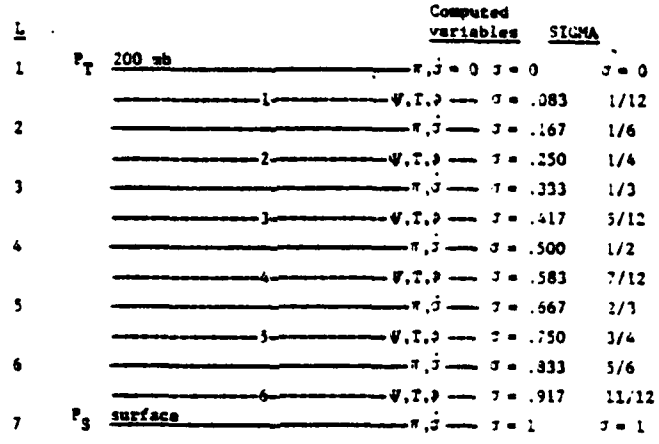

Figure 4. Vertical Distribution of Variables Used in the 6-Layer Version of the Sigma Coordinate System

by expanding the zonal components of the pressure gradient force and mass flux in a Fourier series around each latitude circle. The amplitude of each wave component is then reduced by a factor S when S<1, where

$$S = \frac{d \, \text{Cos} \, \phi}{c_0 \Delta t \, \text{Sin} \, (m\Delta\lambda)} \qquad (2\text{-}2)$$

where S = stability coefficient,

d = 2° grid distance at the equator,

c_0 = phase speed of the fastest gravity wave,

Δt = time step (180 s),

m = wave number,

$\Delta\lambda$ = 2° in radians, and

ϕ = latitude.

III. INITIAL CONDITIONS

The initial conditions consisted of a weak perturbation superposed on an analytically-derived, baroclinically unstable mean flow over a flat earth. The mean ground pressure was $p_o = \pi + p_T = 1000$ mb. The axis of the westerly jet structure was initially placed at 60°N. This configuration was designed to generate an amplifying disturbance in the northern latitudes that would interact with mountains representing those found in Alaska.

The mean flow contained a baroclinic jet with horizontal and vertical shear. The $\bar{v}$ component of the wind was initially set to zero at all points. The $\bar{u}$ component on the spherical earth was in gradient balance:

$$\bar{u} = -A + A\sqrt{1 + \frac{2u_g}{A}} \qquad A = \Omega a \cos\phi \qquad (3\text{-}1)$$

where

$$u_g = \frac{U}{2}\left[1 + \cos(6\phi)\right], \qquad \frac{\pi}{6} \leq \phi \leq \frac{\pi}{2}$$

$$u_g = 0 \quad , \qquad 0 \leq \phi \leq \frac{\pi}{6}$$

while U varied in the vertical by the factor;

$$U = U_o\left(\frac{p_o - p}{p_o - p_T}\right)$$

The velocity varied from zero at the surface to U_o = 40 m sec^{-1} at 200 mb (the defined top of the atmosphere) and from zero at the north pole and at 30°N. The maximum speed at each level was located at 60°N. The initial velocity was set to zero at all grid points south of 30°N.

The supporting temperature field was derived using the thermal wind relation. A correction factor varying with pressure and with latitude was applied to the NACA standard lapse rate [Haltiner and Martin, 1957] at 60°N with the base temperature at 276°K rather than 288°K to simulate a winter-like environment in the Artic. Thus;

$$\bar{T}_{\phi,p} = \bar{T}_{60°N} + \frac{p}{R(p_o - p_T)}\left[-U_o \Omega a\left(-\text{Cos}\ \phi + \frac{\text{Cos}(-5\phi)}{10} - \frac{\text{Cos}(7\phi)}{14}\right) + .4857\right], \tag{3-2}$$

$$\frac{\pi}{6} \leq \phi \leq \frac{\pi}{2}$$

where .4857 is the constant of integration evaluated at 60°N.

and

$$\bar{T}_{\phi,p} = \bar{T}_{\phi = \frac{\pi}{6},p} \quad , \qquad 0 \leq \phi \leq \frac{\pi}{6} \tag{3-3}$$

where

$$\bar{T}_{60°N} = 276°K - 0.0065Z \tag{3-4}$$

and where

$$Z \text{ (meters)} = 44308 \left[1 - \left(\frac{p}{1013.25}\right)^{0.19023}\right] ,$$

for

$$Z \leq 10769 \text{ meters.}$$

The horizontal temperatures at the lowest σ-level varied from -39°C at the north pole to +29°C at 30°N. From 30°N to the equator, the temperatures at each level were set equal to the corresponding temperature at 30°N.

IV. TERRAIN

The mountains used in the model were designed to include the major features of the mountains over south central Alaska, although in an idealized manner. A series of experiments was completed in which the terrain configuration was made successively more complex. This systematic approach to examining topographic effects helped in analyzing the contributions of the various mountain shapes, scales, and features. Table 1 lists the pertinent parameters of the experiments discussed in this paper. Figures 5a through 5f are more detailed schematics of the various mountains used in the experiments. Figure 6 shows a more realistic depiction of the relative sizes of the mountains within 60° sectors. A schematic of Alaska is included for comparison.

The terrain was incorporated in the model in a manner similar to Tibaldi, Buzzi, and Malguzzi (1980) and Hayes and Williams (1977). The mountain was allowed to "grow" with time to minimize the time required for geostraphic adjustment. The "growth" of the mountains in the model was controlled by the scheme presented in Hayes and Williams (1977);

$$\Phi_t = \Phi_m \, \mathrm{Sin}^2 \left(\frac{\pi}{2} \frac{t}{t_p}\right) , \qquad t \leq t_p$$

$$\Phi_t = \Phi_m \qquad , \qquad t > t_p \tag{4-1}$$

Table 1. Summary of Pertinent Features of the Experiments

MOUNTAIN SHAPE	EXP. #	MAX. ELEV.	INITIAL CONDITIONS PERTURBATION*	NUMBER OF NORTH-SOUTH GRID POINTS
None	Control	0	With	24
	1a	1500m	Without	24
	1b	3000m	Without	24
	2a	1500m	With	24
	2b	3000m	With	24
	3a	1500m	With	24
	3b	3000m	With	24
	3c	3000m	Without	24
	4a	1500m	With	24
	4b	3000m	With	24
	5a	1500m	With	24
	5b	3000m	With	24
	5b	3000m	With	47
	5c	3000m	Without	24
	6b	3000m	With	24
	6c	3000m	Without	24
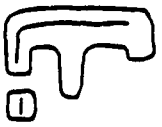	7b	3000m	With	24
	7c	3000m	Without	24

* With/Without Initial Superposed Disturbance.

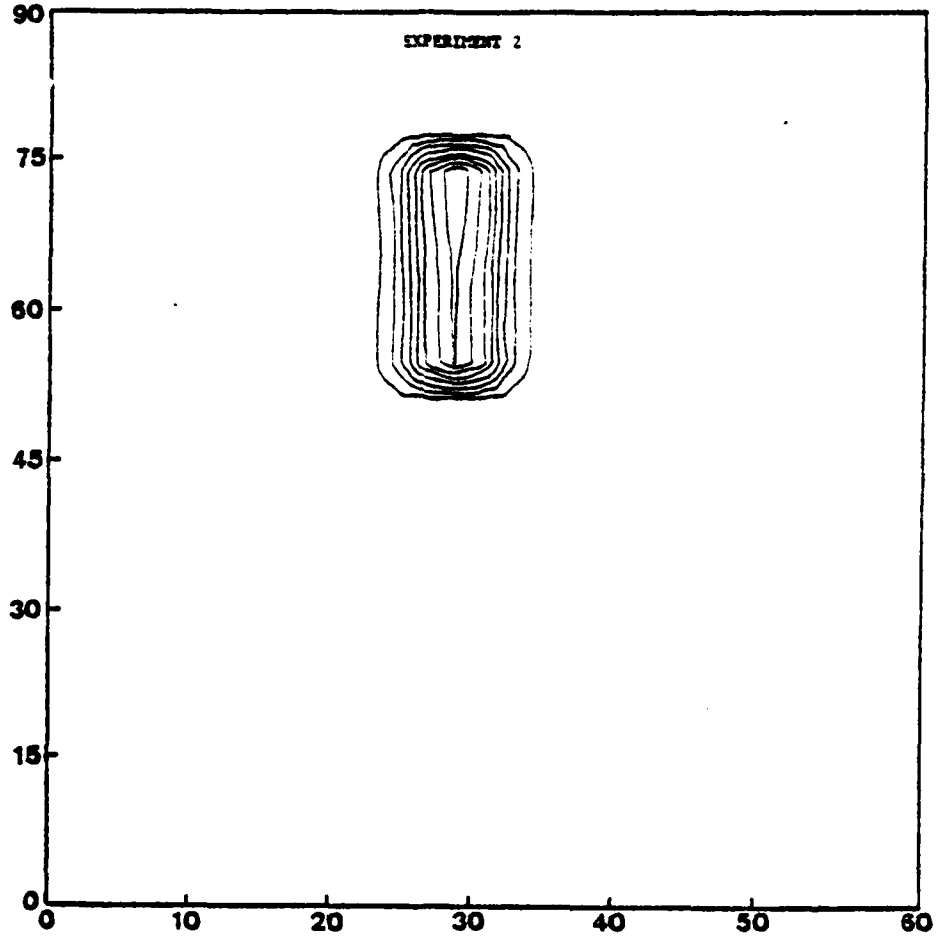

Figure 5a. View of Mountain Used in Experiments 1 and 2

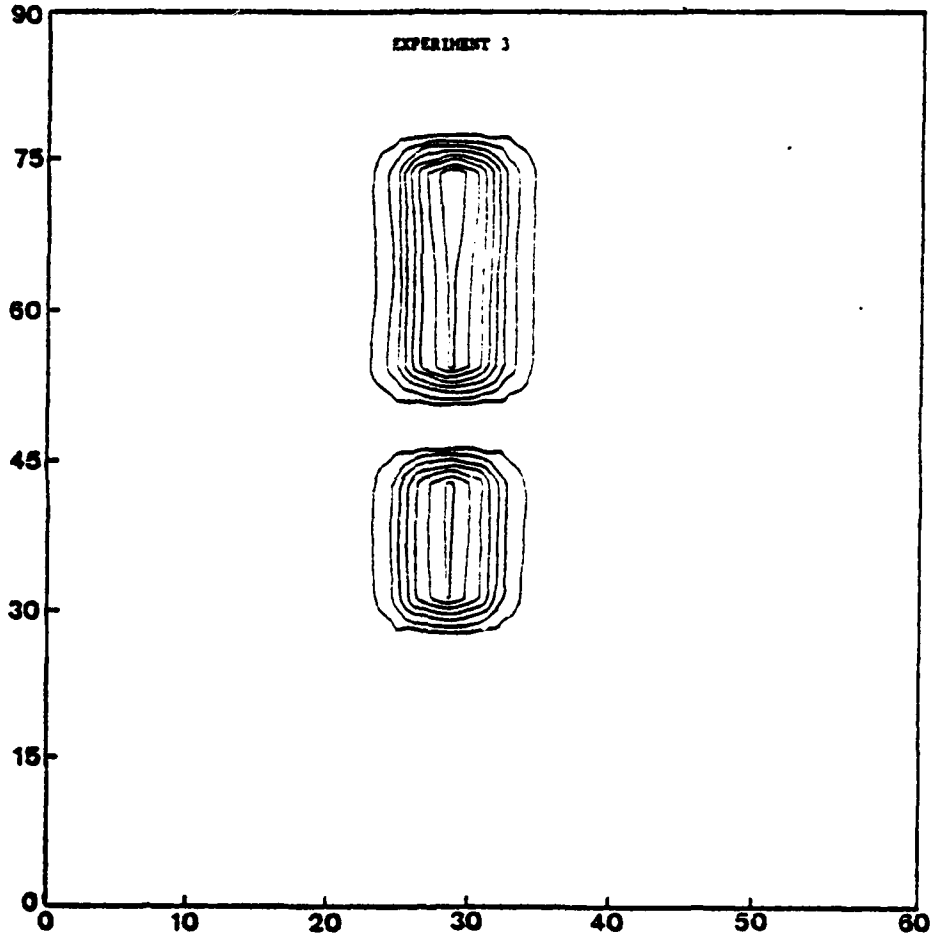

Figure 5b. View of Mountain Used in Experiment 3

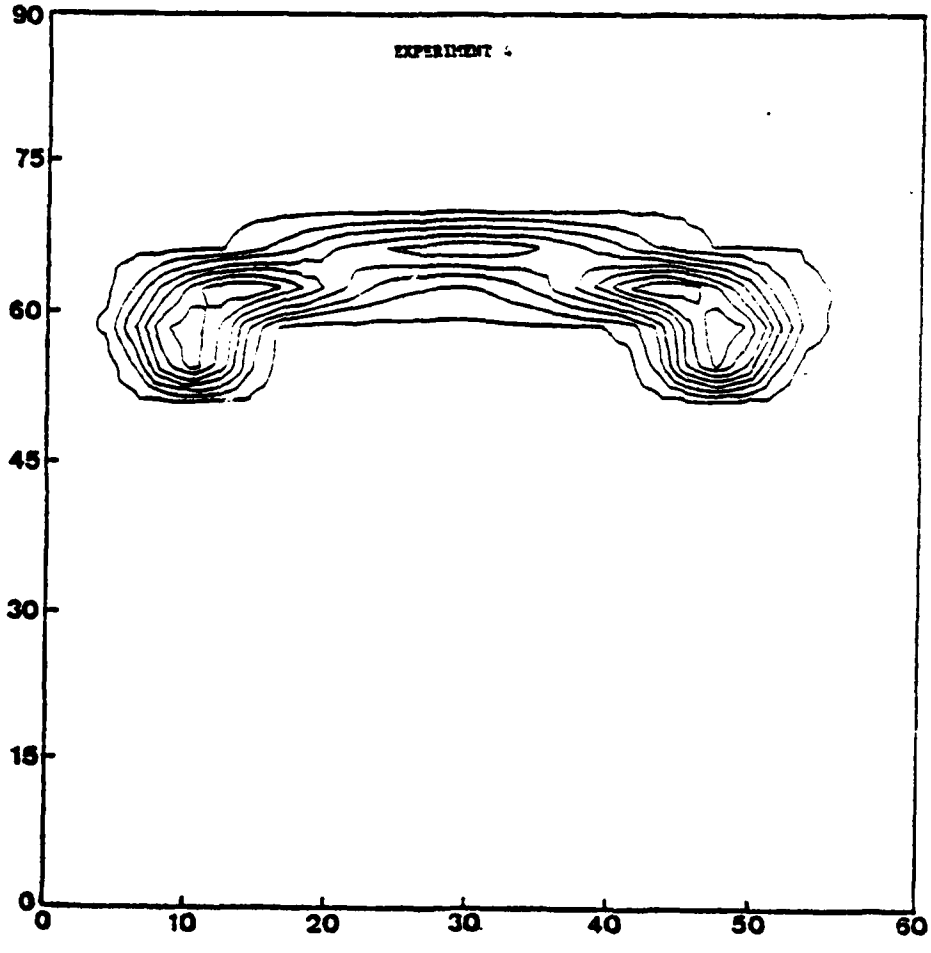

Figure 5c. View of Mountain Used in Experiment 4

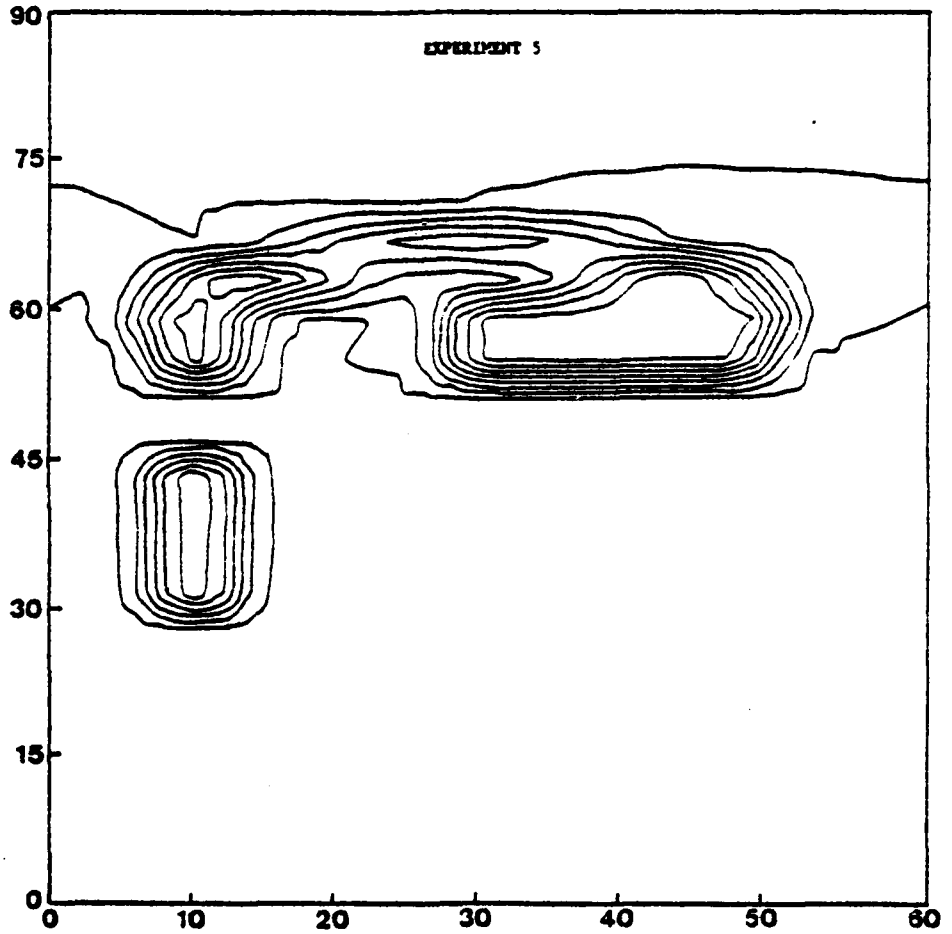

Figure 5d. View of Mountain Used in Experiment 5

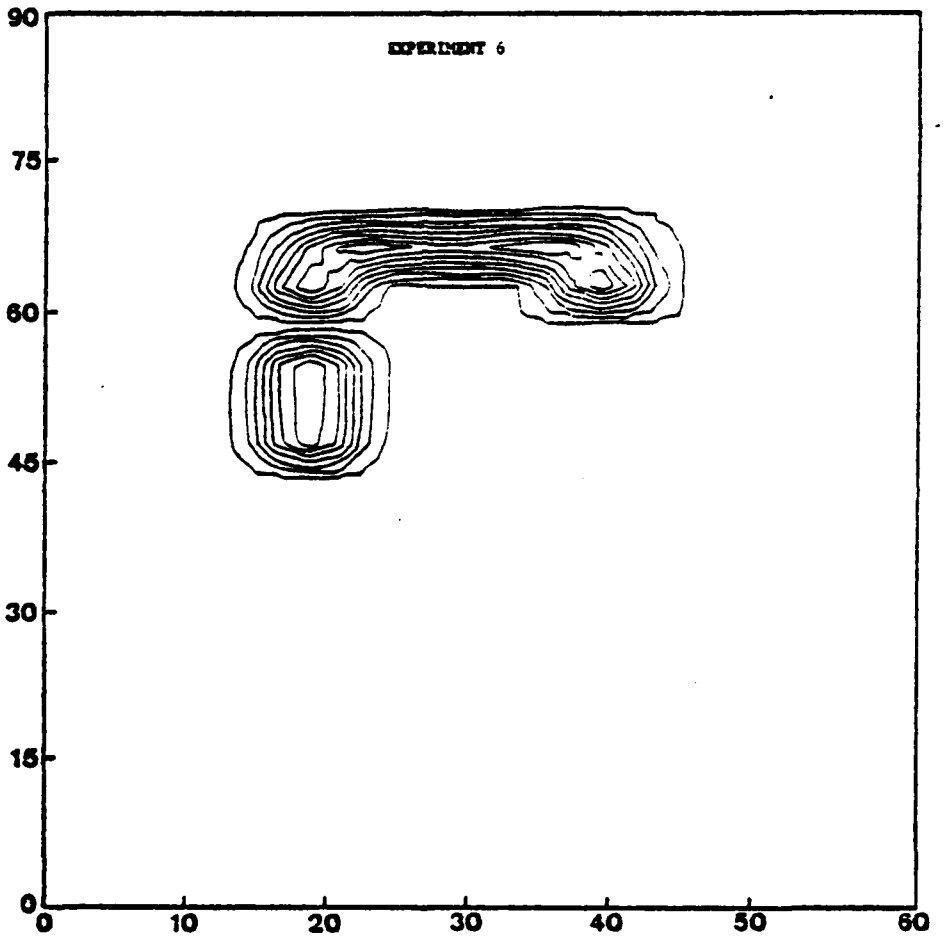

Figure 5e. View of Mountain Used in Experiment 6

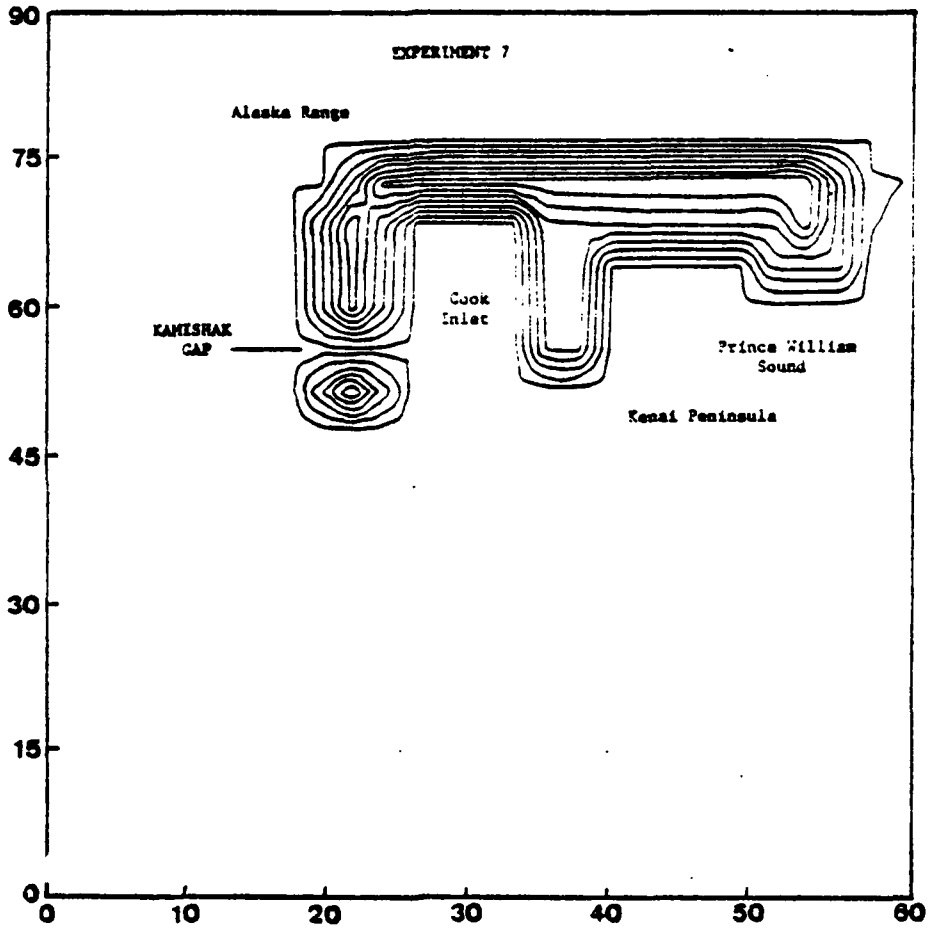

Figure 5f. View of Mountain Used in Experiment 7

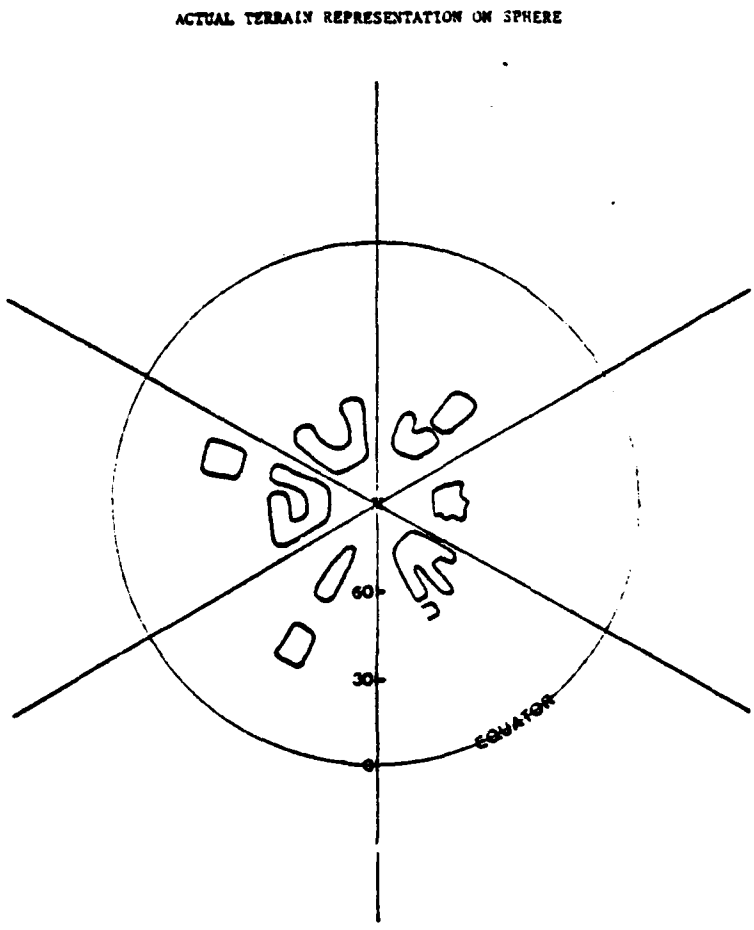

Figure 6. Polar Projection of Mountains Used in Experiments. State of Alaska Included for Comparison

Here, the mountain height ϕ_t was incremented during the model integration until it reached its maximum height ϕ_m at t_p = 12 hr. The value of ϕ_m was either 1500m or 3000m.

The actual profiles of the mountains were constructed by various schemes that adjusted this time-dependent mountain height. For example, the north-south ridge used in experiments 1 through 3 was constructed using the following scheme;

$\phi = .25\ \phi_t$ at east-west grid points 13 and 17,

$\phi = .75\ \phi_t$ at east-west grid points 14 and 16, and

$\phi = \phi_t$ at grid point 15.

The following scheme, devised by Dr. F. J. Winninghoff, produced the "horseshoe-shaped" mountain in experiment 6;

$$\phi = \phi_t \sin \left\{ [9 - 3\ (9 - R)\ ] \frac{\pi}{18} \right\}, \qquad 6 \leq R \leq 12$$

$$\phi = 0 \qquad , \qquad 6 > R > 12$$

where R = the number of increments from a central point to other model grid points.

This scheme produces a circle with the maximum elevation of the mountain located a radius of nine grid increments from the center. The maximum elevation decreases to zero at radii of 6 and 12 grid increments and so forth. The horseshoe shaped was obtained by excluding those grid points

south of a given latitude from the mountain calculation. Other features of the more complex mountains, as in the mountain used in experiment 7, were constructed in a more piecewise fashion and then added together.

Hayes and Williams (1977) found that for an atmosphere in solid rotation (no vertical shear), the surface pressure tendency at a point in the vicinity of the growing mountain reached a quasi-steady state in 16h when the mountain was raised to its full height in 16 h. When the time to raise the mountain was reduced to 12h, the adjustment time was longer. Furthermore, it was necessary to increase the growth time to 36h for a coarse resolution model. In Tabaldi, et al. (1980), the mountain was raised in the path of the oncoming frontal system and only 8h were allowed for progressive readjustment. Their model resolution, however, was finer.

The time to raise the mountain in the present experiments was set at 12h. Although some increase in adjustment time is expected because the growth period has been reduced, the mean flow in the low levels was not as strong as the solid rotation case investigated by Hayes and Williams (1977). It is felt that reduced low-level flow offsets any increase in adjustment time caused by reduction of the growth period.

V. CONTROL RUN

A control run with terrain heights set to zero over the entire domain was made for comparison with the subsequent mountain experiments. The initial conditions included a disturbance superposed on the baroclinic, sheared mean flow described in Section III. A finite amplitude baroclinic wave developed in the sector and was allowed to evolve through 192h of integration to monitor its characteristics over a flat earth.

The model produced stable simulations through at least 192h. Small-scale ($2\Delta X$) waves appeared as the run progressed, however, their amplitudes remained relatively small. Due to the lack of frictional dissipation, diffusion, and external smoothing, some noise in the model was expected.

Fields of surface pressure at 96, 108, 120, and 132h are shown schematically (subjectively smoothed to show the major features at 4 mb intervals) in Figure 7. The pattern developed by the model is quite realistic. Also notice the stronger north-south pressure gradient compared to the east-west gradient at 108h and 132h (Figure 7). This distortion of the output domain is due to the graphics output routine which displays the 60° sector from the northern hemisphere of the globe onto an equally-spaced Cartesian grid. The actual latitudinal distance is more than twice the longitudinal distance in the northern latitudes on this Cartesian grid.

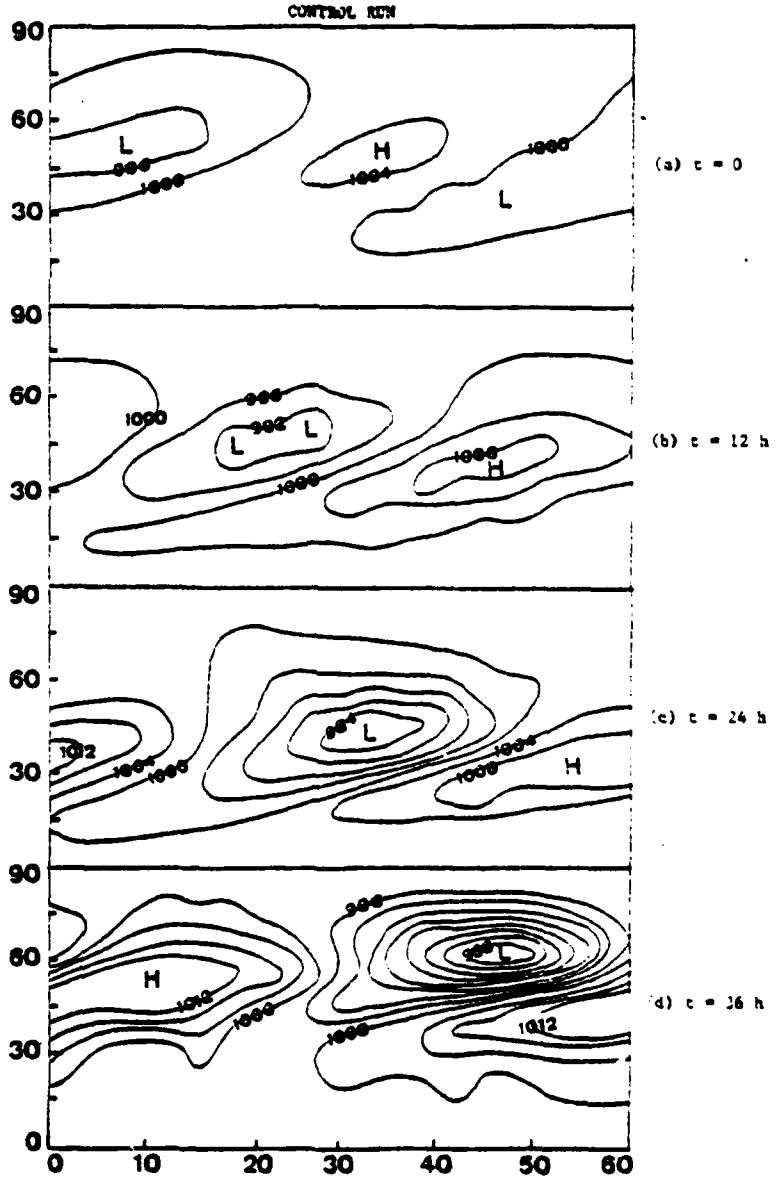

Figure 7. Subjectively Smoothed Surface Pressure Fields From Control Run: a) t_0+96h; b) t_0+108h; c) t_0+120h; d) t_0+132h

Figure 9 shows the position of the surface low at 12h intervals from 96h through 168h. The general movement of the low is toward the east-northeast. Figure 10 shows the upper-level patterns of height and temperature at 120h. Notice that the low is closed off at 850 mb, the system tilts westward with height indicating a developing system, and frontogenesis is apparent in the temperature fields through the 500 mb level. In the mountain experiments, this time will correspond to 12h after the mountain is raised to its full height.

A time to begin raising the mountains for subsequent experiments was chosen based on the position of the amplifying disturbance in the sector and on its degree of development. The u, v, T, and π fields at 96h were selected because, at this point, the disturbance had just appeared on the west side of the sector (Figure 7) and it had just begun its rapid deepening (Figure 8). Raising the mountain in 12h from the 96h point would allow it to interact with the deepening low. Because of the slowly increasing amplitude of the short waves, it was decided that a further delay in raising the mountain would likely allow the amplitudes of these waves to begin masking the important features in the solutions.

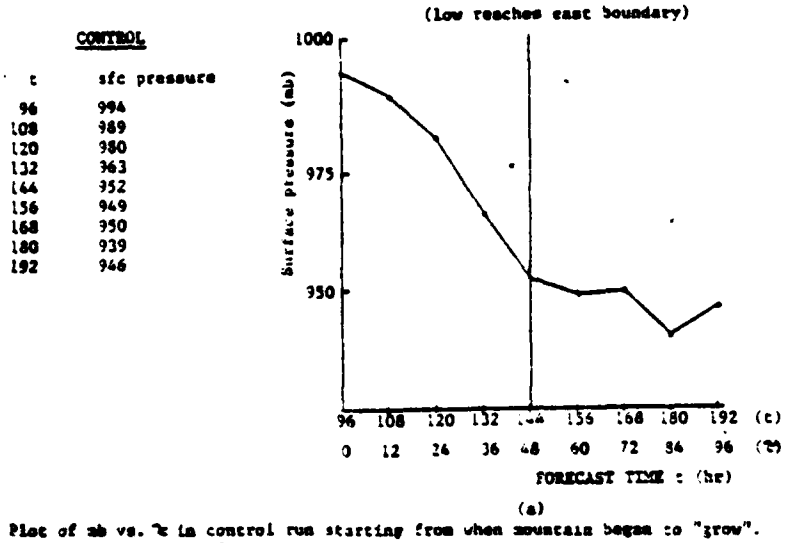

Plot of mb vs. τ in control run starting from when mountain began to "grow". $\tau = t_c + t$ hr. $t_c = 0$ beginning of control run.

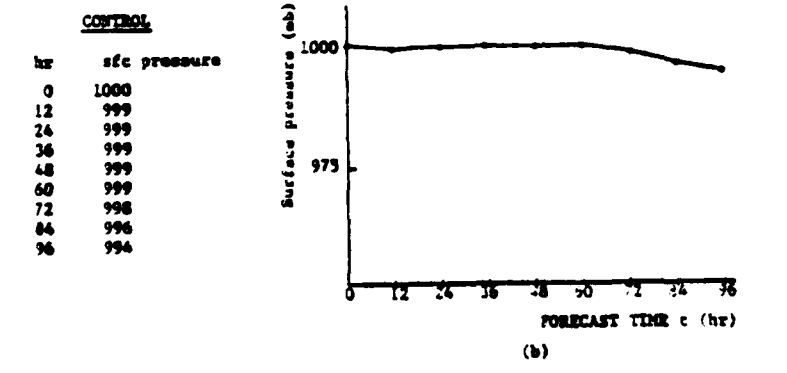

Figure 8. Plot of Surface Pressure (π) Versus Forecast Hour: a) Experiment 2a; b) Experiment 2b

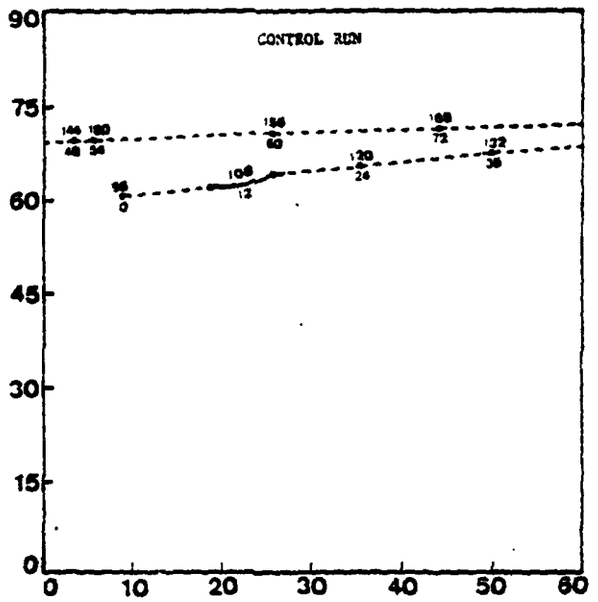

Figure 9. Surface Low Pressure Center Positions From Control Run From t_o+96h Through t_o+168h

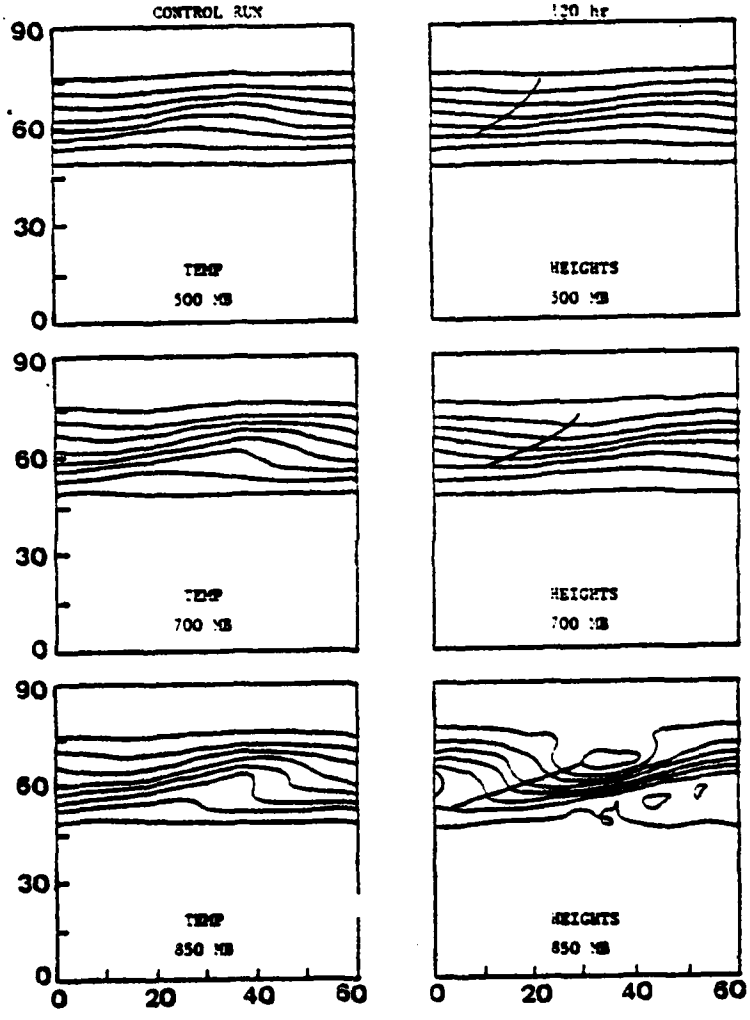

Figure 10. Heights and Temperatures on Pressure Levels for t_0+120h of Control Run

VI. RESULTS OF MOUNTAIN EXPERIMENTS

A. EXPERIMENT 1 - MEAN FLOW

The initial conditions for this experiment were the fields representing the initial state of the baroclinically unstable mean flow described in Section III without the superposed perturbation. The terrain used in this experiment was a simple mountain of finite north-south extent (Figure 5a). The mountain was raised to its maximum height of 1500m (case a) and 3000m (case b) in 12h of model integration. The fields were averaged over the period t_0+12h to t_0+36h (t_0 represents the initial conditions) to eliminate the inertia-gravity waves generated by the growing mountain. The output consisted only of these averaged data fields.

In a recent investigation (Williams, et al. 1981), a similar mountain was allowed to grow in a balanced, uniformly stratified, westerly current in solid rotation with no vertical shear. Based on a study by Merkine (1975), Williams, et al. (1981) determined that a mountain height of about 1700m was necessary to produce flow around the mountain. Based on their results, flow around the mountain should occur with a mountain height of 3000m, but not with a mountain height of 1500m.

This blocking effect was not observed in experiments 1a and 1b as seen in the wind fields at σ = 11/12 (Figure 11). Very little deflection of the flow is observed on the windward side of the mountain in experiment 1a. On the lee side, a trough is seen in the wind field

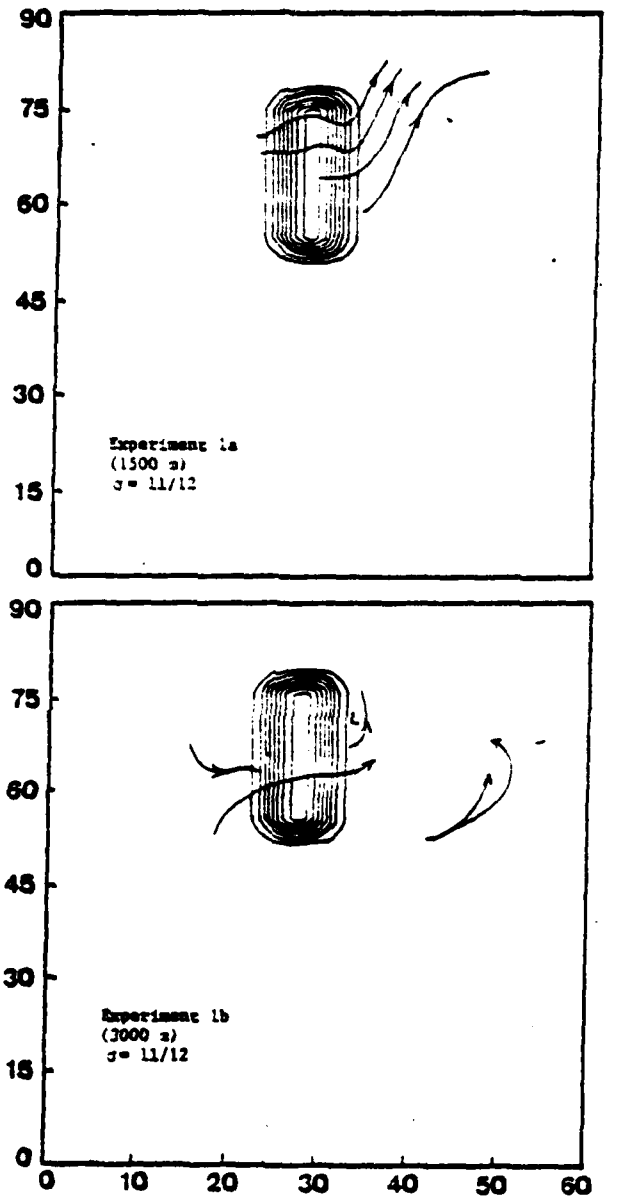

Figure 11. Average Wind Vectors on $\sigma = 11/12$ for Experiment 1

along the base of the mountain. In experiment 1b, the flow on the windward side is deflected toward the northern end of the mountain at the lower elevations. Due to the mean flow starting from zero at the ground, velocities remained small in the lower levels such that continuous flow around the mountain is not easily determined. On the other hand, in the lee, a more intense trough is seen in the wind field at the base of the mountain. The wind pattern suggests that the trough has a nearly closed circulation.

A more intense low was observed over the lee slope in experiment 1b (3000m) compared to the one in experiment 1a (1500m). The low in experiment 1a was more of a surface trough and appeared to be centered close to the crest of the mountain rather than over the lee slope (Figure 12). Since the rate of growth of the mountain apparently affects the geostrophic adjustment time [Hayes and Williams, 1977], the intensity of the low over the lee slope may be related to inertia-gravity waves generated by the use of a 12h period to raise the mountain. However, these waves should have been damped by the averaging of the fields. Therefore, the persistence of this low over the lee slope may be due to other inherent problems in the model such as truncation error in the vicinity of steep terrain. Another possibility is the accuracy of the vertical interpolation scheme in the graphics output package. The temperature and height fields showed wavelengths on the order of two grid intervals over the mountain up to the 700 mb level in experiment 1a (Figure 13) and through the 500 mb level in experiment 1b (Figure 14). Although lee troughs due to downslope motion have been observed in Rocky

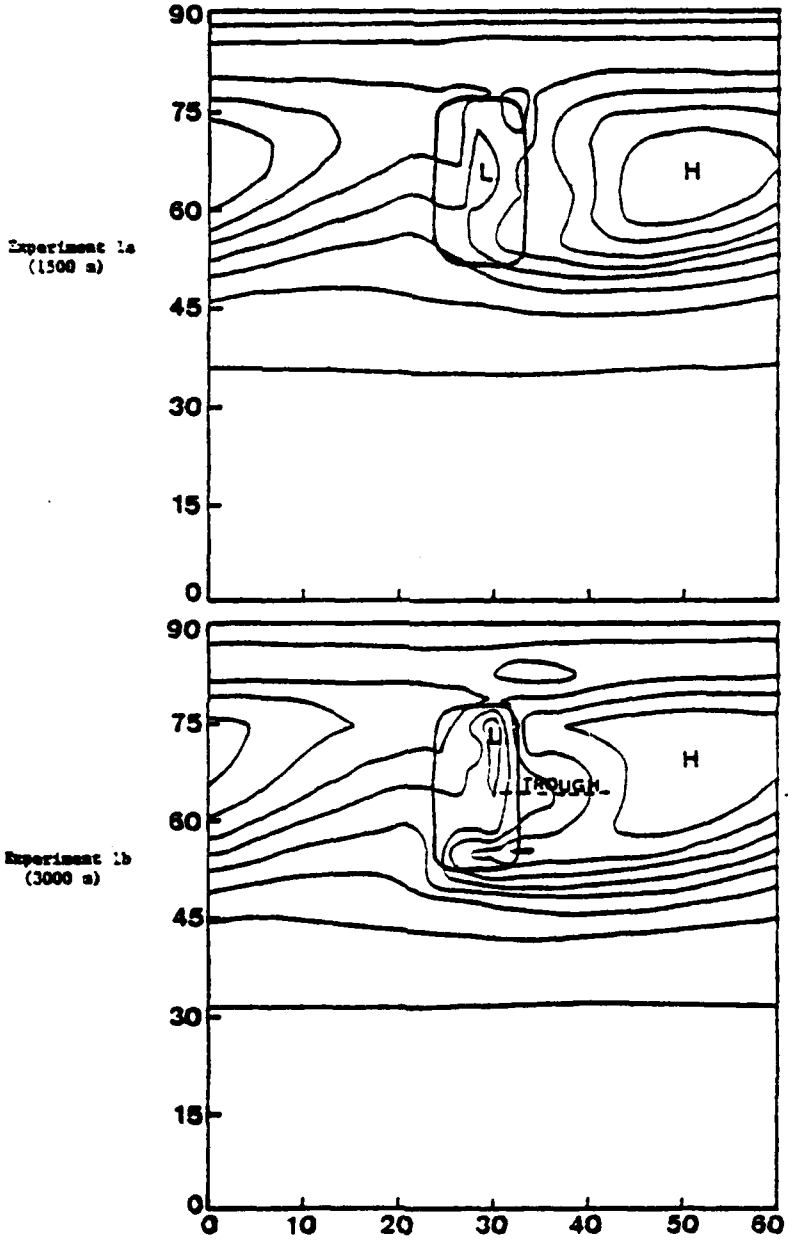

Figure 12. Surface Pressure (π) Fields for Experiment 1

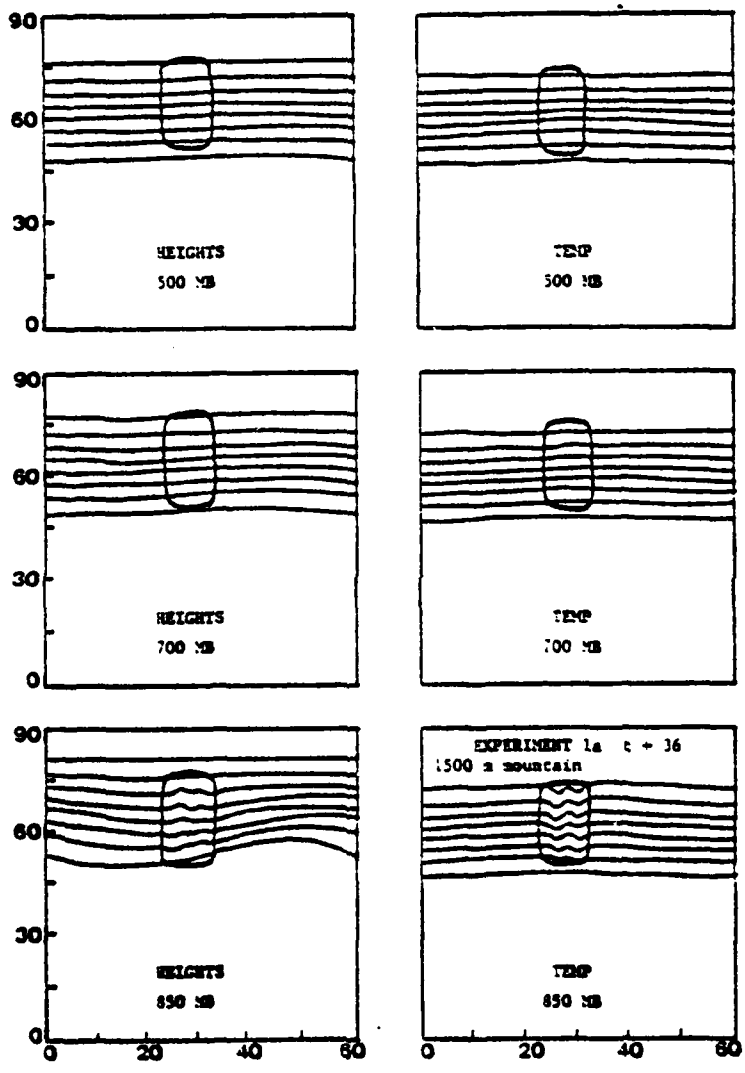

Figure 13. Height and Temperature Fields on Pressure Surfaces for Experiment 1a

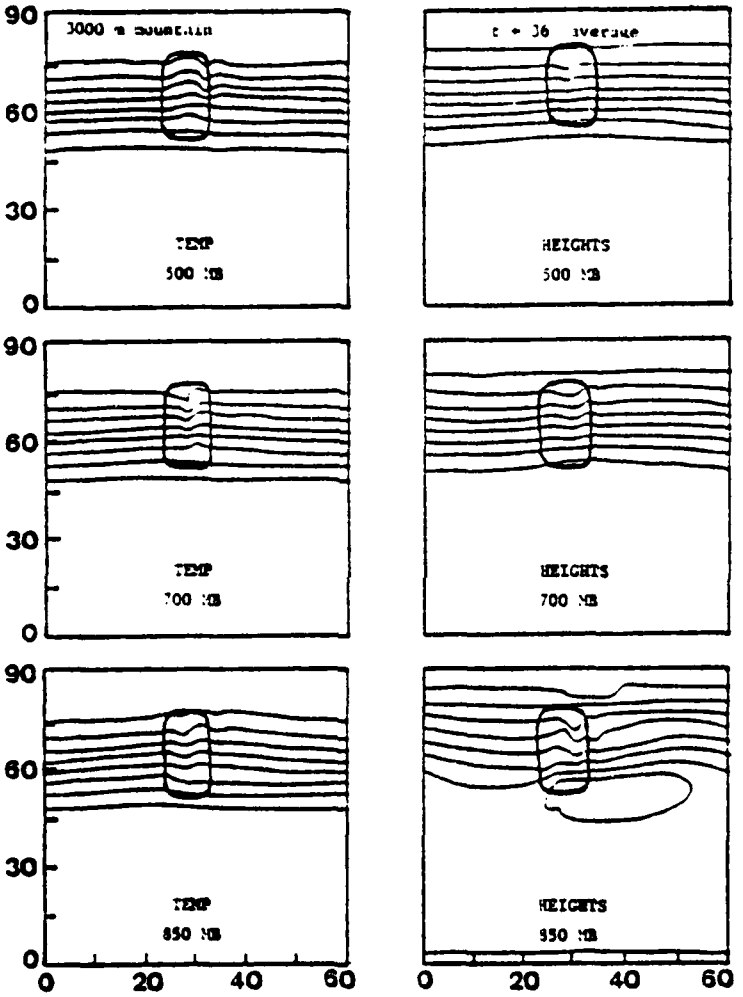

Figure 14. Height and Temperature Fields on Pressure Surfaces for Experiment 1b

Mountain cyclogenesis cases [Newton, 1956; McClain, 1960; Bonner, 1961; and Schallert, 1962], further investigation of this feature was not pursued in this research due to the small-scale and generally non-hydrostatic nature of the observed phenomenon.

A larger-scale surface trough can be seen extending eastward from the center of the mountain in the lee in experiment 1b (Figure 12). This trough is not observed in experiment 1a which has a lower mountain.

In summary, the results of experiment 1 suggest that, although the mountain height is above the critical height of 1700m [Merkine, 1975], flow around the mountain was not achieved in case a or case b due to the magnitude of the shear of the baroclinic current and the lack of a surface mean flow. Further, the lee troughs in case a and case b were closer to the mountain (Figure 11) than the trough observed by Williams, et al. (1981) downstream from the mountain. Finally, a lee trough is generated, as seen in the surface pressure field in experiment 1b (Figure 12), which apparently resulted from the interaction of the mountain and the mean flow.

B. EXPERIMENT 2

In this case, the mountain from experiment 1 was allowed to grow in the path of an amplifying, finite amplitude disturbance. The initial conditions were from t_o+96h of the control run. The mountain was raised to its full height in 12h (i.e. by t+12h where t = t_o+96h). Times for the mountain experiments are referenced to the time the mountain started to "grow". The maximum height of 1500m will again be referred to as

case a and for 3000m, base b. These fields and the fields in the remainder of the experiments were not averaged as in experiment 1. Rather, the fields show the solutions at the end of those time steps in the model integration.

It will become evident that the results of experiments 2 and 3 were very similar north of the latitude of the gap between the two mountains (Figure 5b). Therefore, only analyzed fields from experiment 3 will be shown to avoid duplication. However, a separate discussion of the solutions from experiment 2 will be presented in order to point out the effects of the single mountain (Figure 5a) independently.

The results of experiment 2a were very similar to the control fun. However, the low in experiment 2a was not as intense as the one in the control run. The results of experiment 2b showed the amplifying perturbation approaching the west slope of the mountain at t+18h (Figure 15). The perturbation then filled or was absorbed by the trough over the lee slope which then intensified (Figure 16). This low over the lee slope, also observed in experiment 1b, persisted through t+42h while drifting slowly southward along the lee slope and weakening (Figure 17). Although computational errors such as truncation error may be responsible for this phenomenon, this latter sequence is very similar to the one described by Schallert (1962) for his Type B disturbances. He attributed the presence of these disturbances as mainly due to orographically induced vertical motions. Schallert characterized them as distrubances that developed to maximum intensity within 6h after their

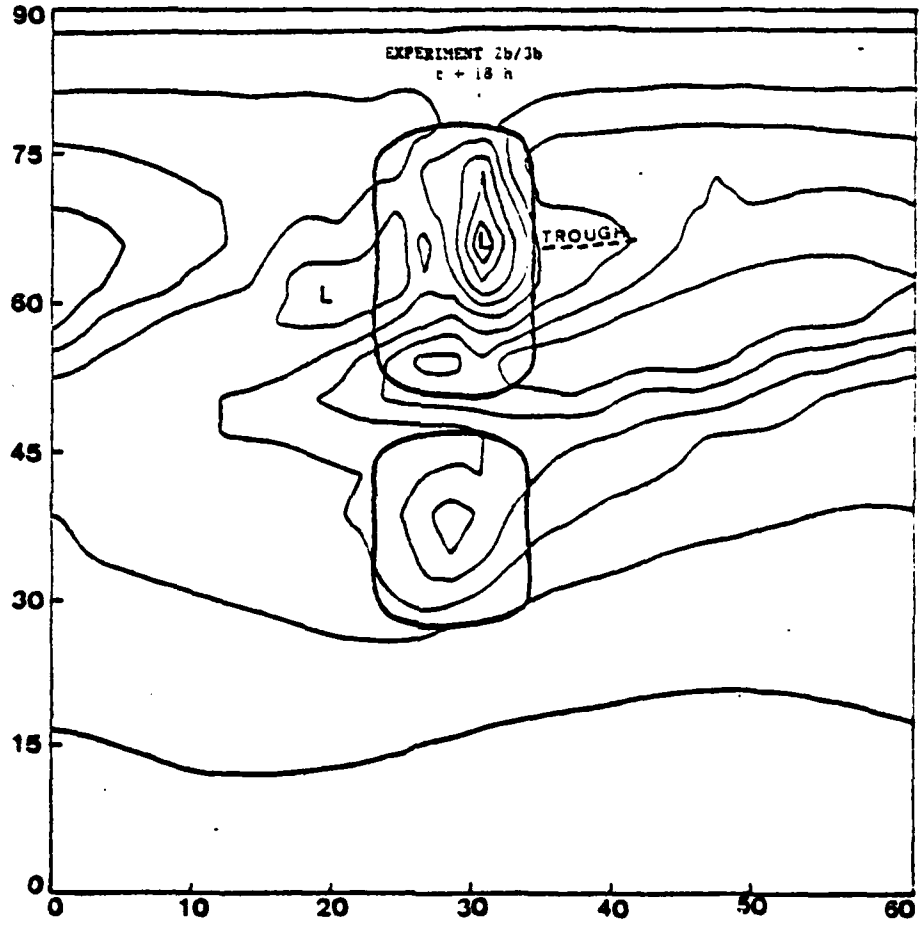

Figure 15. Surface Pressure Field at t+18h for Experiment 3b

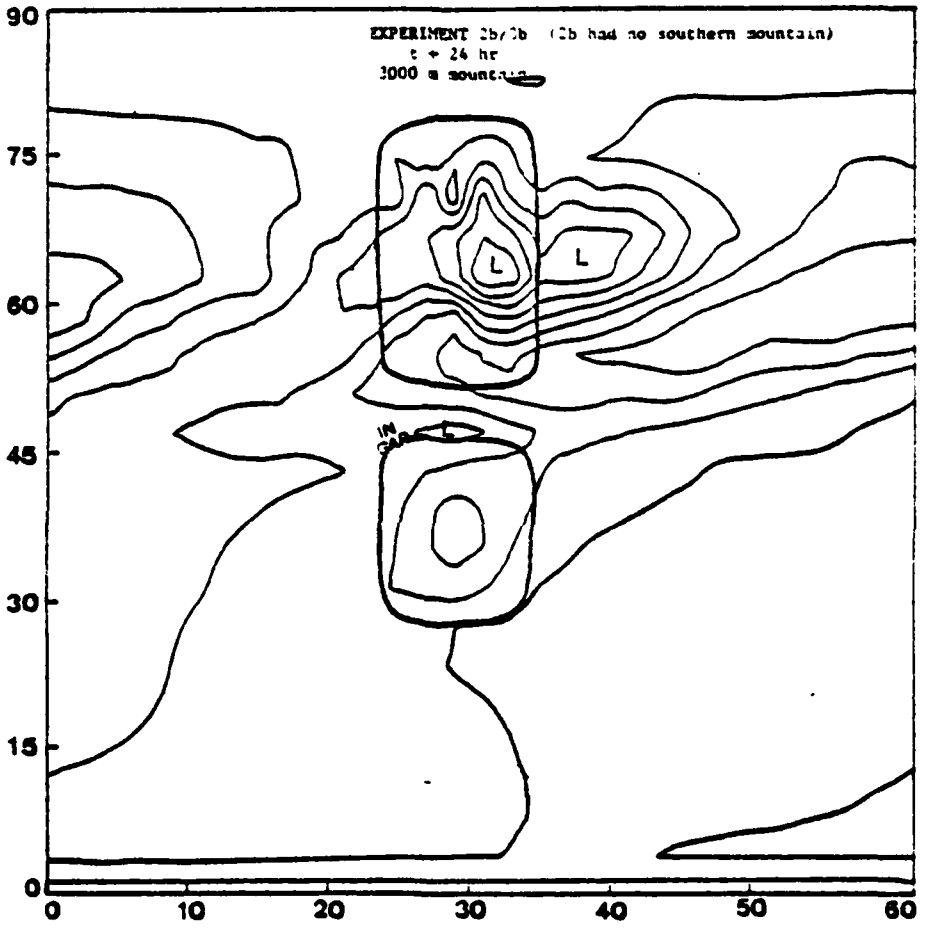

Figure 16. Surface Pressure Field at t+24h for Experiment 3b

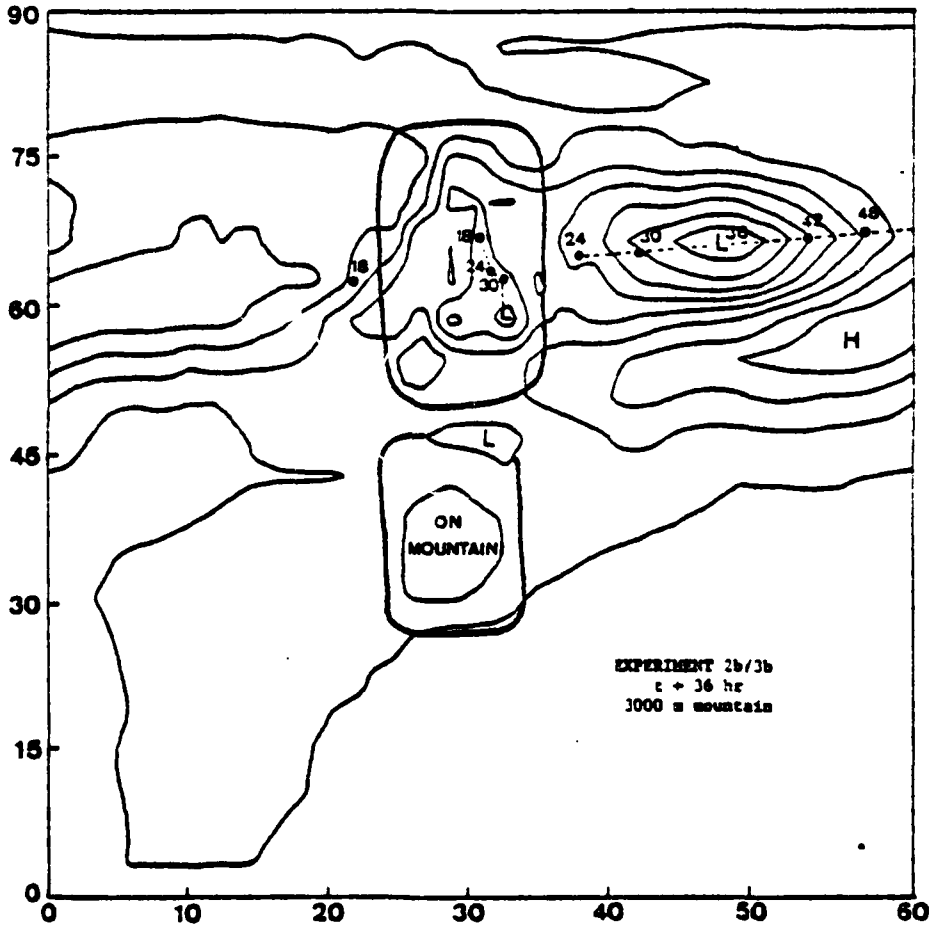

Figure 17. Surface Pressure Field at t+36h for Experiment 3b

appearance, remained over the lee slopes, and move southward and weakened. Schallert's Type A1 development had both an orographically-generated lee low over the lee slope, and a lee low that resulted in an intense cyclone that moved eastward away from the mountain. Both types are observed in experiment 2b. After t+24h, a low rapidly developed in a pre-existing trough just east of the base of the mountain, near the center (Figure 16). This pre-existing trough was also observed in the results of experiment 1b (which had no initial perturbation). In experiment 2b the pressure at grid points in this lee trough fell approximately 15 mb between t+18h and t+24h. This pressure change contrasts with results obtained by Egger (1974), who calculated a pressure fall of only 25 mb in 30h (average of 5 mb per 6-h period) at a grid point in the lee of a mountain intended to simulate Greenland. The sequence of events in experiment 2b was similar to the sequence in Egger's Greenland experiment. Because of the similarity between the results of his experiments with and without the mountain, Egger suggested that the process could be described as a low pressure system crossing a mountain barrier, rather than true lee cyclogenesis. He found that the mountain barrier blocks the lower part of the cyclone but the upper part continues over the mountain and forms a new center in the lee at the surface in the same place as the case without a mountain. This is also apparent in the results of experiments 2a and 2b.

Deepening rates of the primary lows in experiments 2a and 2b (Figure 18) and the control run (Figure 8) were compared. Between t+12h and t+36h, the three lows deepened at approximately the same rate. However,

Exp 2a	
6	996
12	994
18	994
24	988
30	978
36	966
42	965
48	962
54	956
60	956
66	954
72	963
78	970
84	966
90	965
96	966

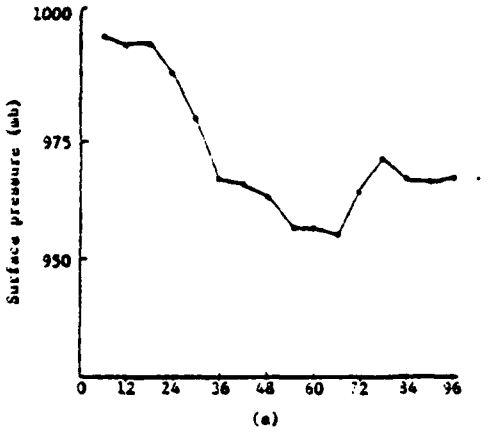

Exp 2b	
6	1000
12	1000
18	1002
24	996
30	991
36	978
42	973
48	976
54	978
60	975
66	966
72	975
78	978
84	990
90	990
96	997

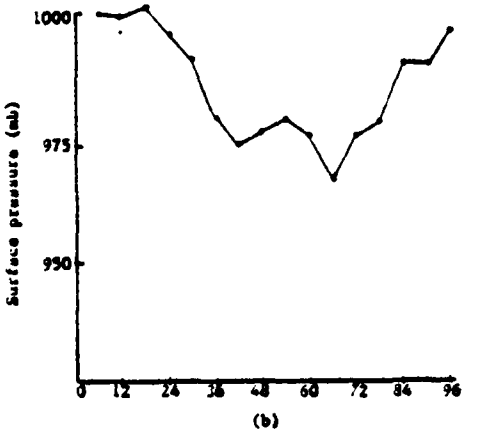

Figure 18. Plot of Surface Pressure (π) Versus Forecast Hour for Experiment 2a and 2b

at grid points in the lee during the rapid development, experiment 2b showed a faster rate of fall than experiment 2a, while experiment 2a, in turn, showed a faster than the control run. The higher mountain appeared to cause a more rapid pressure fall in the lee region but had little overall effect on the rate of fall of the central pressure travelling with the low. The more rapid deepening at points in the lee is likely due, at least in part, to the slower eastward translation speeds of the lows in the mountain cases.

Blocking of the cold air by the mountains is one of the commonly observed phenomena in lee cyclogenesis cases and it has been strongly emphasized as an imprtant contributor to lee development in research studies [Finch and Walker, 1979; Buzzi and Tabaldi, 1978; Egger, 1974; and Radinovic, 1965]. Blocking of the cold air to the west was not simulated as effectively as initially desired in the present experiments. This lack of blocking was due to the manner in which the mountain was introduced in the baroclinic flow. The initial conditions (i.e. the time when the mountain began to "grow" were such that the amplitude of the cold thermal trough approaching the windward side of the mountain was not large enough to allow the mountain to remain in a quasi-homogeneous warm sector as the mountain grew to full height. Rather, the mountain grew amidst the nearly east-west oriented isotherm pattern supporting the westerly jet (Figure 19). As a result, cold air in the northern lee region has a similar temperature to that found in the cold airmass west-northwest of the mountain. However, in both experiments 2a and 2b, a cold front formed west of the mountain in a

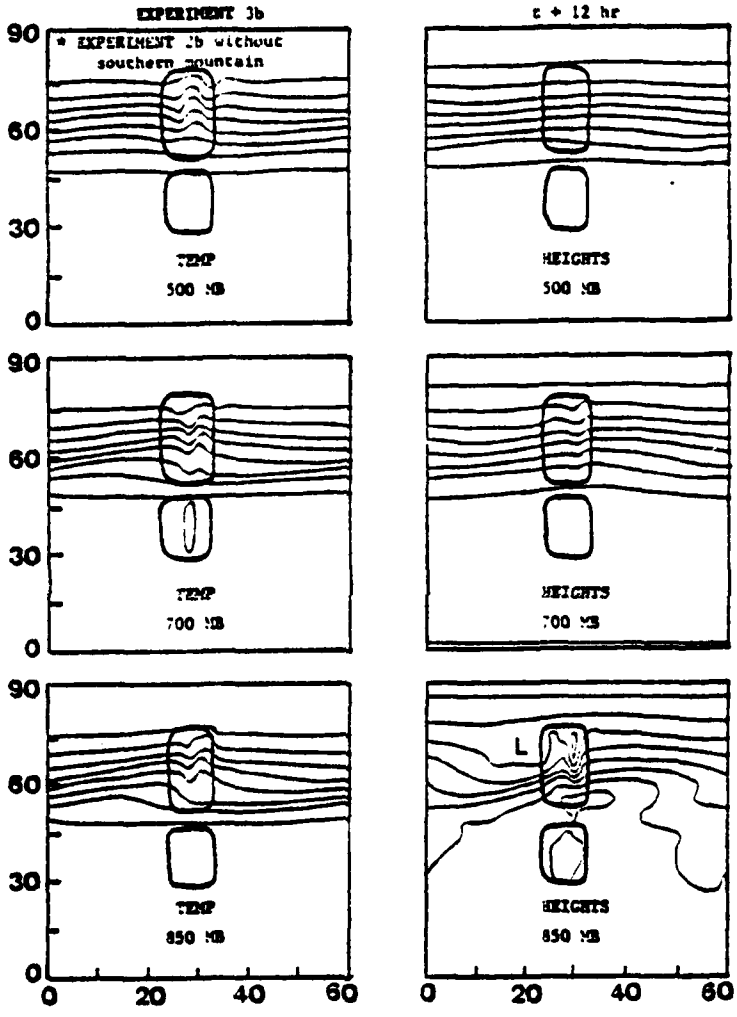

Figure 19. Height and Temperature fields at t+12h on Pressure Levels for Experiment 3b

manner similar to the control run during the normal development of the low. By t+36h (Figure 20), the front was retarded in its eastward movement by the mountain. No strong thickness maximum (i.e. large negative Laplacian of thickness) was observed in the lee prior to the development of the lee low. This maximum in the lee is observed to be an important contributor to the increase of low-level cyclonic vorticity by Egger (1974) and Radinovic (1965).

A comparison of the height patterns at 700 mb and 500 mb for experiments 2a and 2b (Figure 20) reveals a "shearing" of the upper-level trough in experiment 2b. As the trough approaches the windward side of the mountain, the northern part of the trough apparently "slips" around or over the northern end where the terrain drops rapidly to sea level. Subsequently, the trough apparently contributes to cyclogenesis in the lee of the mountain. Typically, a trough aloft is one of the major mechanisms contributing to lee development. An upper-level trough contributes the positive vorticity advection and the associated upper-level divergence needed to deepen the pre-existing trough at the surface. The southern part of the trough is retarded west of the mountain due to the effects of the barrier on the cold air mass.

The phase speeds of the low pressure centers in experiments 2a, 2b, and the control run were approximately the same. The low in experiment 2b reached the eastern boundary approximately 6h later than in experiment 2a and in the control run.

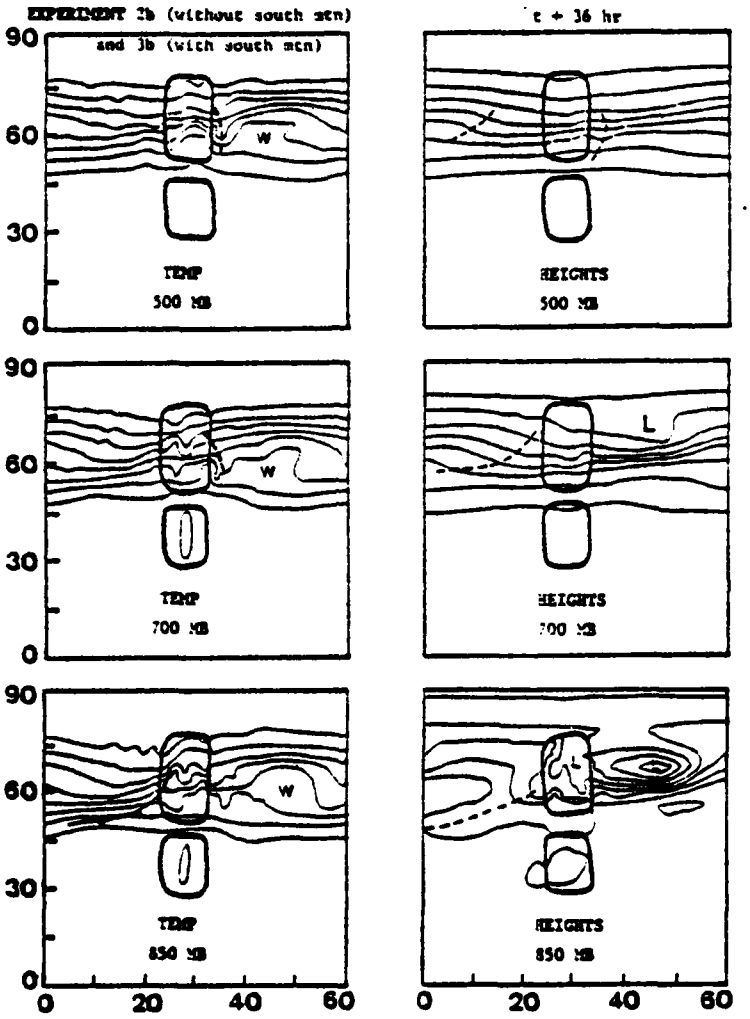

Figure 20. Height and Temperature fields at t+36h on Pressure Levels for Experiment 3b

C. EXPERIMENT 3

In this experiment a smaller mountain was inserted to the south of the mountain used in experiment 2 in such a way that if forms a gap between the mountains (Figure 5b). Tibaldi, Buzzi, and Malguzzi (1980) concluded that the cold air flowing around the Alps contributed to a baroclinic development in the lee of the mountain. Trevisan (1976) investigated cyclogenesis in the lee of the Alps by adding another mountain to simulate the gap between the Alps and the Pyrenees. She concluded that the break in the Mountain allowed cold air to flow through the pass, which forced a secondary branch in the jet, and subsequently contributed to the development of a cyclone in the lee of the Alps. Finch and Walker (1979) suggested that a similar mountain gap contributes to cyclogenesis in the lee of the Alaska Range.

Experiment 3 followed the same procedure as in experiment 2. The results of experiment 3a (1500m mountain) were quite similar to those of the control run. Both had closed contours at 850 mb by t+24h and at 700 mb by t+36h. Neither the control run nor experiment 3a ever had closed contours at 500 mb. Runs with 2° north-south resolution showed closed contours aloft where no closed contours were observed with 4° resolution. This indicates that the vertical development is smaller scale and not adequately resolved with 4° resolution. As in experiments 1a and 2a, no significant trough formed over the lee slope in this experiment.

Experiment 3b (3000m mountain) showed results nearly identical to those from experiment 2b in development, intensification, and speed of

translation. A comparison of Figures 18 and 21 shows very similar changes in central pressure of the low with time. The patterns at 850 mb, 700 mb, and 500 mb were also nearly identical. The retardation of the cold front on the windward slope was again observed as in experiment 1b (Figure 20). The formation of a strong closed low over the lee slope that drifted southward with time was observed in experiment 3b as in experiment 2b (Figure 17).

The main difference between experiments 2 and 3 was the presence of a gap between the mountains. This gap appeared to force a weak low-level cyclonic eddy. Initially, this eddy did not appear to have much baroclinic support. The eddy appeared to originate in a trough that was formed between two independent anticyclonic flows (i.e., between the east winds caused by anticyclonic flow through the northern part of the gap and west winds through the southern part of the gap caused by anticyclonic flow associated with a topographically bound high over the southern mountain (Figure 22)). Once the eddy formed in the gap, it moved slowly eastward (Figure 22). The eddy then appeared to draw energy through a weak baroclinic conversion process as seen by the weak differential advection in low levels (Figure 23). The eddy continued to drift eastward but developed little through t+66h. Cyclonic circulation in the wind field at $\sigma = 11/12$ was apparent through t+96h, and the 850 mb and 700 mb levels showed some upper-level support for the eddy in the contour pattern (Figure 23).

At t+54h the more northern low that had deepened in the lee (as in experiment 2b) reached the east boundary and had closed contours through the 700 mb level (experiments 2a and 3a had closed contours by t+36h).

	Exp 3a
6	997
12	997
18	997
24	988
30	980
36	967
42	966
48	964
54	956
60	956
66	956
72	961
78	973
84	969
90	961
96	965

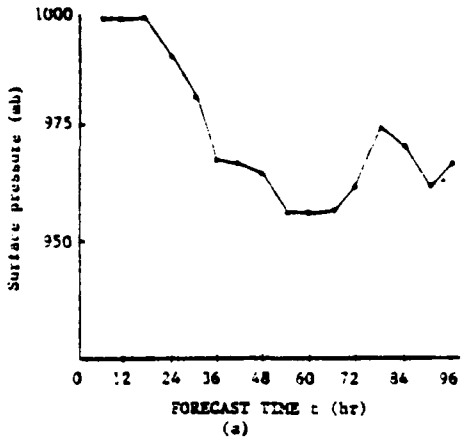

	Exp 3b smin low
6	1003
12	1004
18	1008
24	998
30	994
36	980
42	978
48	980
54	983
60	978
66	966
72	972
78	973
84	990
90	995
96	998

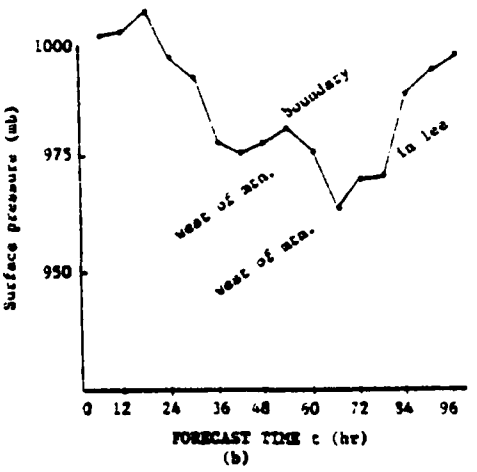

Figure 21. Plot of Surface Pressure (π) Versus Forecast Hour for Experiment 3a and 3b

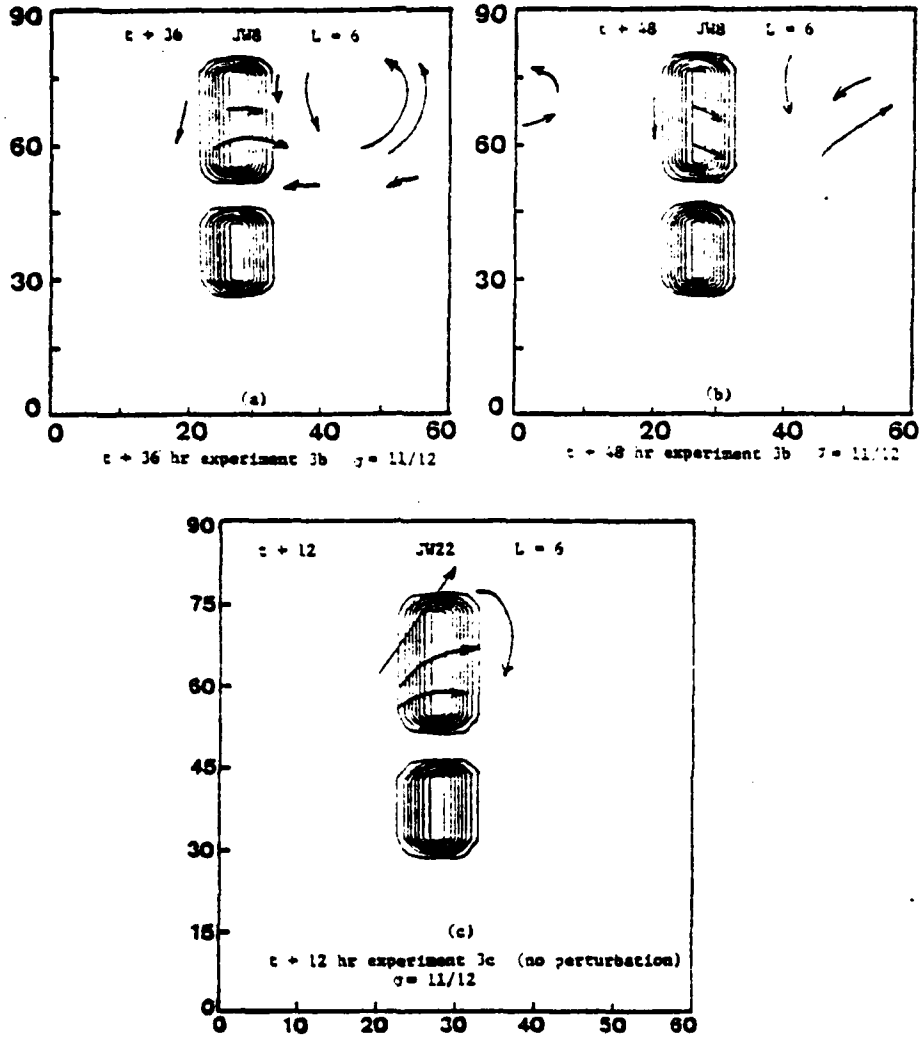

Figure 22. Wind Vectors on σ = 11/12: a) Experiment 3b t+36h; b) Experiment 3b t+48h; c) Experiment 3c t+12h

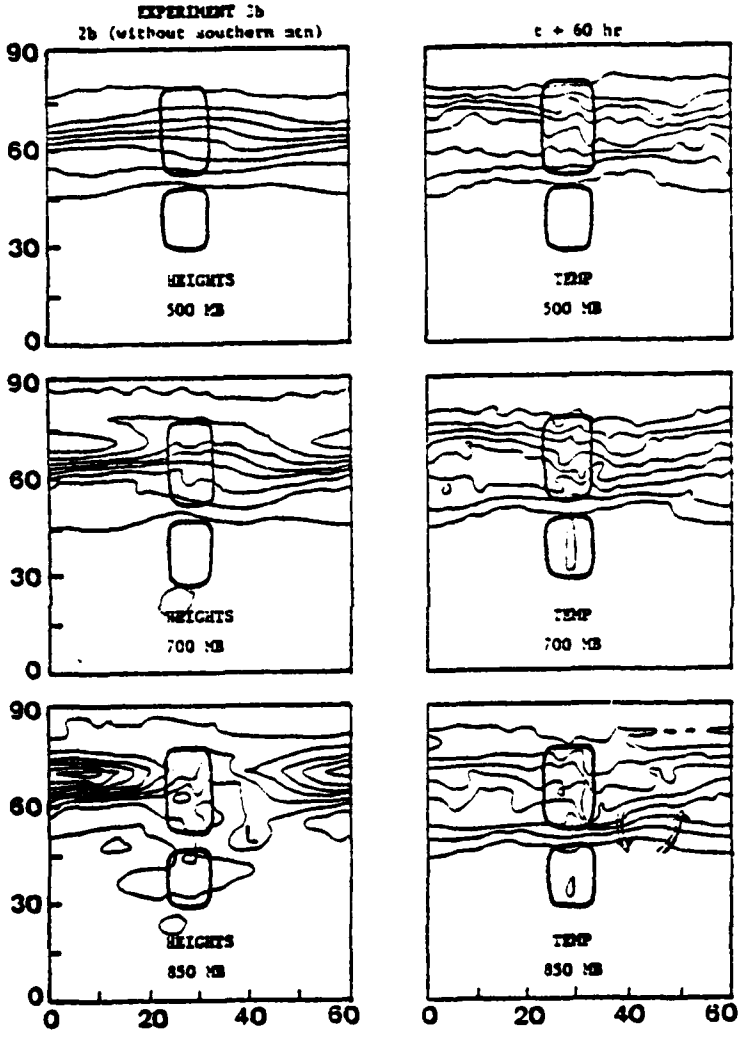

Figure 23. Height and Temperature Fields as t+60h on Pressure Levels for Experiment 3b and 2b

The intensity of the cold northerly flow west of this nearly mature low (and east of the mountain) caused a trough to form in the lee. As a result, the retarded trough on the windward side appeared to "jump" to the leeward side in a somewhat discontinuous manner. The low that had originated in the gap was then observed to intensify rapidly. This "gap low" eventually had closed contours through the 700 mb level by t+96h due to the apparent newly formed energy source (trough). Closed contours at the 500 mb level were observed over the northern low by t+96h.

The "primary" lee low deepened further as it approached the windward side of the mountain (Figure 24) from t+56h to t+66h (it was approaching the windward side of the mountain again because of the cyclic boundary conditions). A rapid development was not observed in the lee during this nearly mature stage of this low; rather, the low filled. This suggests that, if the mountain is the trigger for the baroclinic instability, the resulting development is a function of the available potential energy remaining in the mean flow. However, the height of the mountain may also be a factor since, in experiment 3a, the low deepened in the lee. Another possible factor could be that the low in experiments 3a and 3b passed over the mountain (or partially around) near the northern end.

In summary, the differences between the control run and the mountain experiments include:

(1) More rapid pressure fall at the grid points in the lee in experiment 3b;

(2) Generation of a separate low due to the gap between the mountains;

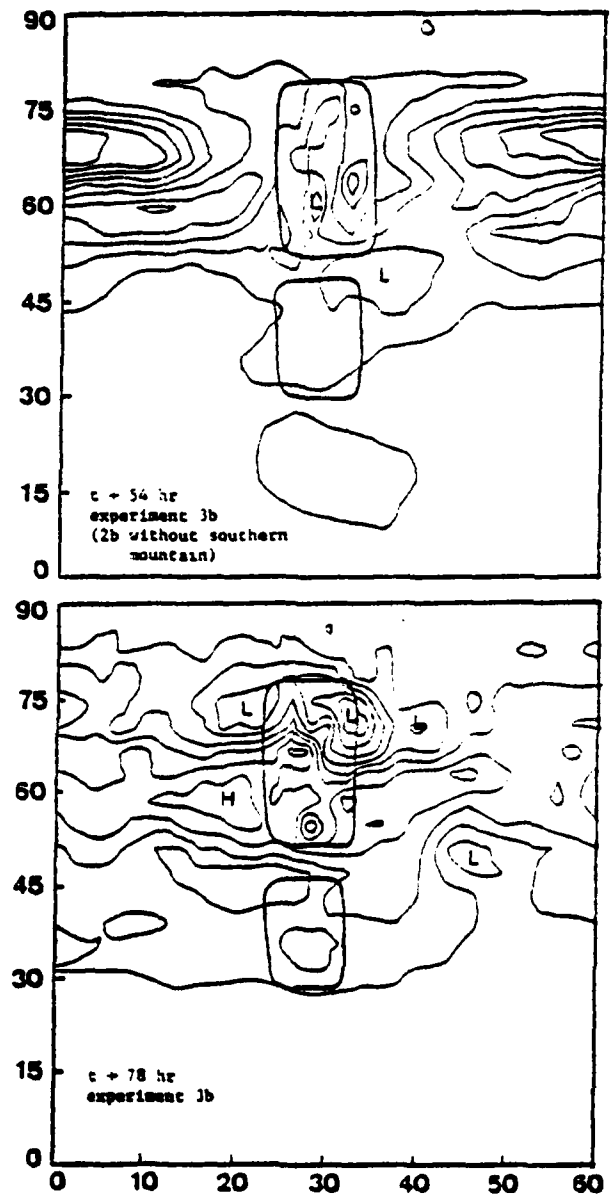

Figure 24. Surface Pressure Fields for Experiment 3b at t+54h and t+78h

(3) Retardation of the cold air mass west of the mountain and the shearing, or splitting, of the trough by the mountains which allowed the northern part to move more rapidly eastward;

(4) Slower eastward propagation of the lee low in experiments 2b and 3b (i.e., 3000m mountains);

(5) Lows deepened more rapidly approaching the mountain for the second time compared to the control run during the same time period; and

(6) Lows filled more rapidly after the second encounter with the mountain compared to the same time in the control run.

Experiment 3c was run with the initial conditions as described in Section III except without the superposed perturbation. The mountain was inserted into the model at $t_o = 0$ and raised to its full height of 3000m in 12h. The mountain was identical to the one used in experiment 3b.

The results were suprisingly similar to experiment 3b whose initial conditions consisted of an amplifying disturbance in the flow. A low over the lee slope was present by t_o+12h and drifted southward thereafter (Figure 25) as in experiments 2b and 3b. As indicated above, this lee low is pssibly due to truncation error in the vicinity of the terrain. A trough extending eastward from the base of the mountain in the lee developed at t_o+24h. This trough was nearly identical to the one observed in experiments 2b and 3b except that it had appeared by t_o+18h in those experiments.

A cyclone then developed in the lee trough and moved eastward (Figure 25). The fall of pressure with time, following the low center (Figure 26), was very similar to the control run (Figure 8). However, the eastward propagation of the low center (Figure 25) was much slower

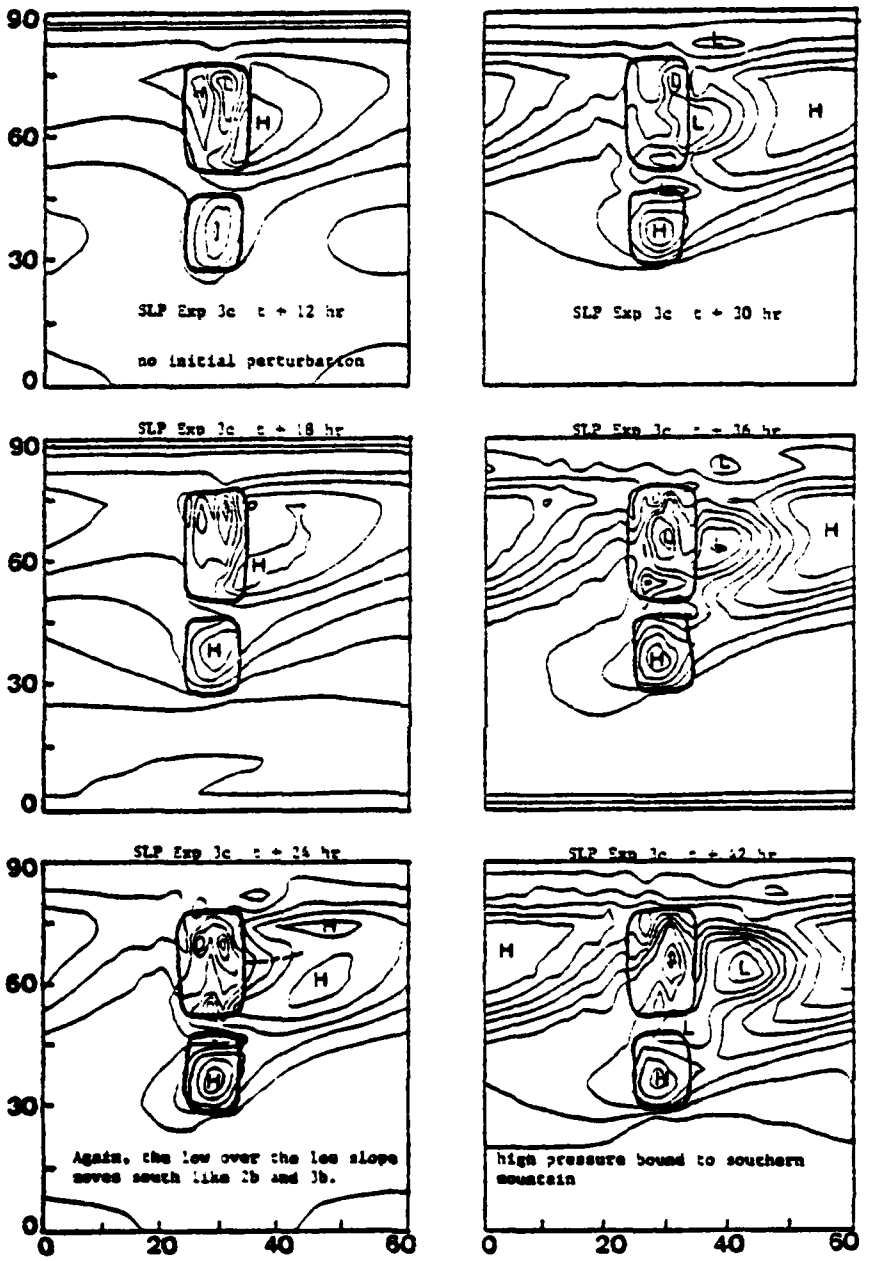

Figure 25. Surface Pressure Fields for Experiment 3c: t+12, 18, 24, 30, 36, and 42h

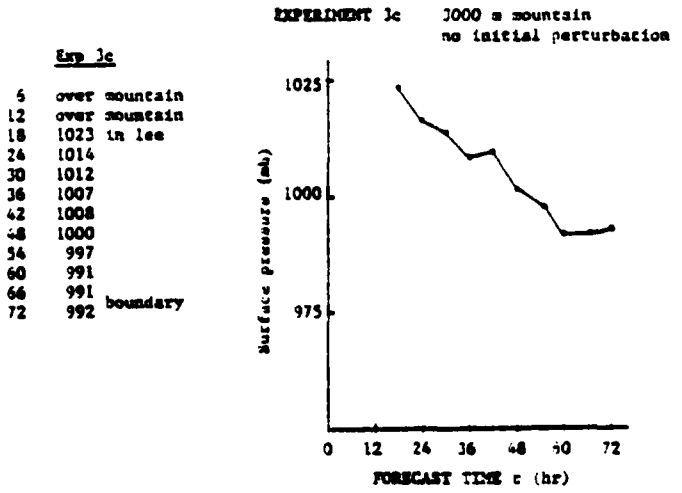

Figure 26. Plot of Central Surface Pressure Versus Time of the Low in Experiment 3c

than that observed for the control run (Figure 9) and in experiments 2b and 3b (Figure 17). Closed contours at the 700 mb level were observed over the low by t_o+66h (this is 12h later than in experiment 3b) and a nearly closed low existed in the 500 mb level by t_o+72h. At t_o+72h, the low was over the east boundary for the first time.

The development of the lee low appeared to be cuased by a short wave trough formed by deflection to the north of the westerly baroclinic current near the northern end of the mountain, as seen in the 700 mb wind field at t_o+12h (Figure 27). At 850 mb, the wind field suggests flow around the mountain (Figure 27, and in Figure 22 for σ = 11/12) in light of the increasing v-component in the windward side of the mountain (Williams, et al, 1981). By t_o+24h, a difluent area over the lee is clearly visible in the wind field (Figure 27). The surface trough is visible in the lee at this time (Figure 25). A comparison of the wind fields (Figure 27) and temperature fields (Figure 28) at the 850 mb level at t_o+24h shows northerly flow in the lee which advects cold air southward and southerly flow farther east which advects warm air northward, indicating conversion of eddy available potential energy to eddy kinetic energy. The low then continues to deepen and move slowly eastward (Figure 25). It appears that the westerly baroclinic current is deflected northward on the windward side of the mountain resulting in difluence aloft, a trough in the surface developes in the lee, and the presence of baroclinicity in the lee provides a source of energy for development to continue.

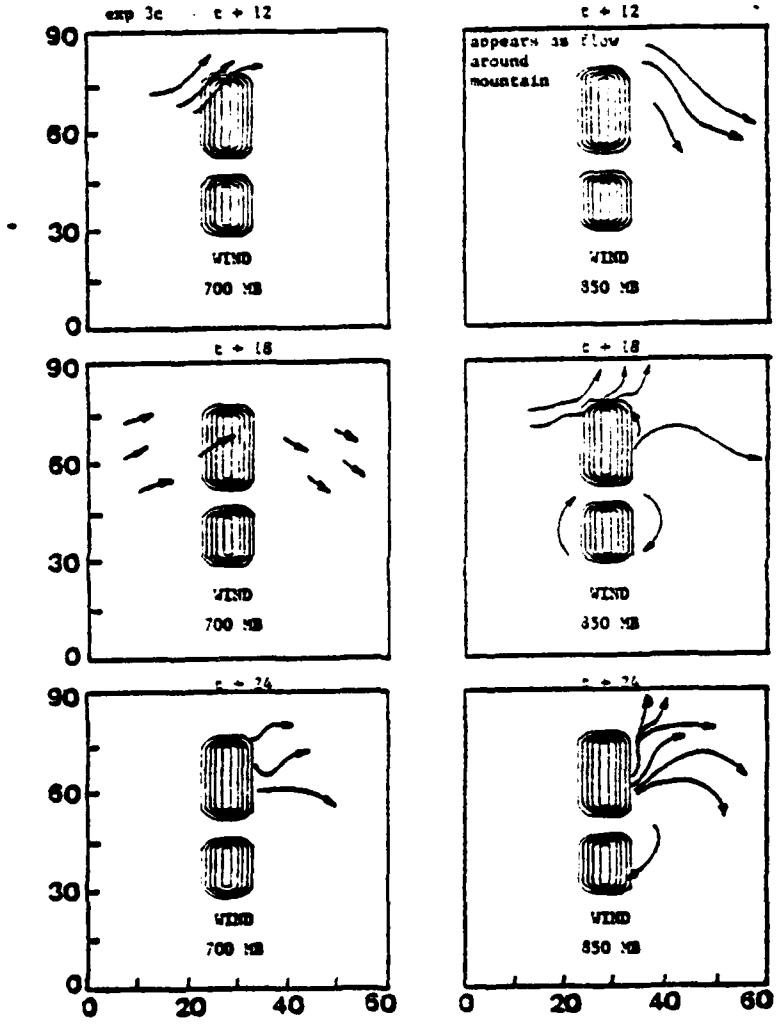

Figure 27. Wind Vectors From Experiment 3c at 850 and 700 mb for t+12, 18, and 24h

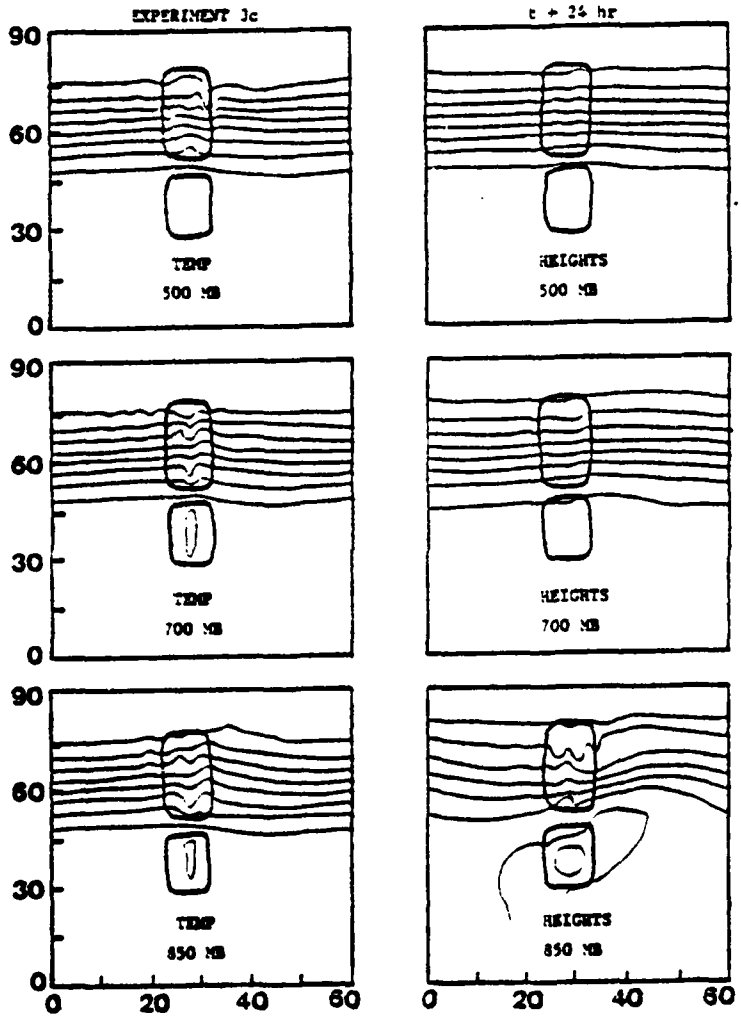

Figure 28. Height and Temperature Fields at t+24h on Pressure Levels for Experiment 3c

The "gap low" developes in the same manner as described in experiment 3b. Further development occurs when the northern low reaches the eastern boundary and the northerly flow to the west caused cold advection southward to feed baroclinic processes associated with the gap low as in experiment 3b.

Evidently, in the frictionless atmosphere, the amplifying perturbation in experiment 3b only served to deepen the lee cyclone more rapidly than was observed in experiment 3c. Further, since it took nearly 108h for significant development to occur in the control run, and the same development occurred within 24h with the mountain forcing, it would appear that the presence of the mountain amplified locally the degree of instability. In addition, the development began in the lee and not downstream from the mountain. This further supports the findings of others [Buzzi and Tibaldi, 1978; and Tibaldi, et al., 1980] that orography serves to trigger the release of available potential energy of the baroclinic flow.

It was concluded, based on these results, that the model simulates some of the characteristics of lee cyclogenesis in the lee of the Rockies and in the lee of Greenland. The presence of the gap did not appear to contribute to this development. Rather, the presence of the gap was responsible for generating an eddy that subsequently underwent "sympathetic" development due to the northerly flow behind the lee cyclone.

D. EXPERIMENT 4

The mountain in this experiment was "horseshoe-shaped" and had a rather large scale (Figure 5c). A gap in the mountain on the west side was not included in this experiment to analyze independently the effect of the "horseshoe-shape". This shape was an attempt to model the mountain rages over south central Alaska, although the horizontal dimensions of the mountain were quite large compared to the Alaska mountain complex (Figure 6). At 60°N the mountain was of the order of 1400 nm longitudinally and 1200 nm latitudinally, whereas the Alaska mountain complex is only about 800 nm by 500 nm, respectively. In this experiment, the initial conditions (t_o+96h from the control run) consisted of a disturbance moving up the windward side of the mountain as the mountain was raised.

In experiment 4a (1500m mountain), the disturbance moved down the lee side of the mountain and deepened only slightly (Figure 29) compared to experiments 2a and 3a (Figure 30). At the time the mountain reached full height (t+12h), the low was "trapped" south of the east-west ridge of the mountain complex (i.e. within the "horseshoe"). The low also moved much more slowly (Figure 31) than in previous runs.

The central pressure of the low in the horseshow vascillated with a period of 6h (Figure 30). This pattern suggests the presence of internal gravity waves propagating through the area as observed by Elias (1973) and McCollough (1974). However, a plot of pressure versus time at specific grid points within the horseshoe area show much smoother profiles. Therefore, the oscillations in the pressure pattern may only

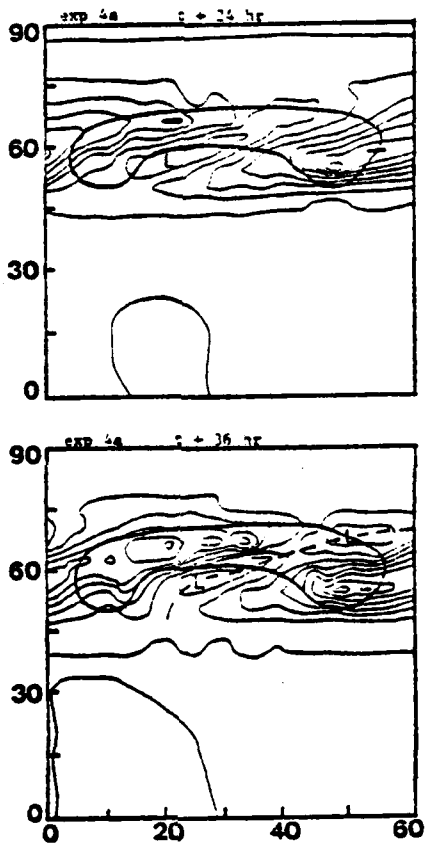

Figure 29. Surface Pressure Fields for Experiment 4a at t+24 and t+36h

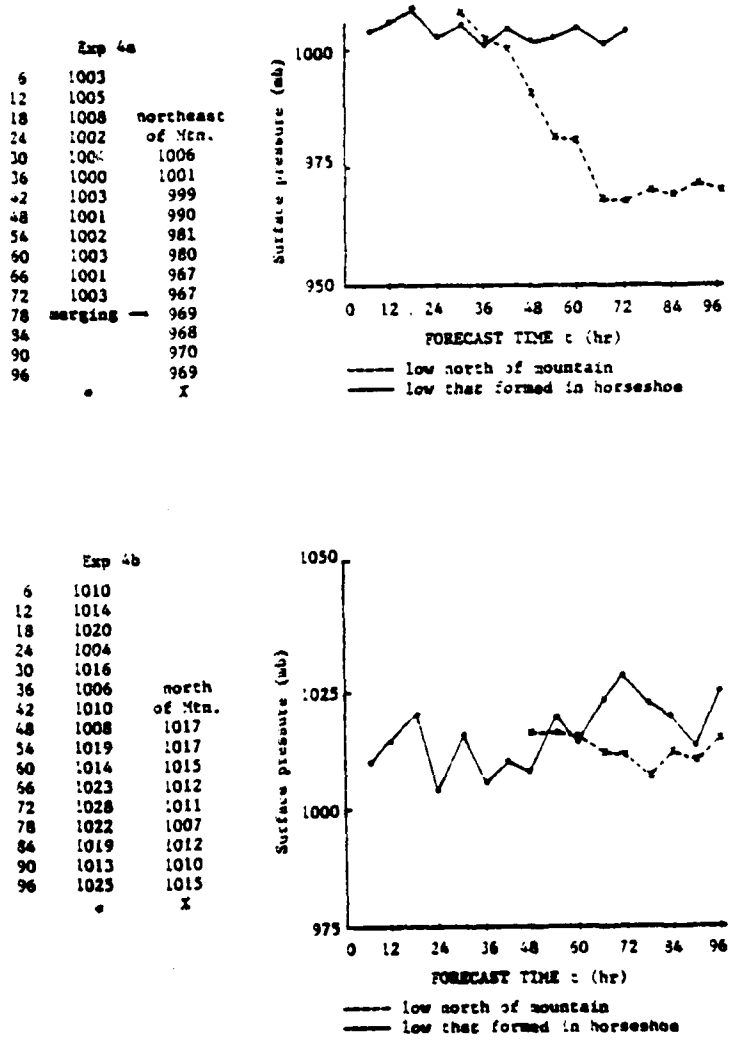

Figure 30. Plot of Surface Pressure (π) Versus Forecast Hour for Experiments 4a and 4b

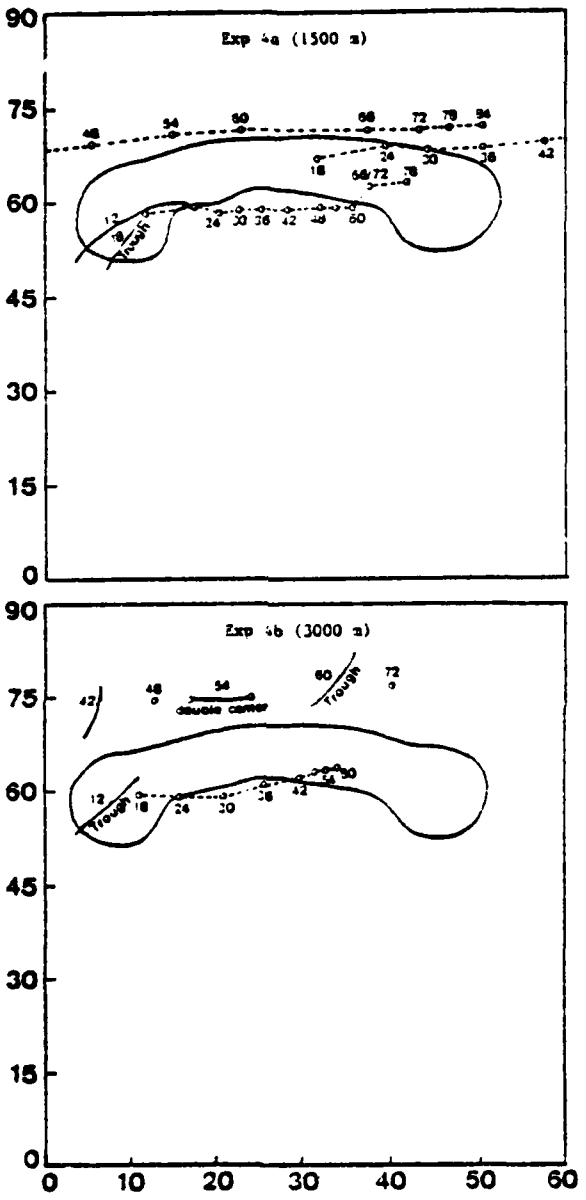

Figure 31. Positions of Suface Low Pressure Centers Versus Time for Experiment 4a and 4b

be due to insufficient resolution in the model as the low center falls between grid points. If this is true, then the profile shown in Figure 30 suggests that the low is persistent and non-deepening (no decrease in central pressure). This however, does not preclude the possibility of intensification of the low (increasing horizontal pressure gradient).

By t+24h the low in the "horseshoe" split into two parts with the northern portion deepening as it continued eastward (Figure 29). The split was a result of an elongation of the low in the direction of the flow where a trough extended across a low point in the east-west ridge. (This low point was due to the decreased resolution in the north-south direction and the manner in which the mountain generating scheme discussed in Section IV forms the mountain.) The northeast-southwest orientation of the trough can be better seen in the surface pressure output of the control run at t+12h (Figure 7b). The residual low to the south remained behind and continued to move slowly eastward and filled slowly (Figure 31). The northern low became quite strong (Figure 30) and eventually dominated the entire synoptic picture. At t+36h the deepening low north of the mountain was in the same location as the low in the control run. Subsequent positions were also near the positions in the control run for the corresponding times (Figure 9).

Although the deepening low north of the mountain was in the same location as the low in the control run at t+36h, it was much weaker at this stage. At t+42h, the low then began deepening rapidly (Figure 30) and nearly reached the intensity of the low in the control run by t+66h.

The low in the horseshoe had closed contours at the 850 mb level by t+36h (Figure 32). However, closed contours at the 700 mb level were never observed through t+84h. The northern low had closed contours at 850 mb by t+48h, became more intense than the low in the horseshoe by t+60h and then dominated the pattern. The northern low had closed contours at the 700 mb level at t+84h.

The sequence of events showed cold air south of the growing mountain forming a front oriented east-northeast to west-southwest (Figure 33). As the upper trough moved eastward over the mountain, the low in the horseshoe developed in response to warm advection due to southerly flow over the eastern section ahead of the trough and cold advection to the west due to northerly flow west of the trough. This differential advection appeared to cause a weak baroclinic conversion until the east end of the horseshoe was encountered, which cut off the warm advection to the east. Meanwhile, the low to the north developed normally in the northern part of the trough which had "sheared off" by t+48h (Figure 32).

These results suggest that the 1500m mountain had an effect on the disturbance but not enough to alter totally the large-scale dynamics. Further, they suggest that the mountain shape diverts some of the energy away from the northern wave which in the control run was the only development.

The results of experiment 4b (3000m mountain) showed that the higher mountain may have a stronger effect on the large-scale dynamics. The low that formed in the horseshoe in experiment 4b (Figure 34) was more

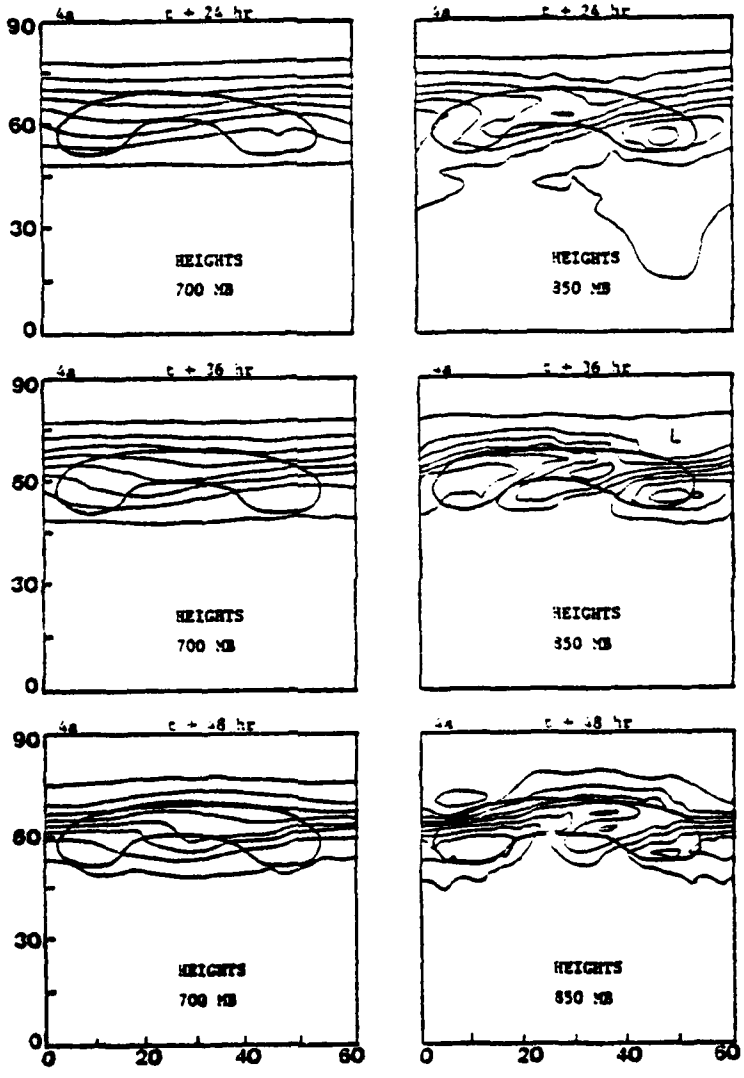

Figure 32. 850 and 700 mb Height Fields for Experiment 4a at t+24, 36, and 48h

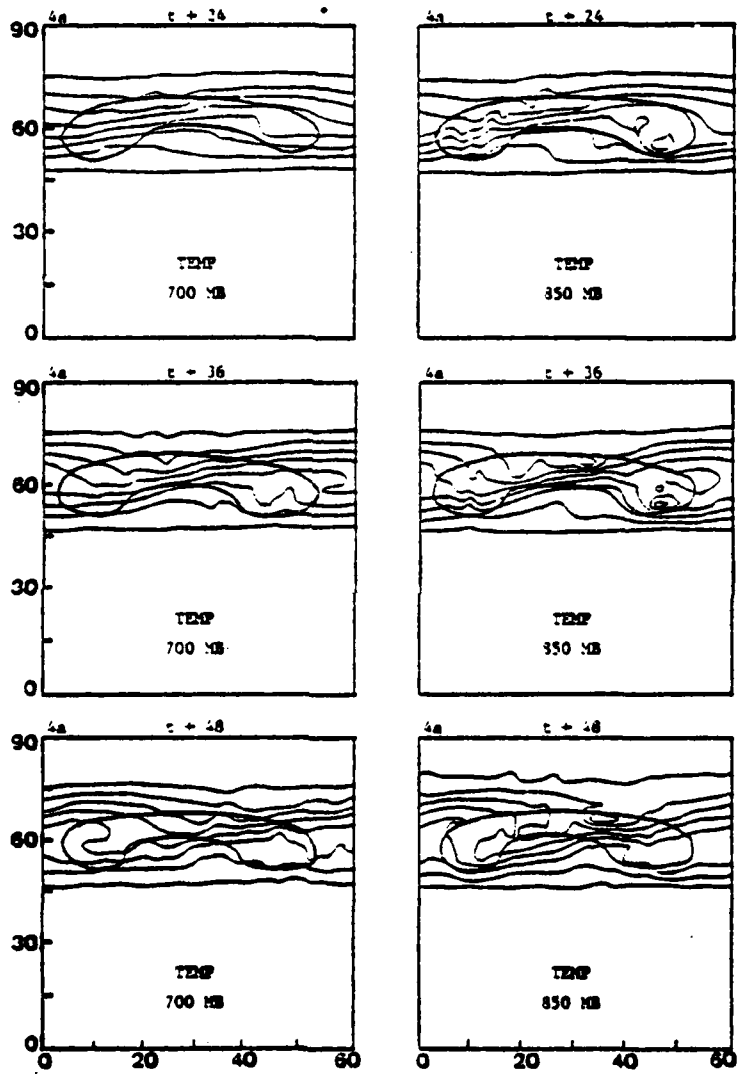

Figure 33. 850 and 700 mb Temperature Fields for Experiment 4a at t+24, 36, and 48h

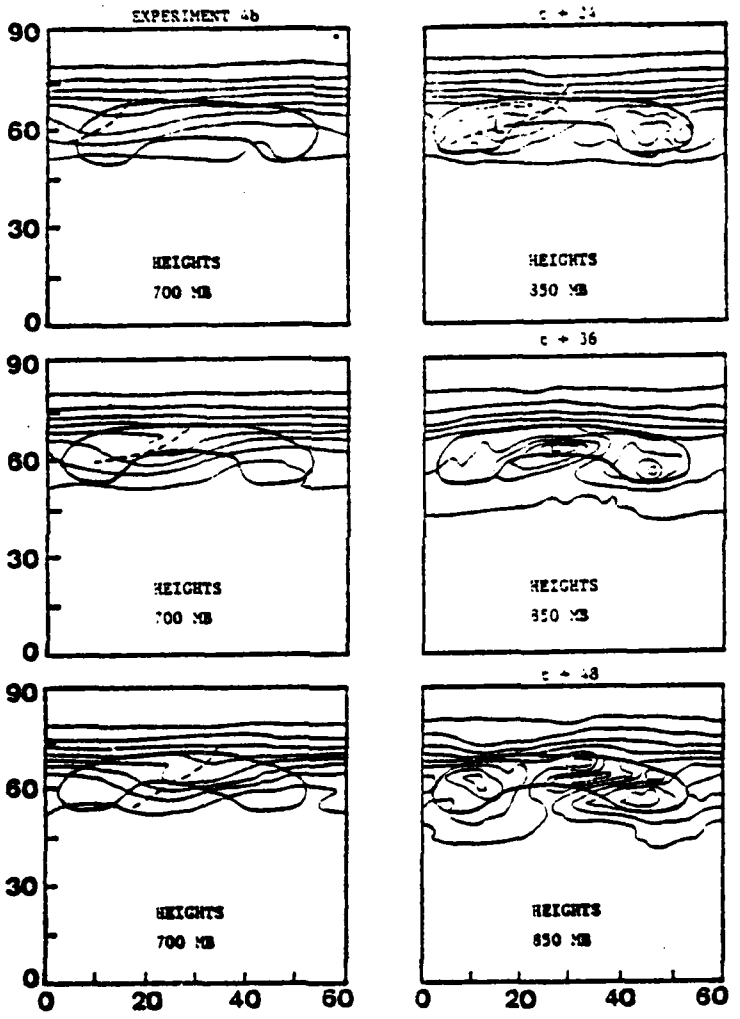

Figure 34. 850 anc 700 mb Height Fields for Experiment 4b at t+24, 36, and 48h

intense and had a better defined circulation at the 850 mb level than in experiment 4a. This low remained the dominant low throughout the experiment. Only weak troughing was observed over the low area of the east-west ridge to the north. This was likely due to the more effective blocking due to the higher mountain height, which together with the shape, appeared to have a strong "trapping" effect on the cyclone in the horseshoe.

As in experiment 4a, a nearly east-west front formed as a result of cold air being forced southward in the horseshoe by the growing mountain (Figure 35). This front that formed in the northwest corner of the horseshoe in experiment 4b became more intense than the front in experiment 4a, possibly because of the increased steepness of the mountain slope in experiment 4b. The strength of this front increased from t+12h through t+36h (Figure 35). During this period, the low in the horseshoe reached its lowest pressure (Figure 30). As in experiment 4a, the pressure changed vascillates with a 6h period. However, smoother pressure traces were observed at individual grid points within the horseshoe. Notably, the western-most grid point in the horseshoe showed a pressure fall of 13 mb in 6h between t+18h and t+24h. This type of pressure fall was also observed in experiments 2b and 3b.

Winds at the lower σ-levels at t+36h (Figure 36) suggest a baroclinic conversion process taking place. There is cold air being advected southward with northerly winds to the west and warm air moving northward in the southerly flow to the east of the low.

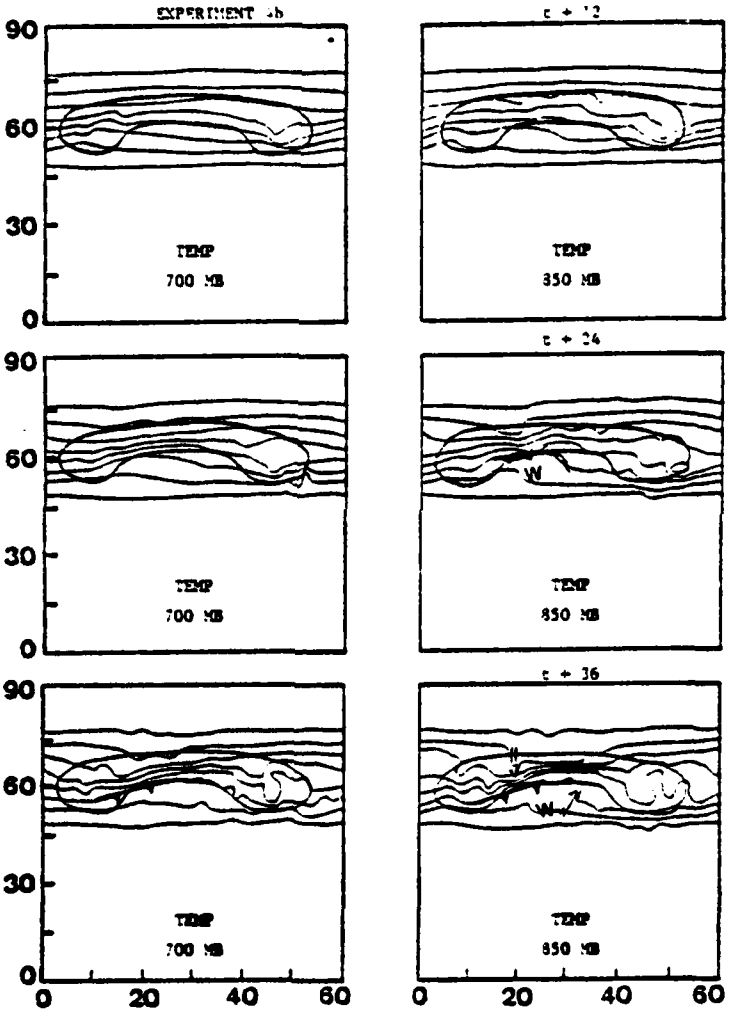

Figure 35. 850 and 700 mb Temperature Fields for Experiment 4b at t+24, 36, and 48h

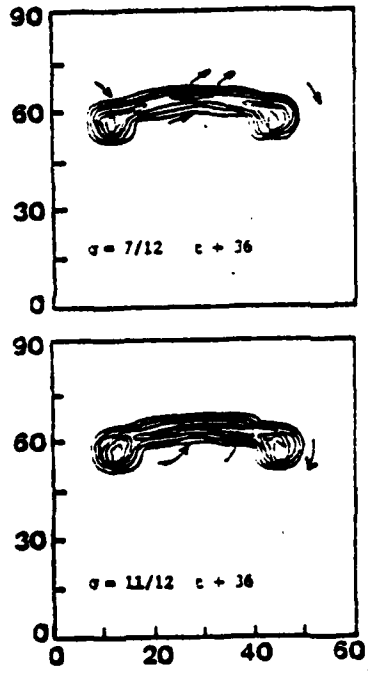

Figure 36. Wind Vectors on σ = 7/12 and 11/12 at t+36h for Experiment 4b

While results in experiment 4b showed a much stronger development process occurring within the horseshoe than to the north of the mountain (Figure 37), the results of experiment 4a showed the reverse. Mountain height appears to be the key difference. After the low in the horseshoe in experiment 4b filled, the low north of the mountain eventually attained a lower pessure than the low in the horseshoe, but it did not deepen as fast as in experiment 4a.

Development aloft was never very strong at 500 mb. No closed contours were observed at the 700 mb level either. A persistent low of moderate intensity was observed moving eastward with the upper trough. The system tilted westward with height, which indicated development until t+36h, when the central pressure began to rise and the system appeared vertical through the 700 mb level. As the low in the horseshoe was filling, the northern low deepened slightly after t+60h (Figure 30).

Tibaldi, et al. (1980) prcposed that the amplification of an initial disturbance produced by a cold front associated with the large-scale wave that moves over the Alps is caused by a small-scale baroclinic process. Further, they proposed that this process reduced the efficiency of the baroclinic conversion over the whole domain, even though it increased the energy conversion locally.

A similar effect appears to be occurring in experiment 4b. The initial disturbance in the horseshoe appears to be amplified by a cold front moving down the southern slope and by the associated upper trough. The mountain height appears to contribute to this more local development, which also appears to reduce the baroclinic conversion over the whole domain as evidenced by the less intense low to the north.

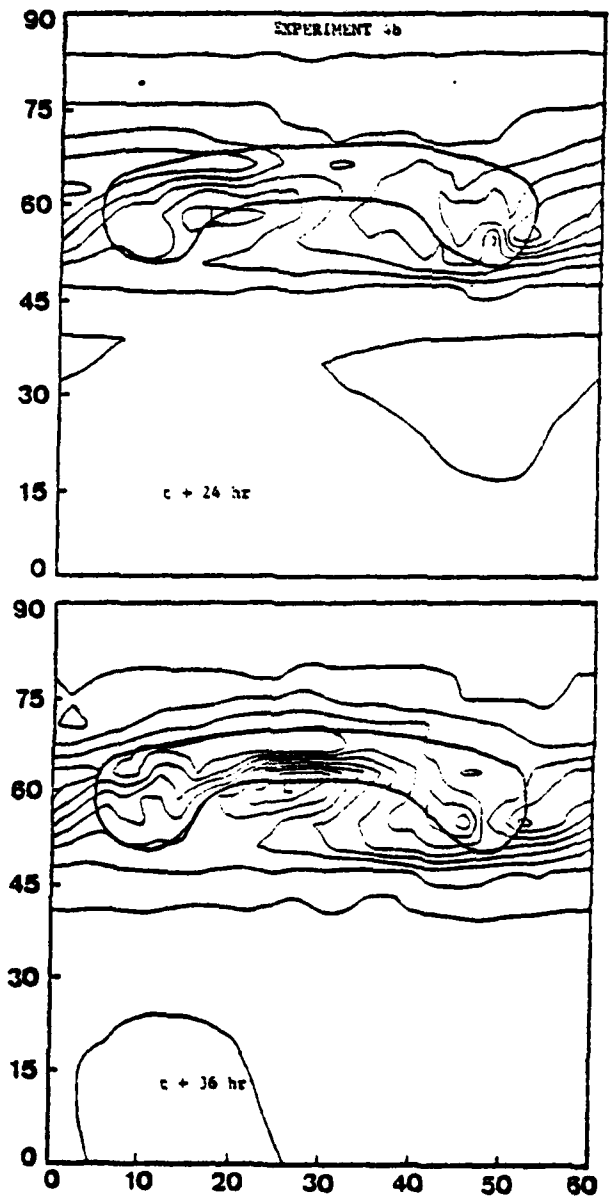

Figure 37. Surface Pressure Fields for Experiment 4b at t+24 and t+36h

A similar situation appears to occur in Alaska, except that a cold front and an upper trough amplifies, intensifies, or localizes a pre-existing depression over Cook Inlet, which reduces the efficiency of the baroclinic conversion over the northern Gulf of Alaska.

Three important features were observed in experiment 4b;

(1) The height and shape of the mountain appeared to be responsible for the lack of deepening observed in previous runs as well as the lack of vertical support through the 500 mb level;

(2) The horseshoe appeared to "trap" the low and contribute to the localization of a baroclinic conversion within the horseshoe at the expense of development to the north of the mountain; and

(3) The main low within the horseshoe was far behind the control run in its eastward movement.

E. EXPERIMENT 5

The terrain in this experiment (Figure 5d) was formed with the mountain from experiment 4 by adding a mountain which extended westward from the eastern-most ridge. The area within the horseshoe was therefore decreased. There was an opening to the northeast with was an attempt to simulate Cook Inlet and the valley to the north and northeast. The extremely large scale was used to better resolve any atmospheric features that would be generated. The initial conditions again consisted of the amplifying disturbance from the control run at t_o+96h, and the mountain was raised in 12h.

In experiment 5a (1500m mountain), the low developed as in experiment 4a, except that the eastward translation was much slower and the low filled by t+54h (Figure 38). A low again developed by t+24h north

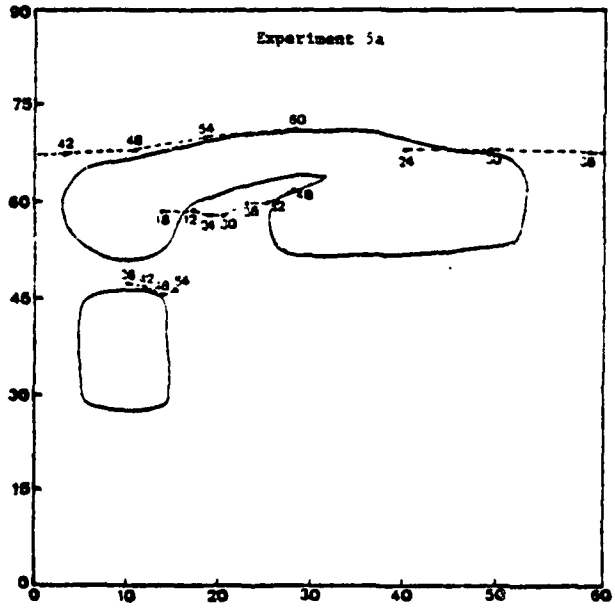

Figure 38. Positions of Surface Low Pressure Centers at 6-h Intervals for Experiment 5a

AD-A125 301 NUMERICAL SIMULATION OF THE INFLUENCE OF SMALL SCALE MOUNTAIN RANGES ON A BAROCLINC WAVE(U) NAVAL POSTGRADUATE SCHOOL MONTEREY CA J P WALKER DEC 82 2/2

UNCLASSIFIED F/G 4/2 NL

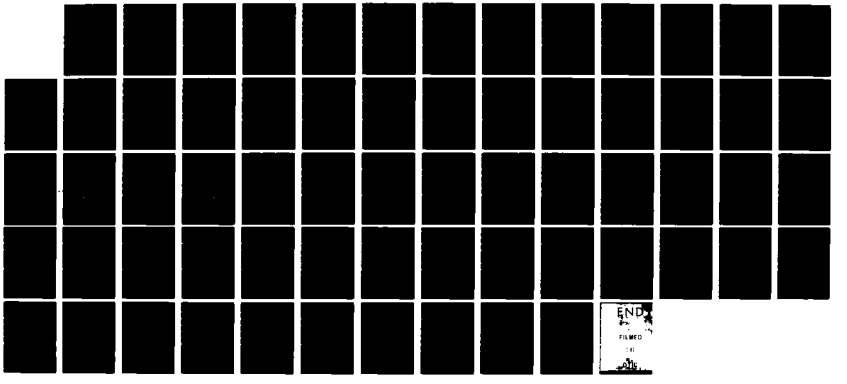

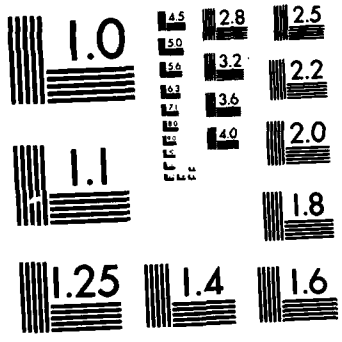

of the mountain (in the trough that extended from the low in the horseshoe northeastward over the low area in the east-west ridge). This low continued to deepen (Figure 39), and eventually dominated the surface pattern.

A low developed in the gap by t+36h (Figure 41) and drifted eastward. A similar low did not form in experiment 4a. It dissipated by t+60h (Figure 39) after very little eastward movement (Figure 38). The low from the gap developed after a large amplitude 850 mb trough (Figure 42) passed over the mountain and "closed off" over the low in the horseshoe. The reason for the development of this low in the gap was not readily apparent.

A short-lived development of the low in the horseshoe occurred with cold air moving southward to the west and warm air moving northward to the east of the low as in experiment 4a. The low in the horseshoe in this experiment filled earlier than the one in experiment 4a, apparently because of the warm air being cut off to the east of the low as it encountered the terrain to the east. The vascillation in the pressure tendency (Figure 39) can be seen again in this experiment. As in experiment 4a, the low in the horseshoe persists but never deepens significantly.

Experiment 5b (3000m mountain) started out similar to 5a. Whereas experiment 5a had developed a low northeast of the mountain complex by t+30h, the low in experiment 5b did not (Figure 44). The low north of the mountain formed at t+42h and gradually deepened thereafter. The central pressure of this low was generally less than the one in the horseshoe, but they had a similar decrease in pressure with time through

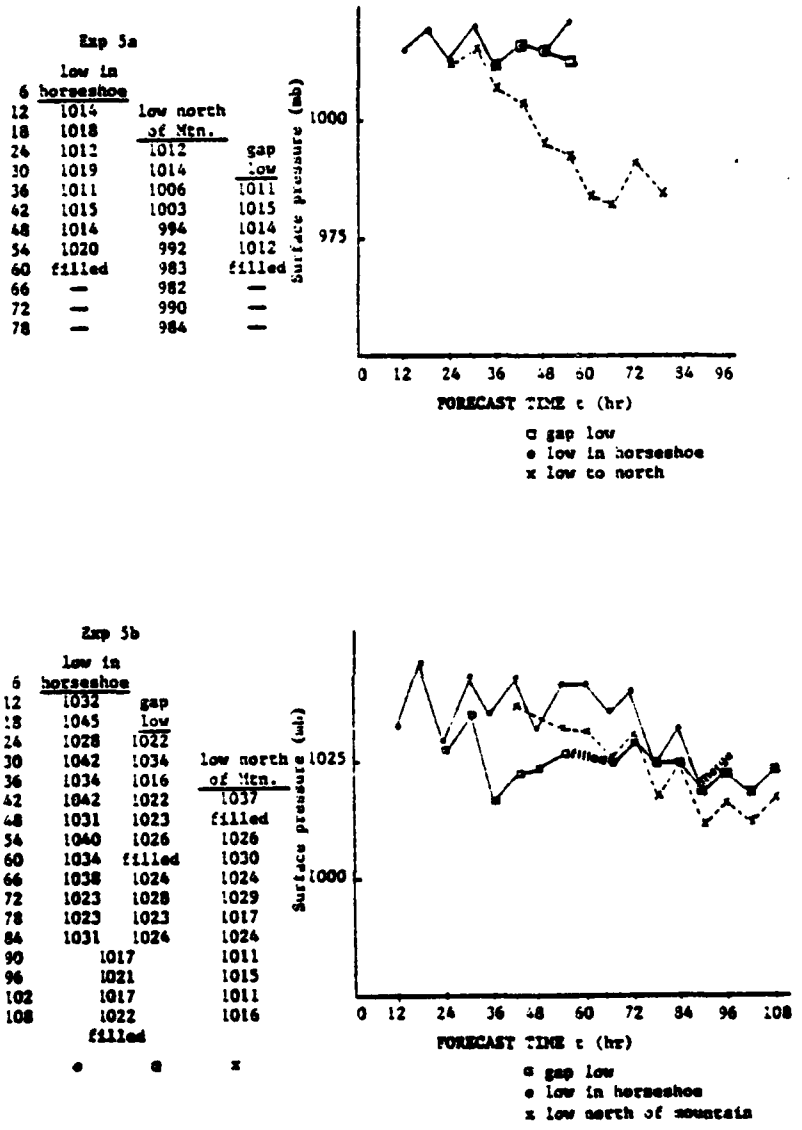

Figure 39. Plot of Surface Pressure (π) Versus Forecast Time for Experiments 5a and 5b

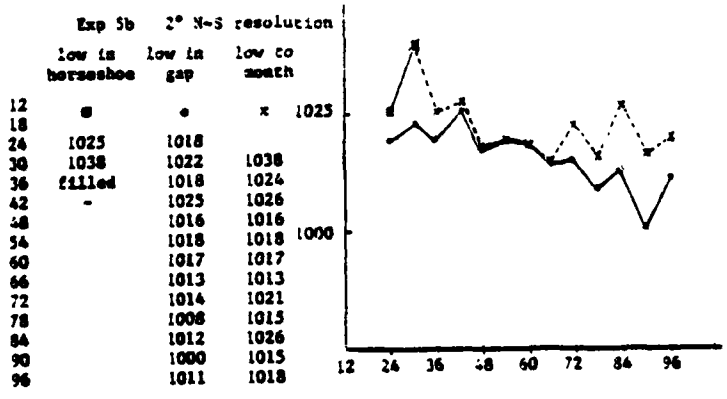

Figure 40. Plot of Surface Pressure (π) Versus Forecast Time for Experiment 5b (2° North-South Resolution)

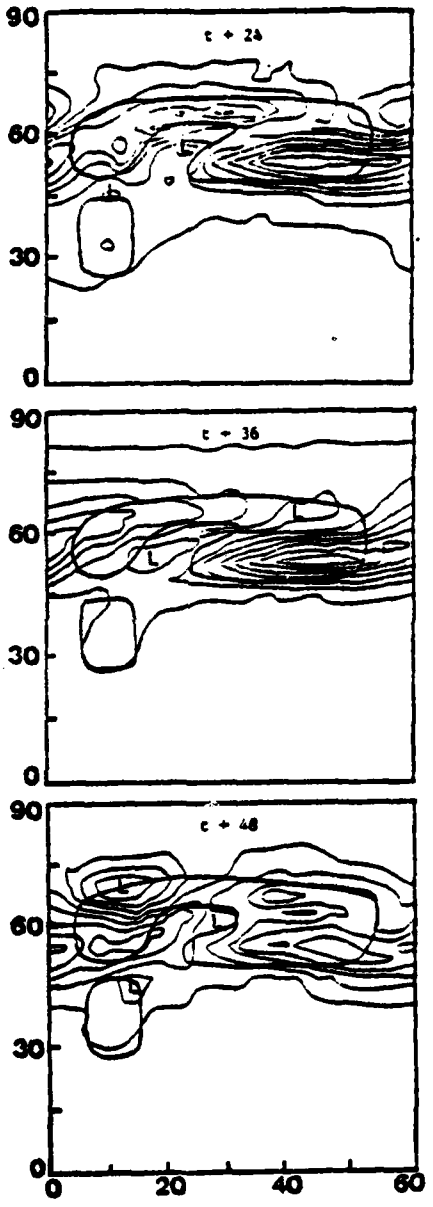

Figure 41. Surface Pressure Field for Experiment 5a at t+24, 36, and 48h

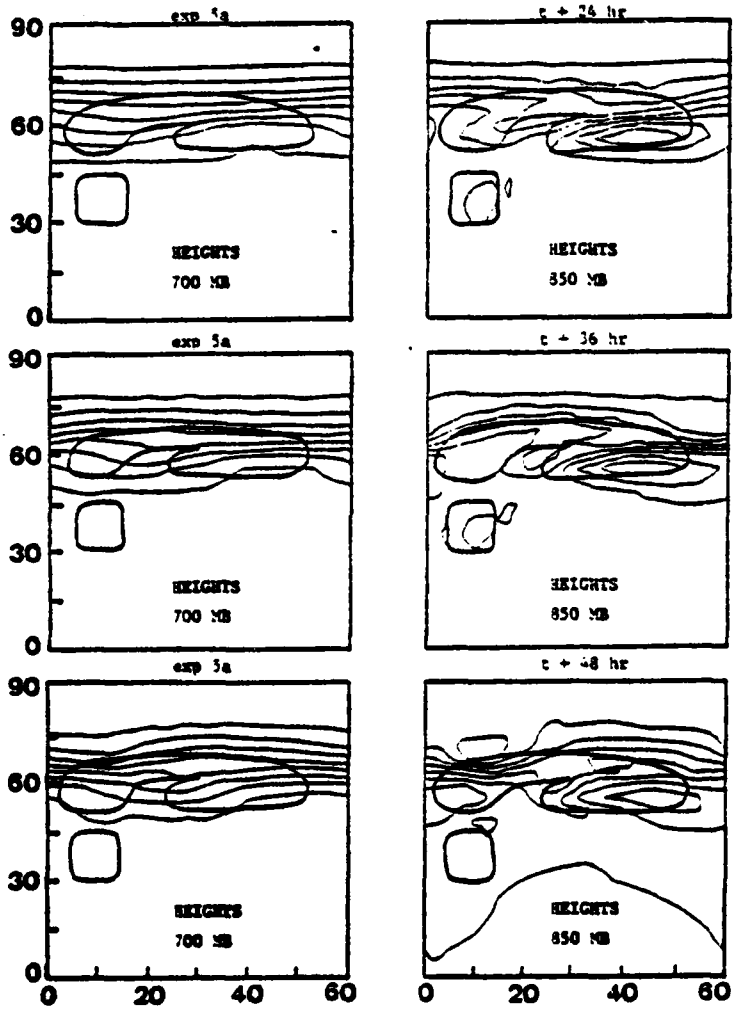

Figure 42. 850 and 700 mb Height Fields for Experiment 5a at t+24, 36, and 48h

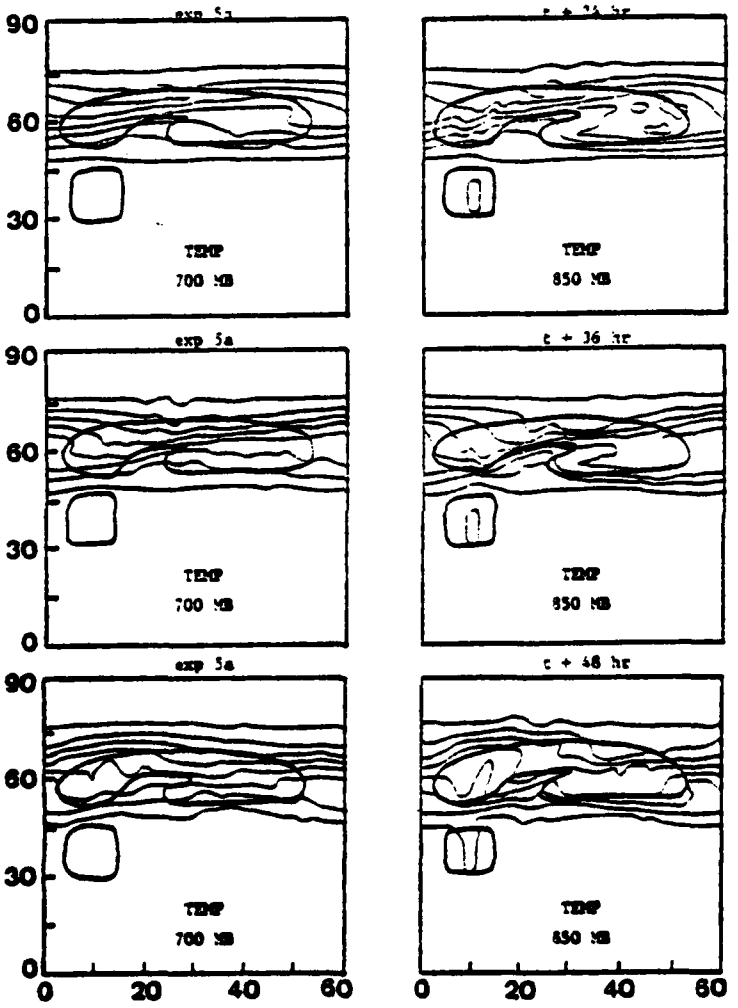

Figure 43. 850 and 700 mb Temperature Fields for Experiment 5a at t+24, 36, and 48h

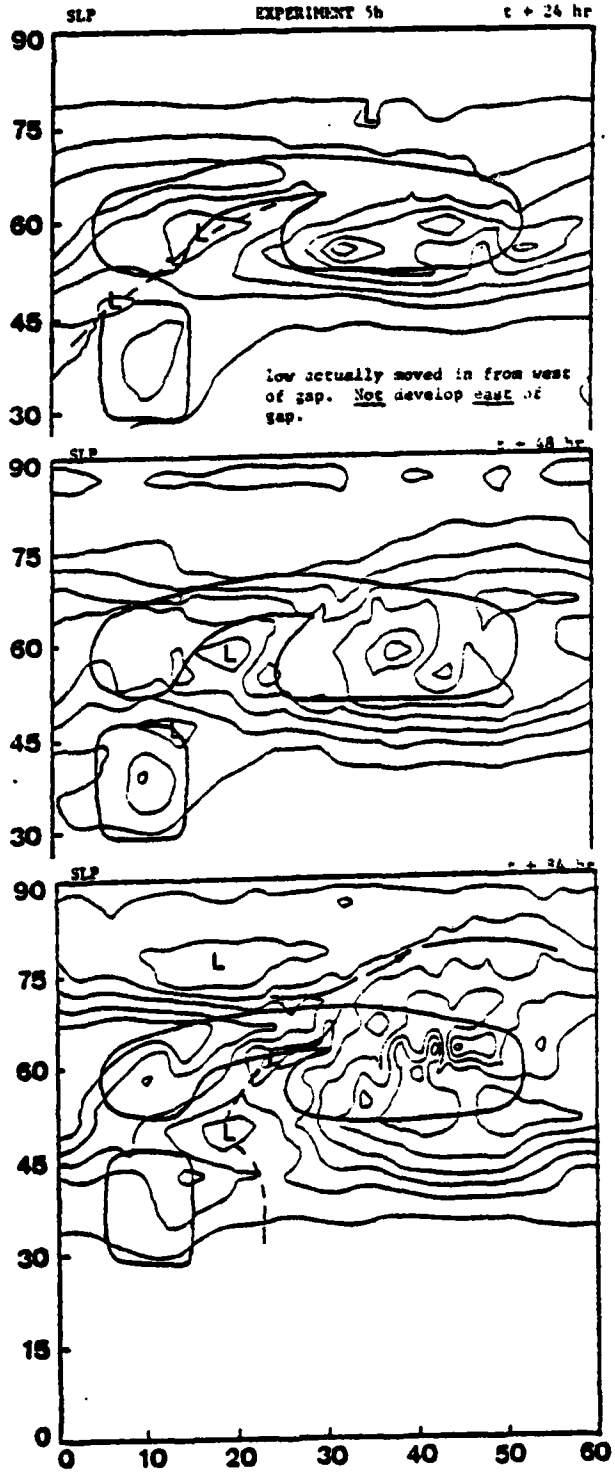

Figure 44. Surface Pressure Field for Experiment 5b at t+24, 48, and 84h

t+102h (Figure 39). This trend differs from the results of experiment 4b, in which the low north of the mountain did not deepen until the low in the horseshoe was nearly filled.

The overall sequence of events in experiment 5b occurred in a slowly changing fashion. By t+24h, a low had formed in the gap and a low was present in the horseshoe (Figure 44). The central pressure of both of these lows became nearly equal by t+66h (Figure 39). Figure 39 shows that the low from the gap had the lowest pressure early in the experiment. An experiment with 2° north-south resolution showed central pressures to be lower in the low that originated in the gap rather than in the low north of the mountain (Figure 40). In fact, the low from the gap was the only low within the horseshoe after t+36h. This shows that the resolution of the model affected the simulation of the important features. The wind and height fields also showed this same increase in detail. In the 4° resolution run, the low that formed in the gap moved slowly east-northeast along the mean low-level isotherm pattern and apparently merged with the low in the horseshoe by t+90h (Figure 45).

The long period of time during which the lows remained drifting eastward prior to t+60h (Figure 44) appears to be partially a result of the retardation of the upper trough (Figure 46) to the west by the mountain and also the constraint of cyclic lateral boundary conditions. The upper-level trough over the western mountain moved very slowly eastward throughout the experiment and gradually became more vertical. Closed contours were observed at the 500 mb level at t+72h (Figure 47) in the run with 2° north-south resolution. With 4° resolution, no

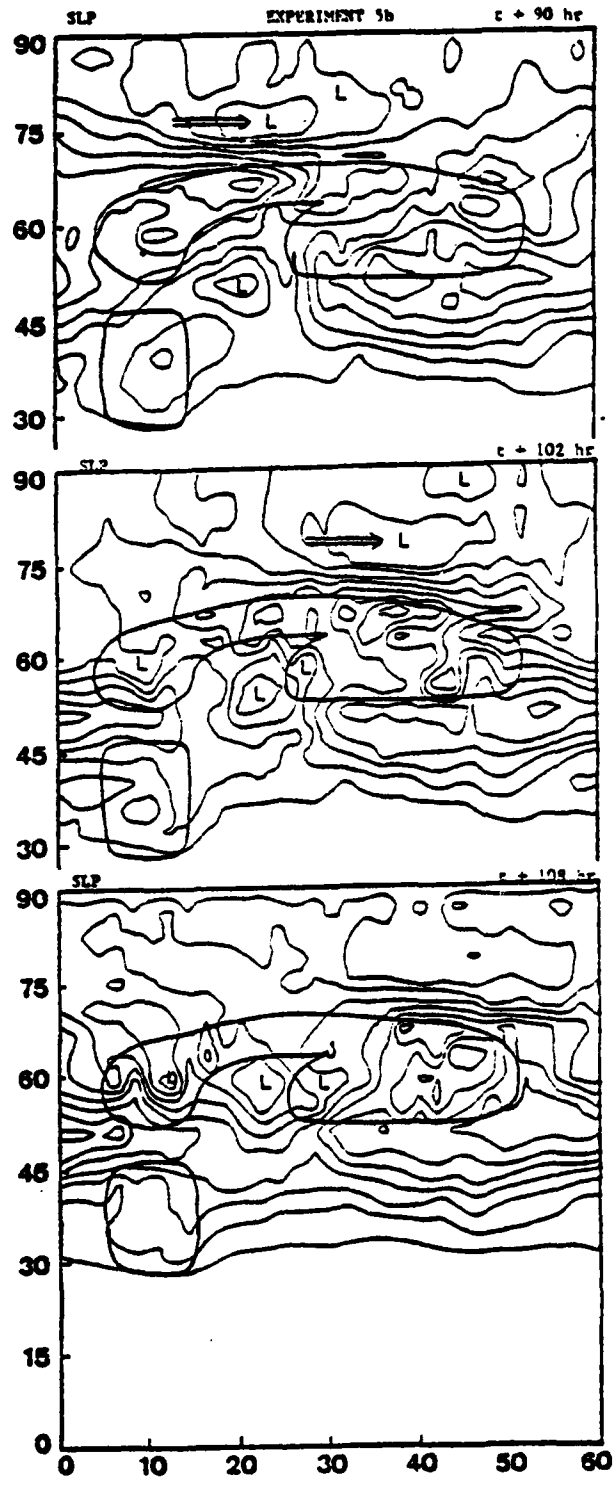

Figure 45. Surface Pressure Field for Experiment 5b at t+90, 102, and 108h

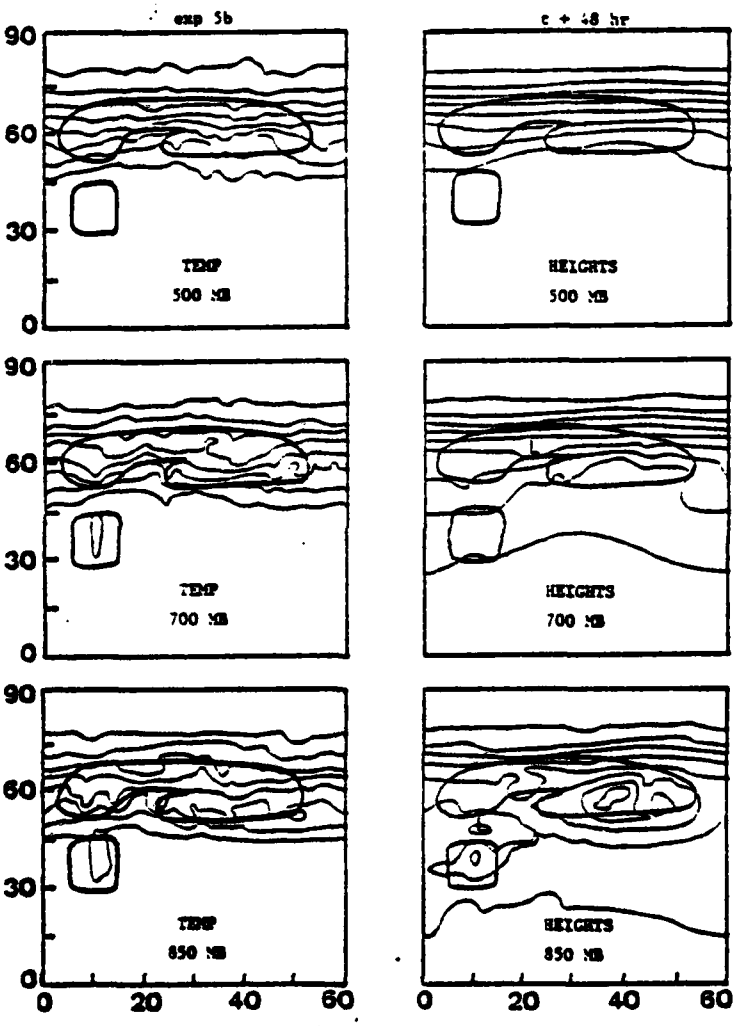

Figure 46. Height and Temperature Fields at t+48h on Pressure Levels for Experiment 5b

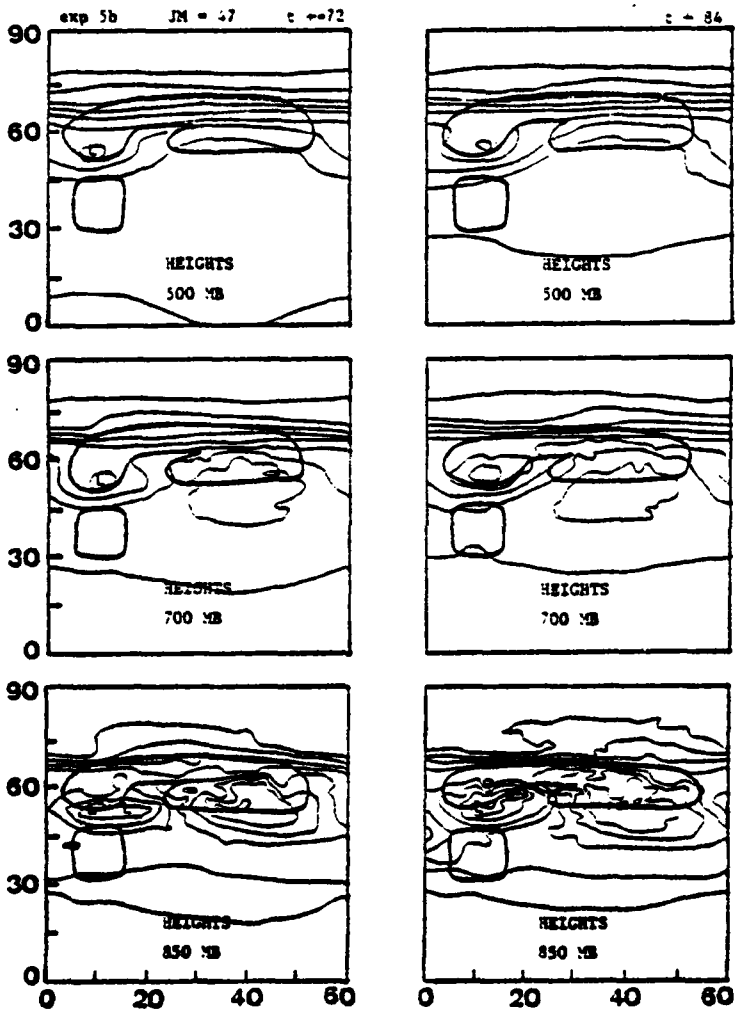

Figure 47. 850, 700, and 500 mb Height Fields for Experiment 5b at t+72 and t+84h (2° North-South Resolution)

closed contours were observed at 500 mb until t+108h (Figure 48). After t+72h the surface pressure of the horseshoe low showed a distinct falling trend (Figure 39).

The remainder of the results of experiment 5b will be discussed using solutions from the 2° north-south resolution runs. In Figure 48, the wind field at t+72h shows westerly flow through the gap at all levels. In addition, easterly flow in the south side of the 850 mb high over the eastern mountain becomes southerly flow over the east side of the horseshoe, and a trough northwest of the mountain can be seen in the wind field. This trough moves eastward through the remainder of the run but appears to have little interaction with the features south of the mountain.

The temperature field at 850 mb showed a warm ridge in the horseshoe and a cold trough over the gap. These two features support a thickness maximum east of the gap. The wind field acts to maintain this pattern and also has the potential to intensify it. As mentioned before, the thickness maximum contributes to the generation of low-level cyclonic vorticity [Patterssen, 1956; and Radinovic, 1965].

The height fields at t+72h (Figure 47) show that the low near the gap is nearly vertical and has closed contours through 500 mb. In addition, a short-wave trough aloft, extending eastward from the closed low over the gap, is rotating northward within the horseshow. A much smaller scale low at 850 mb and at the surface is observed here compared to the 4° resolution run. The smaller-scale low is also apparently more strongly associated with the terrain to the west compared to the low east of the gap in Figure 47.

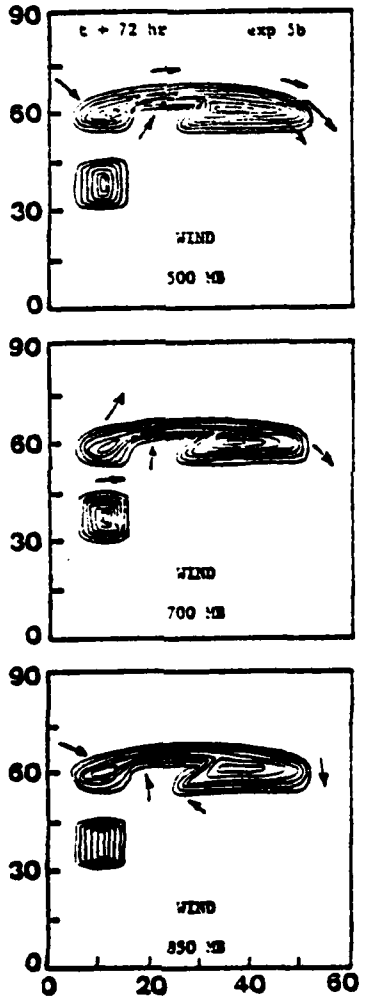

Figure 48. Wind Vectors on Pressure Levels for Experiment 5b at t+72h (2° North-South Resolution)

The evolution of features shown in the results of the high resolution run (experiment 5b) is similar to the one observed over Cook Inlet. In experiment 5b the upper trough west of the mountain and a surface trough in the lee of the mountain are quasi-stationary as in the Alaska case. Cold air flows southward west of the mountain and eventually flows through the gap. Closed contours are seen aloft over the gap and a relatively small-scale low is found in the surface. The short wave trough that is generated in the experiment may even occur in nature, although this has not been observed due to insufficient data density.

A weak baroclinic conversion apparently occurs within the horseshoe and the low travels along the mean low-level isotherms toward the northeast. This low never deepens appreciably and could even remain in a wave-like stage. A similar behavior of weak perturbations over Cook Inlet is sometimes observed. In the experiment, warm air ahead of the low is advected northward as a result of the southerly flow associated with a ridge of high pressure over the mountain to the east. This ridge is also observed in the Alaska case along the North Gulf Coast. Warm air is present over Cook Inlet. The thickness maximum within the horseshoe is also observed in the Alaska case over Cook Inlet. In the experiment, the low within the horseshow fills as it moves northward and cold advection from the southwest becomes increasingly dominant. This also appears to occur in the Alaska case.

It appears justified to accept these results from the latter part of the run in light of the quasi-steady nature of the synoptic pattern. The developing trough to the west never moves eastward completely through the sector. Further, the surface low that did develop north of

the range, and moved through the sector more than once due to the cyclic lateral boundary conditions, showed little interaction with the low south of the range.

Experiment 5c, as in 3c, used the initial conditions as described in Section III without the superposed perturbation. A 3000m mountain was allowed to grow in 12h starting from t_o=0. The mountain is shown in Figure 5d.

A low in the gap was formed with closed isobars by t_o+30h (Figure 49). Closed contours at the 850 mb level were also present but differed from the surrounding heights by less than 100m until t+60h. This indicates the slowness of the growth of the eddy. No low was present in the horseshoe to the north.

The trough over the western mountain continued to grow in intensity especially after t_o+60h (Figure 50). At this time, a steady decrease in central pressure of the low east of the gap is observed (Figure 51). No closed contours were observed at the 700 mb level with 4° north-south resolution. At t_o+72h, the southerly flow east of the low and the westerly flow west of the low (cold advection) were coming in phase with the northeast to southwest isotherm pattern without the horseshoe. This would allow further development. The change of pressure with time (Figure 51) shows the response to this pattern.

It appears that, in this case, the mountain caused a baroclinic conversion process to occur locally (i.e., within the horseshoe) and hindered the larger-scale conversion as noted in the other experiments.

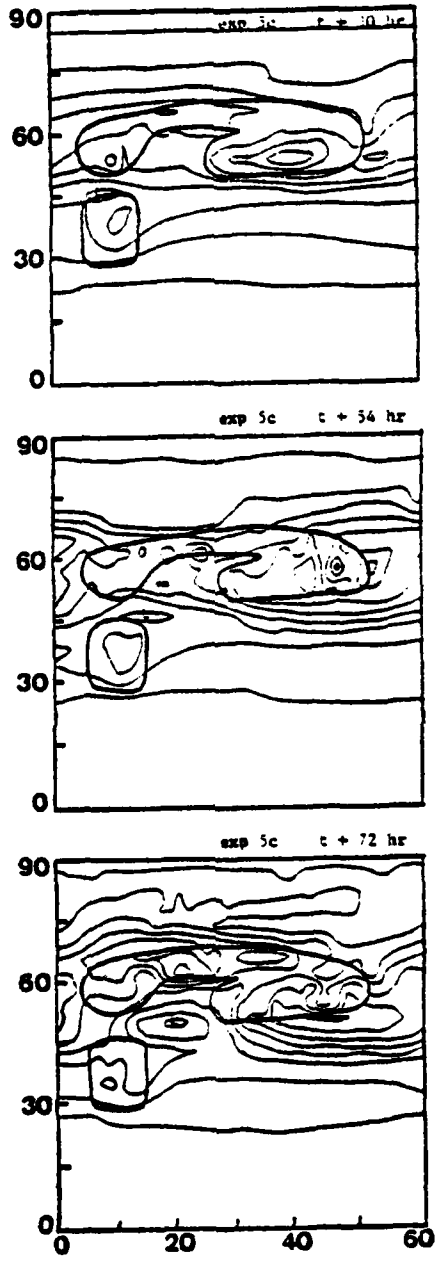

Figure 49. Surface Pressure Field for Experiment 5c at t+30, 54, and 72h

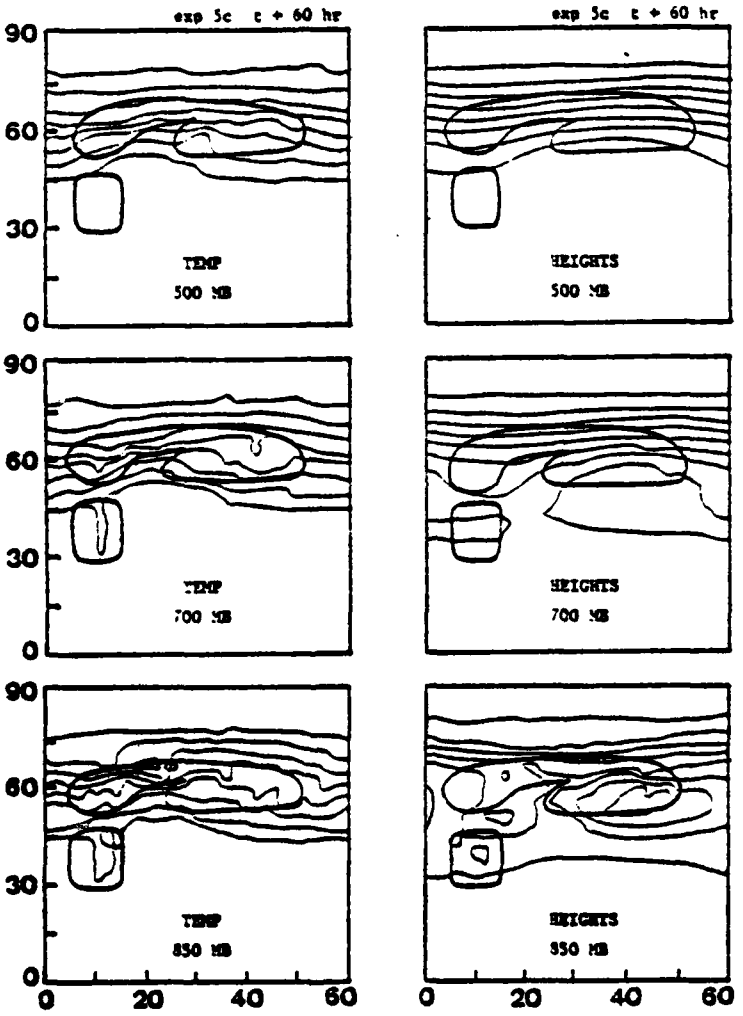

Figure 50. Height and Temperature Fields at t+60 on Pressure Surfaces for Experiment 5c

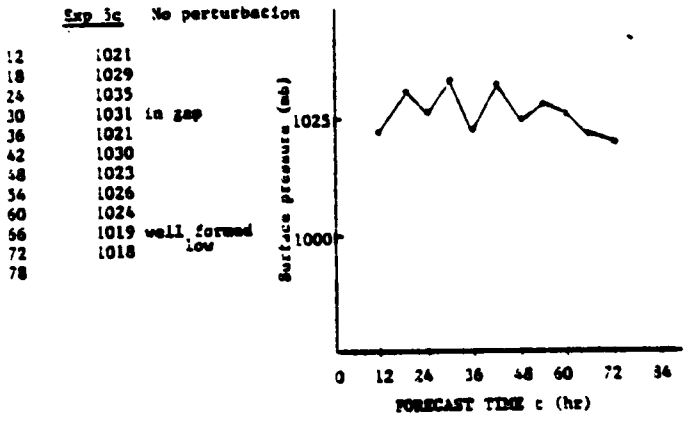

Figure 51. Plot of Surface Pressure (π) Versus Forecast Time for Experiment 5c

The mountain appears to have a significant effect on the type of disturbances (as well as their location and intensity) that can be generated in a large-scale baroclinic flow. Interaction between the mountain and flow having an initial perturbation has resulted in a stronger response than interaction with a basic state with no perturbation. This agrees with results of experiments by Trevison (1976).

F. EXPERIMENT 6

Experiment 6 was conducted with a mountain similar to the one used in experiment 5b, except that the horizontal scale of the mountain was reduced by approximately a third (Figure 5e). There was no experiment 6a (1500m mountain). The height of the mountain remained at 3000m and the width of the new mountain was about 850 nm.

The mountain was placed 4° further north in this experiment compared to the mountain in experiment 5b. This was done in an attempt to block the westerly jet aloft more effectively and to try physically to prevent the amplifying perturbation from moving north of the mountain. Again, the mountain started growing with t_o+96h from the control run for initial conditions.

The disturbance which started out on the west slope at t+12h (the time the mountain was fully grown) deepened rapidly east of the gap at t+24h (Figure 52). Although the temperature gradient increased from t+12h to t+24h west of the mountain (Figure 53), a noticeable increase of the gradient was also evident through the gap and into the northern part of the horseshoe (as in experiments 4 and 5). Westerly flow through the gap (Figure 54) and the low-level thermal pattern, permitted

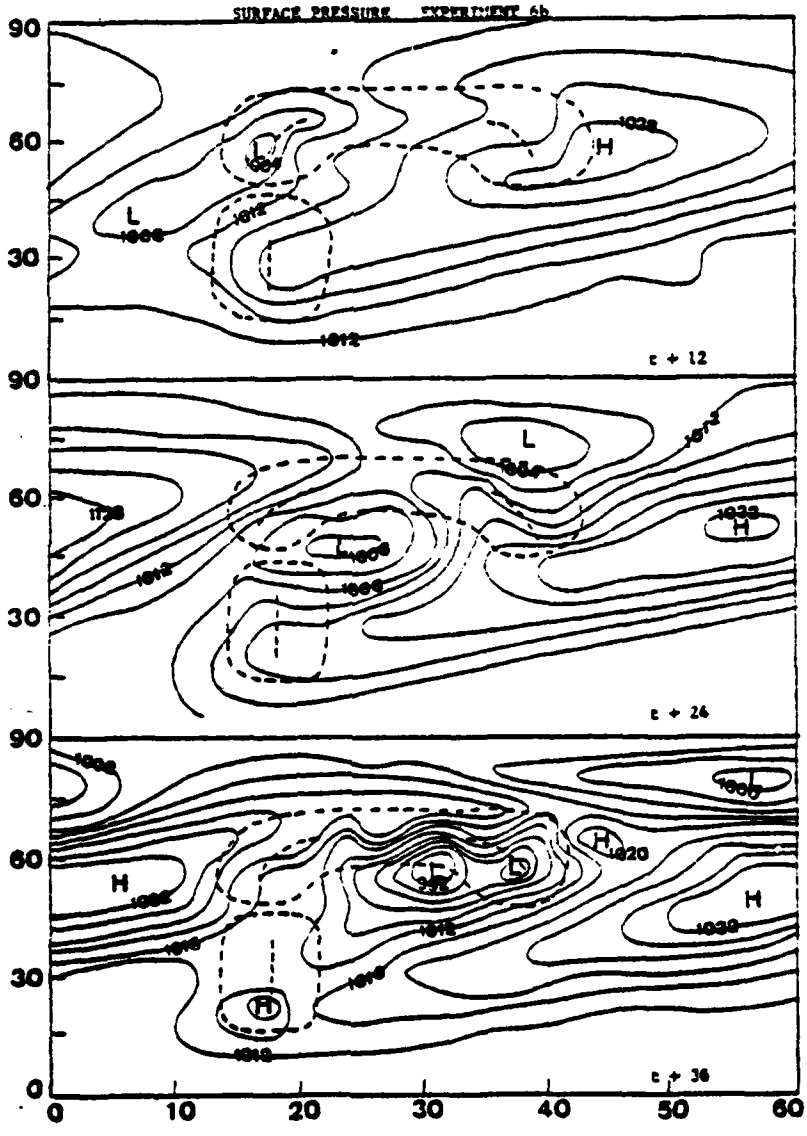

Figure 52. Subjectively Smoothed Surface Pressure Fields From Experiment 6b at t+12, 24, and 36h

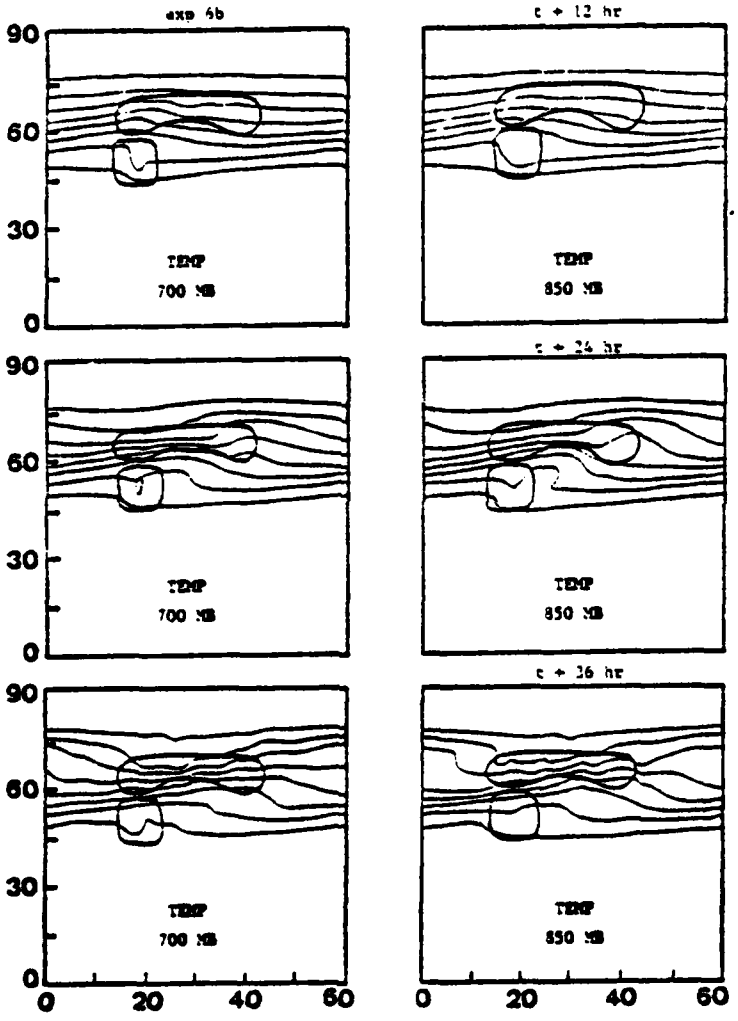

Figure 53. 850 and 700 mb Temperature Fields for Experiment 6b at t+12, 24, and 36h

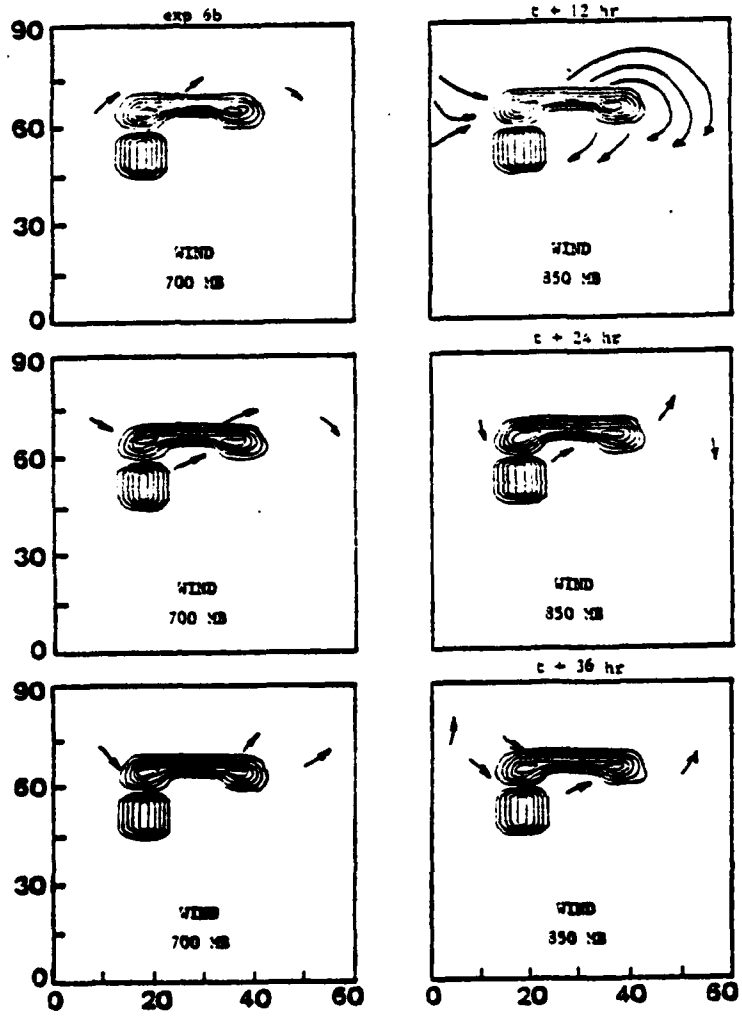

Figure 54. Wind Vectors on Pressure Surfaces for Experiment 6b at t+12, 24, and 36h

only weak cold advection eastward through the gap. At the same time, southerly flow over the eastern part of the horseshoe area suggested warm advection. This apparent weak baroclinic conversion could account for the deepening east of the gap (through the 850 mb level) and the subsequent east-northeast movement of the low across the open area of the horseshoe. In experiment 6b, the low moved from the gap to the west slope of the east mountain range in about 24h (Figure 55). As the low from the gap weakened over the eastern portion of the mountain from t+42h through t+54h, the low north of the mountain deepened (Figure 56) and became the dominant low. Moving the mountain north did not prevent the development of this low. The mountain apparently caused a more localized baroclinic conversion process to occur at the expense of the large-scale conversion. The northern low was only able to develop after the low in the horseshoe weakened. The movement of the features in this experiment was faster than those observed in experiments 4b and 5b. Further, closed contours at the 700 mb level were never observed for either low, which is likely due to the lack of retardation of the upper trough by the mountain.

Evidently a smaller scale of the mountain had less of an effect on retarding the eastward-moving wave than was seen in experiments 4b and 5b. The results of experiment 6b were in better agreement with the results of experiments 2b and 3b (north-south mountain) with regard to the eastward movement of the wave.

Experiment 6c used the initial conditions from Section III without the initial superposed perturbation. The mountain was again rasied to 3000m in 12h starting from t_o=0. The mountain from experiment 6b was

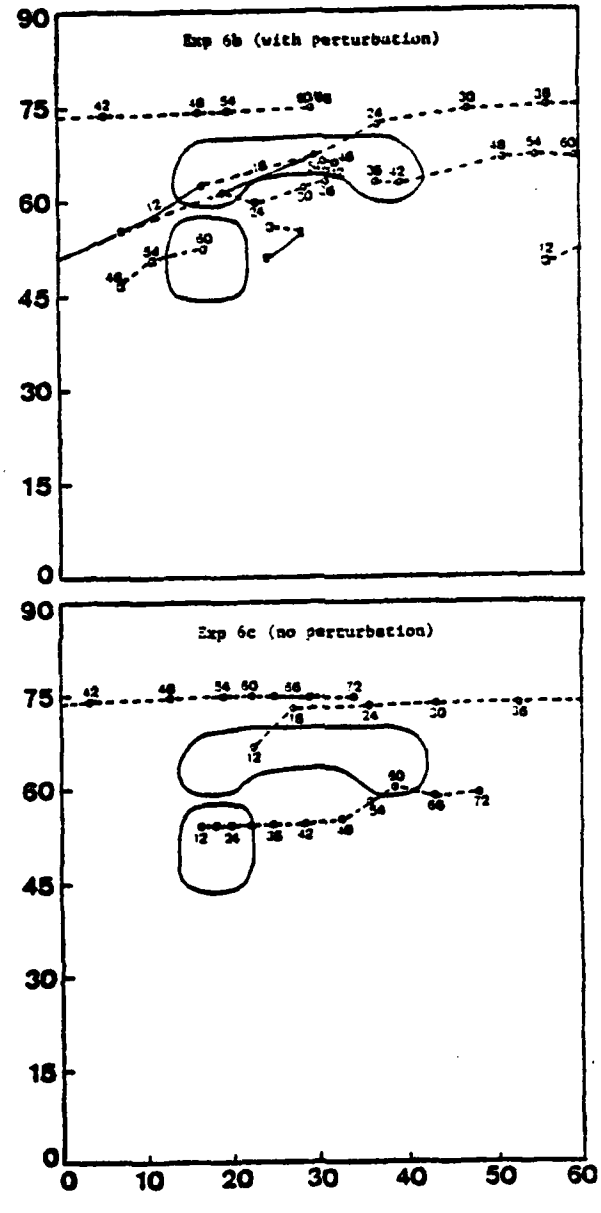

Figure 55. Positions of Surface Low Pressure Centers at 6-h Intervals for Experiment 6b and 6c

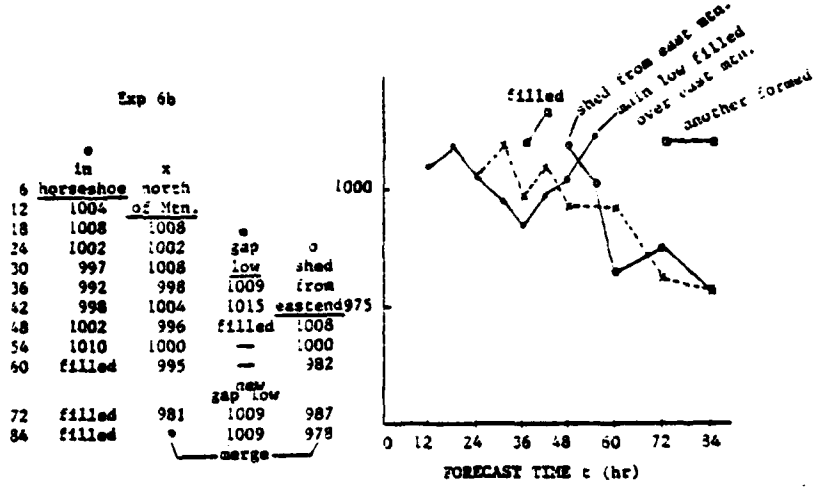

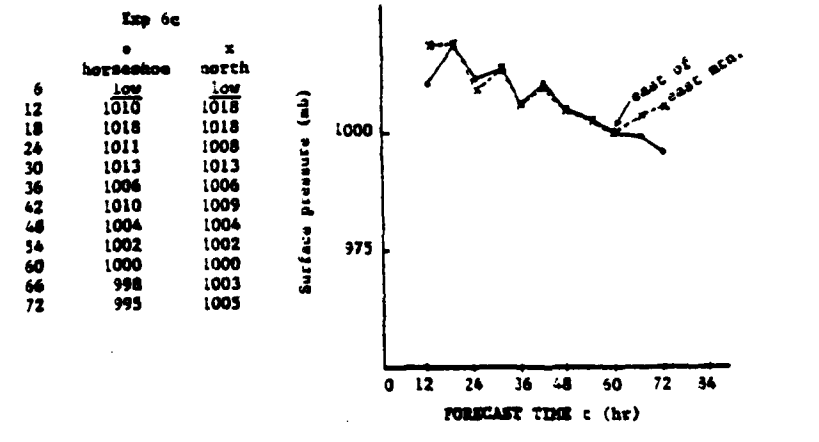

Figure 56. Plot of Surface Pressure (π) Versus Forecast Time for Experiment 6b and 6c

used. Figure 57 shows the surface pressure pattern at t_o+12h and the surface pressure field from experiment 6b at t+12h. The presence of the mountain in experiment 6c forces a pattern very similar to the one for experiment 6b except that 6b shows an amplifying disturbance interacting with a mountain while 6c shown a mountain interacting with a westerly baroclinic mean flow with no perturbation.

The effect of the mountain in the early stage was to deflect the westerly airflow northward (Figure 58). Chung (1977) discusses the mountain's blocking effect on airflow and the orographic divergence inducing ascent on the upslope side and increasing the poleward deflection. The northwest flow on the east boundary, due to cyclic boundary conditions, becomes northwest flow on the west boundary and forms a trough (Figure 58) when it joins the deflected northerly flow west of the mountain. This mountain-forced flow pattern could induce development if the flow is baroclinically unstable.

The presence of the mountain evidently causes a trough to form over the western ridge at the 850 mb level and forms a low in the gap at t_o+24h. There is no obvious reason for the development of this low. A low also formed north of the mountain at t_o+24h (Figure 59), evidently due to the trough aloft that was forced by the northward deflection of the flow at the beginning of the experiment.

From t_o+36h through t_o+60h, the low that formed near the gap and the low north of the mountain deepened slowly at the same rate (Figure 56). From t_o+24h to t_o+36h, the 850 mb and surface troughs continued to deepen. At t_o+36h (Figure 60) northerly flow west of the low and southerly flow east of the low, superposed on the nearly east-west

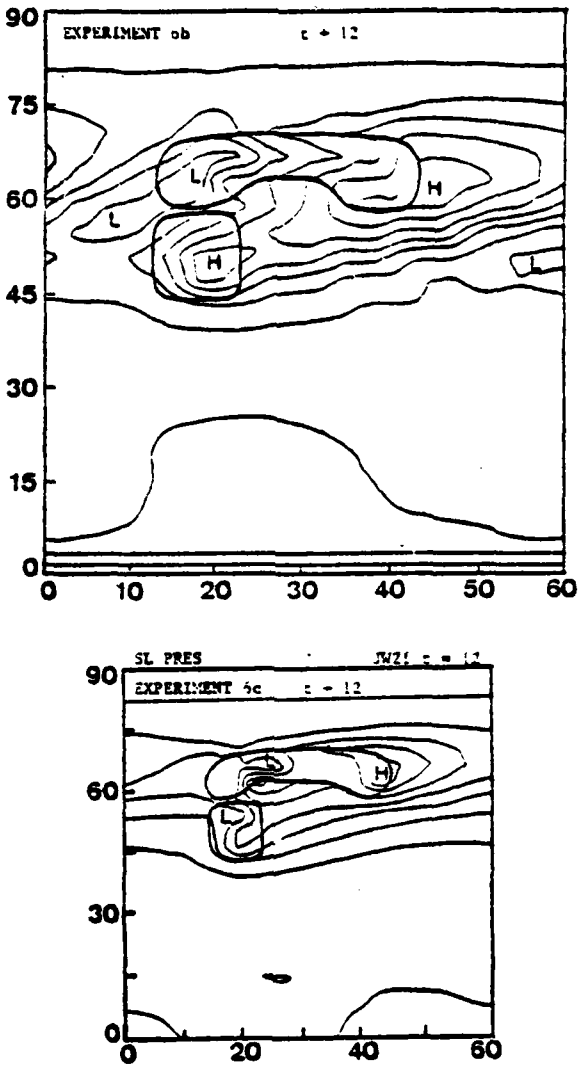

Figure 57. Surface Pressure Fields for Experiments 6b and 6c at t+12h

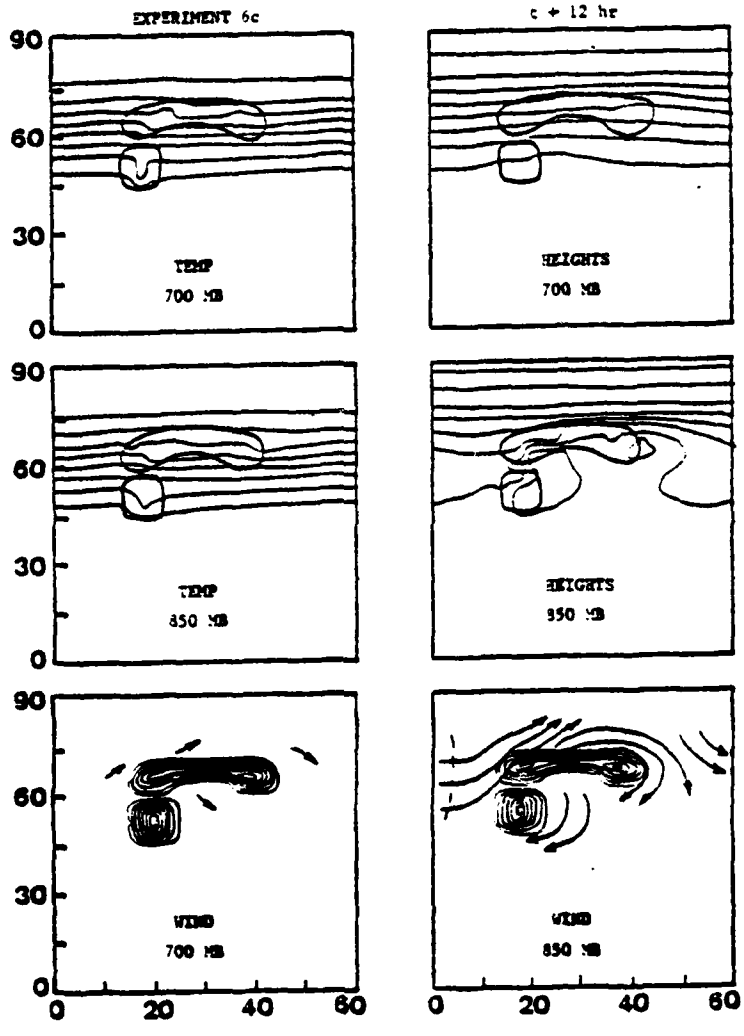

Figure 58. Heights, Temperatures, and Wind Vectors at 850 and 700 mb for Experiment 6c at t+12h

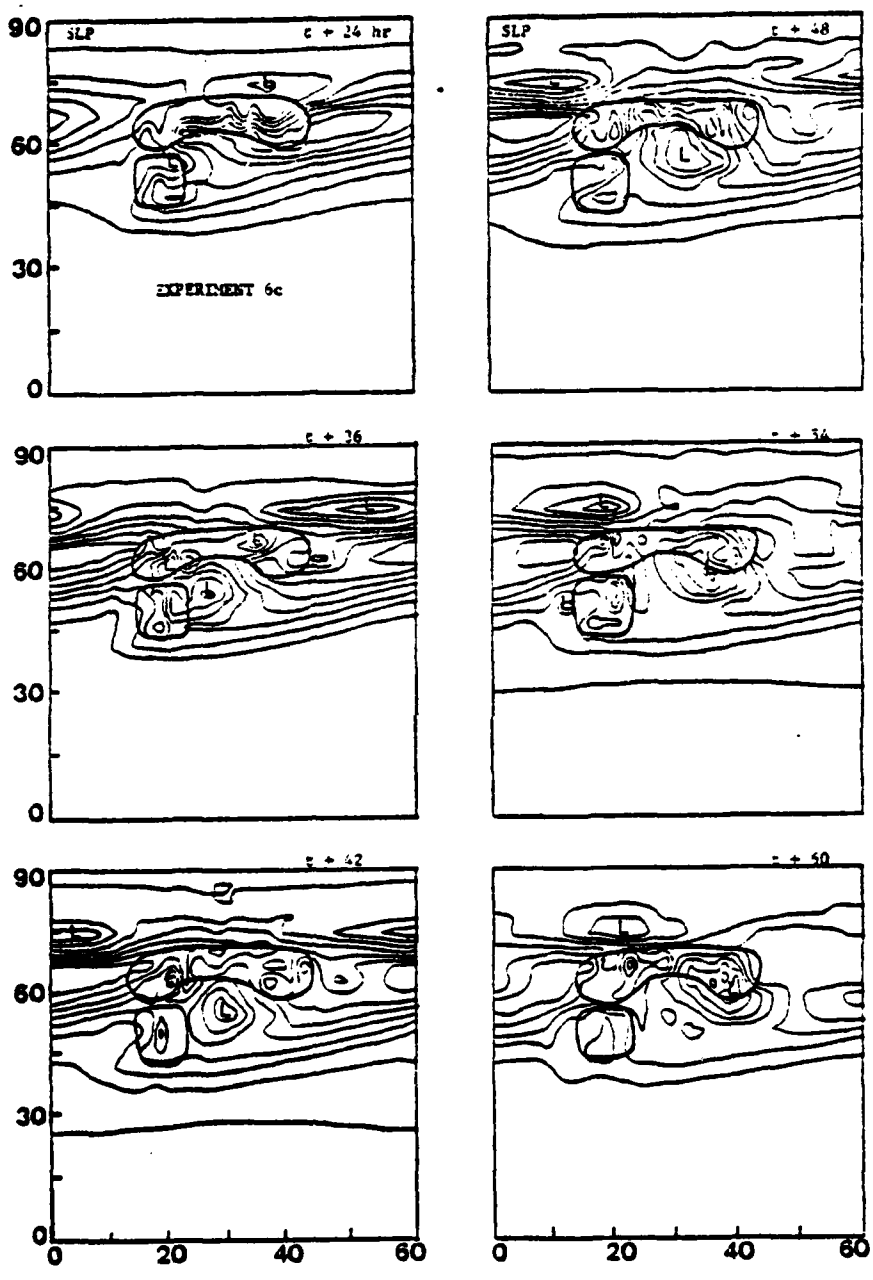

Figure 59. Surface Pressure Fields for Experiment 6c at t+24, 36, 42, 48, 54, and 60h

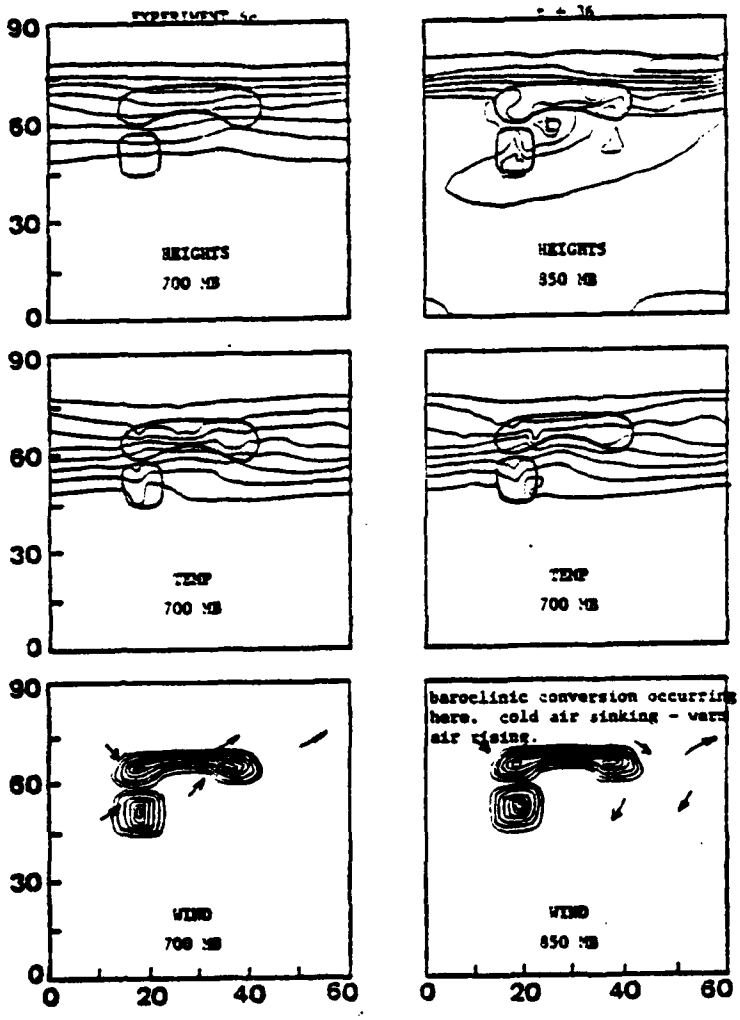

Figure 60. Heights, Temperatures, and Wind Vectors at 850 and 700 mb for Experiment 6c at t+36h

isotherm pattern in the lee, apparently allowed a weak baroclinic conversion to occur. The low never became very intense and no closed contours were observed in the trough at the 700 mb level. This is also true for the low to the north of the mountain. Both lows continued eastward (Figure 55) with the northern low moving at about the same speed as the low in the control run. However, the northern low never reached the intensity of the low in the control run.

It again appears that the type of mountain used in the experiment was responsible for developing a more local disturbance in the lee of the mountain. The circulation around the low appeared to contribute to a local baroclinic conversion.

G. EXPERIMENT 7

Experiment 7 was conducted using a mountain which was somewhat similar to the "horseshoe-shaped" one used in experiment 6, but contained an additional north-south ridge over the central part of the horseshoe (Figure 5f). There again was a gap in the mountain to the west and the mountain was of the order of 1000 nm in width. The height of the horseshoe part of the mountain and the separate mountain forming the gap was kept at 3000m. The central north-south range was only 2000m, as was the plateau to the east. The central range was added to test the mountain's effect on causing an even more local formation and eastward movement of the low that originated near the gap compared to the effect seen in experiments 4, 5, and 6. In the Alaska case, it

appears that cyclogenesis occurs in an area surrounded by a "horseshoe-shaped" mountain. The results of experiments 4, 5, and 6 show a similar phenomenon.

In this experiment, the lower terrain in the center represents the Chugach and Kenai mountains (Figure 2) along the east side of Cook Inlet. The model resolution was too coarse to be able to represent the Cook Inlet area and the surrounding mountains effectively. Therefore, the scale of the mountains was increased in the model in an attempt to better resolve them and any meteorologically significant atmospheric features that might form in the area.

Following the notation in previous experiments, the case using initial conditions from t_0+96h from the control run with a 3000m mountain will be referred to as experiment 7b. The experiment using t_0=0 with no perturbation as initial conditions will be referred to as experiment 7c. There was no experiment 7a with a 1500m mountain.

The results of this experiment revealed features that could apply to cyclogenesis in the lee of the Alaska Range. From t+12h through t+36h, the same disturbance which was amplifying in the control run slowly moved up the windward slope of the mountain and became elongated toward the northeast. By t+30h (Figure 61), the low center rapidly became lost among small low centers, which appear to be due to computational noise because of their $2\Delta x$ scale. The 850 mb trough was well developed and of large amplitude at t+24h (Figure 61). The trough had a substantial northeast to southwest tilt which became more north-south through t+54h. Figure 64 shows that the northern portion of this trough remained bound to the western mountain. A portion of the large amplitude trough breaks

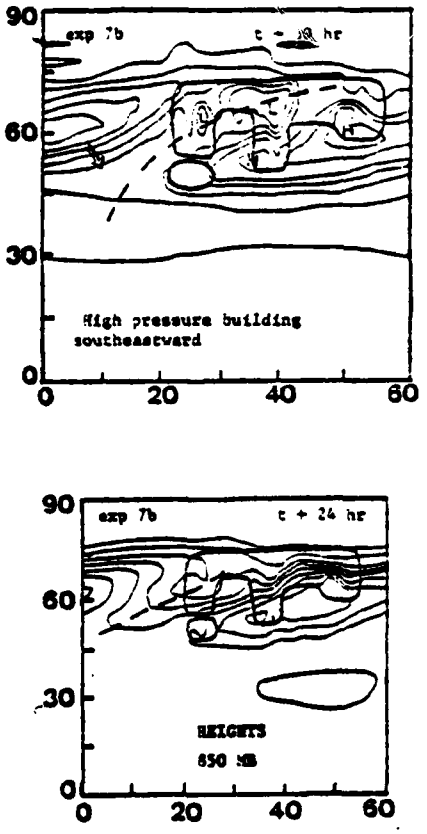

Figure 61. Surface Pressure Field at t+30h and 850 mb Heights at t+24h for Experiment 7b

off north of the mountain and can be seen after it re-entered the west boundary at t+48h (Figure 64).

By t+36h, strong cold advection and frontogenesis is observed west of the mountain (Figure 63), which also occurred in the control run. However, in experiment 7b the flow at 850 mb is more northerly than northwesterly, which is similar to the situation in the Alaska case. In experiment 7b, the troughs at 700 mb and 500 mb appeared to be catching up to the 850 mb trough, and therefore became more vertical. The 850 mb low appears quasi-stationary over the mountain in the northern part of the trough. This also occurs in Alaska lee cyclogenesis, but is not as intense and is apparently due to other reasons. In the Alaska case, the 850 mb low bound to the Alaska Range to the west is possible due to warm advection over the mountains from the east, and its location beneath the upper level divergence associated with the trough to the west. Tibaldi, et al. (1980) point out that upper divergence in the lee of the Alps and retardation of the advection of cold air in low levels are responsible for the depression at the surface.

As the 850 mb trough pivoted southeastward and became more north-south with time, the low over the mountain increased in intensity, the frontal surface on the windward side steepened, southerly winds causing warm advection over the area representing Cook Inlet noticeably increased, and the backward tilt with height of the trough on the windward side decreased. The steepening of the trough's tilt suggests blocking by the terrain in low levels. The reasons for the intensification of the low over the mountain and its apparent tendency to be bound to the

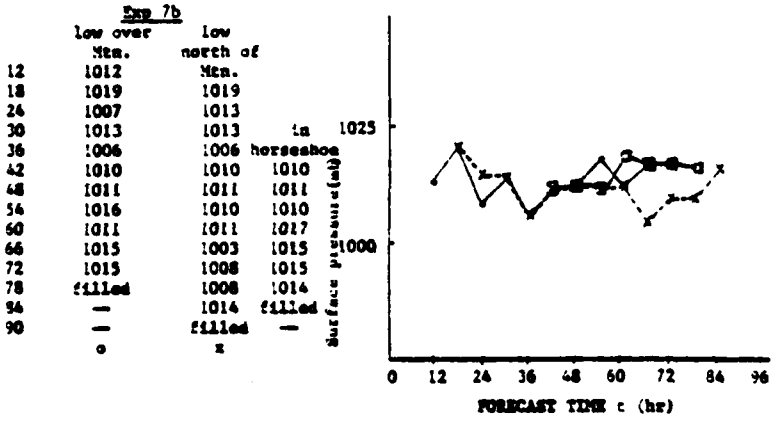

Figure 62. Plot of Surface Pressure (π) Versus Forecast Time for Experiment 7b

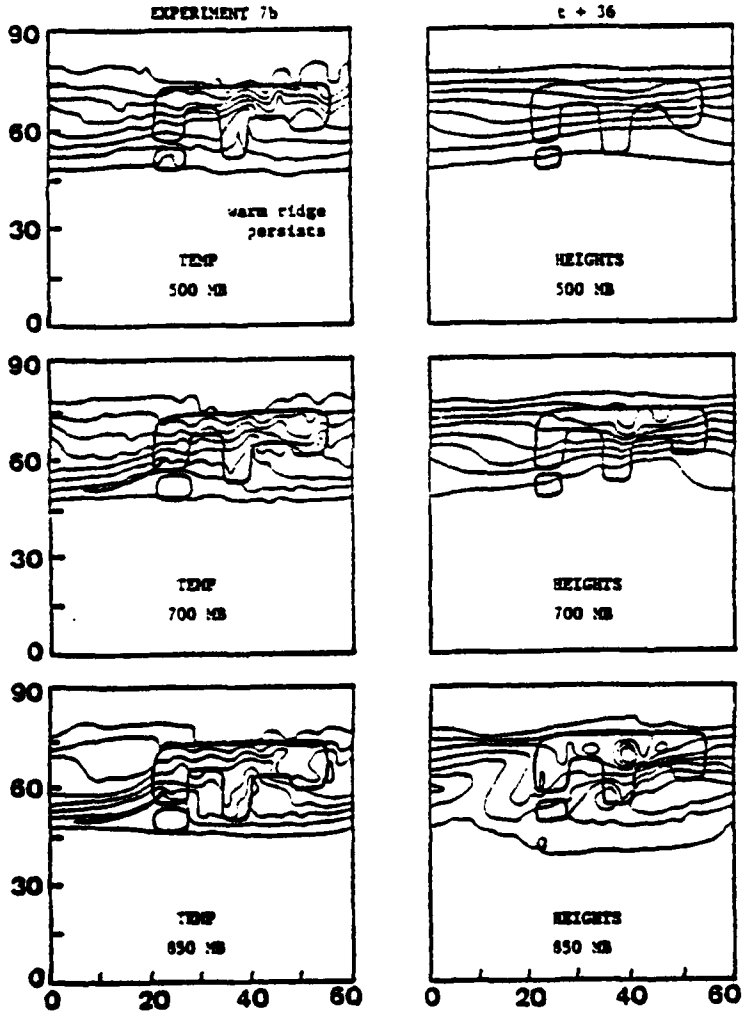

Figure 63. Height and Temperature Fields at t+36h on Pressure Surfaces for Experiment 7b

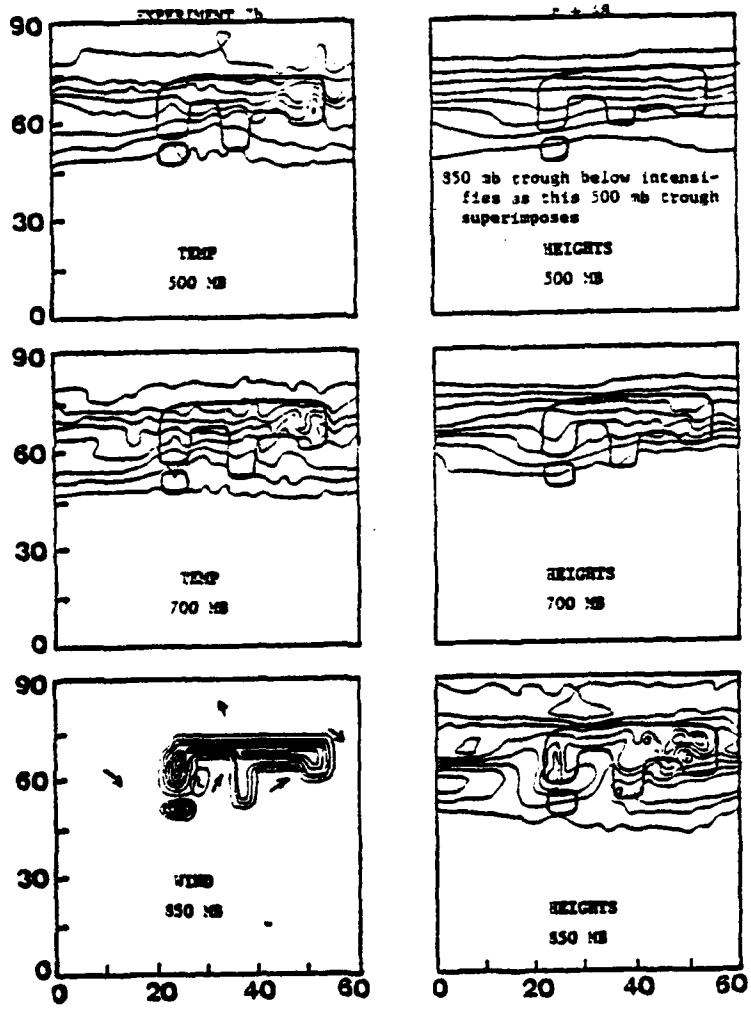

Figure 64. Heights and Temperatures at 700 and 500 mb, Heights at 850 mb, and Wind Vectors at 850 mb for Experiment 7b at t+48h

mountain were not determined. It should be noted that winds aloft were not strong or nearly perpendicular to the mountain except at 500 mb. The upper trough at 700 mb and at 500 mb remained superposed.

At t+42h, the surface front was approaching the western end of the gap (Figure 65). At the same time, the lows over the mountain at the surface and at the 850 mb level were vertical and were more intense, which caused more westerly flow through the gap, as shown by the 850 mb winds (Figure 64). The stronger westerly flow advected cold air through the gap which, when coupled with the warm advection over the east side of the area that represents Cook Inlet, appeared to cause a baroclinic conversion of avilable potential energy to kinetic energy in the lee. This lee low gained strength through t+66h at which time the low over the mountain filled (Figure 67).

Figure 62 shows the change of surface pressure with time of the perturbation. Because of the large amount of computational noise, it was difficult to estimate the actual pressure minimum in the low. The pressure drop as the low crosses the mountain can be seen. This occurred in previous experiments. However, the pressure begins to rise in the lee and has periods when the pressure changes little. In the control run and the experiments with the north-south mountains, the low continued to deepen with time as it moved eastward. This suggests that both the eastward progression and deepening of the low in experiment 7b were retarded by this particular horseshoe-shaped mountain. The surface low remained in a position representing Cook Inlet and the pressure trace shows no consistent deepening or filling. Large 6-hourly pressure

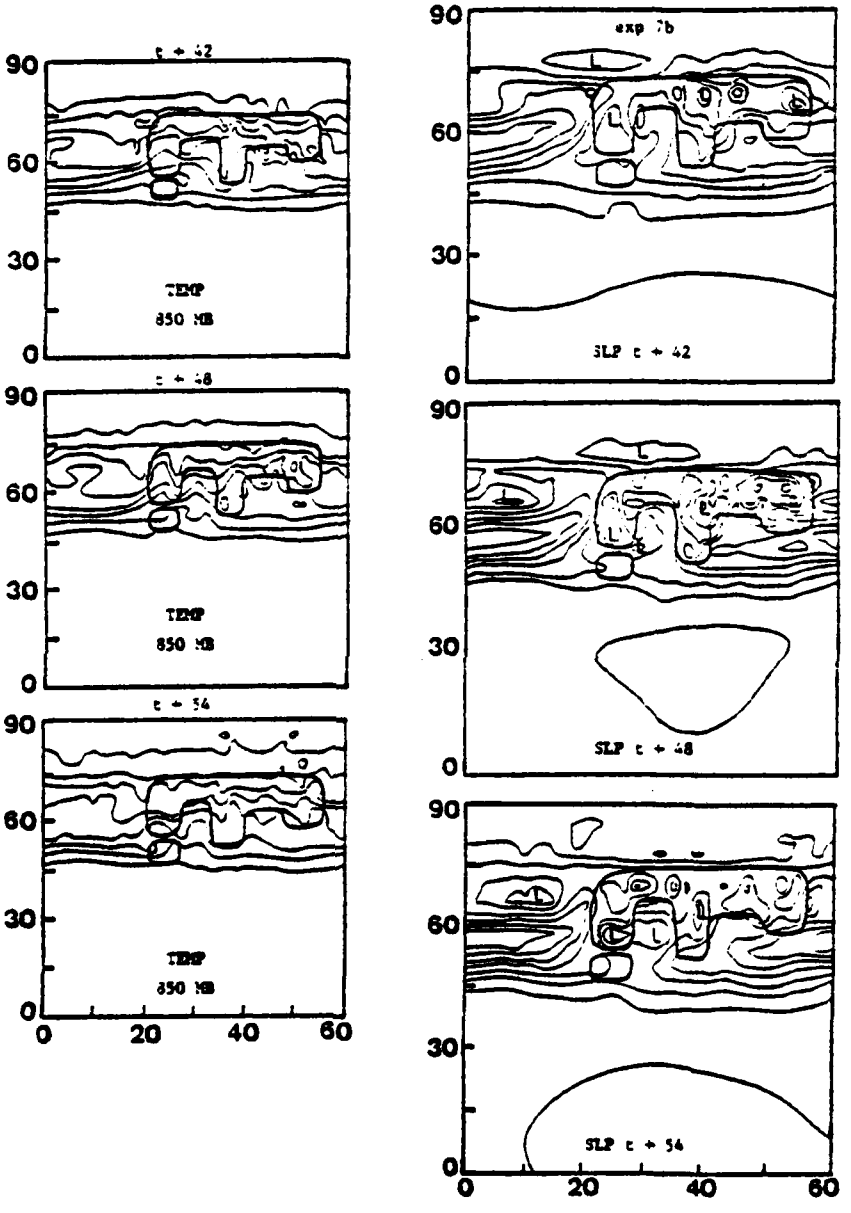

Figure 65. Surface Pressure and 850 mb Temperature Fields for Experiment 7b at t+42, 48, and 54

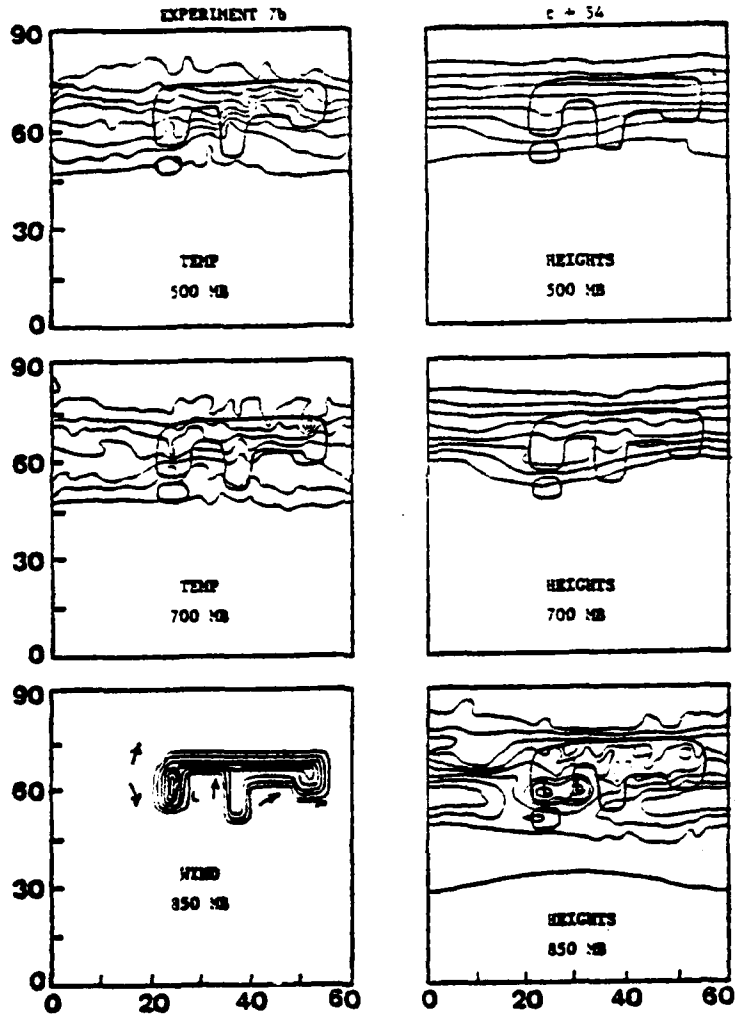

Figure 66. Height and Temperature Fields at t+54h on Pressure Surfaces for Experiment 7b

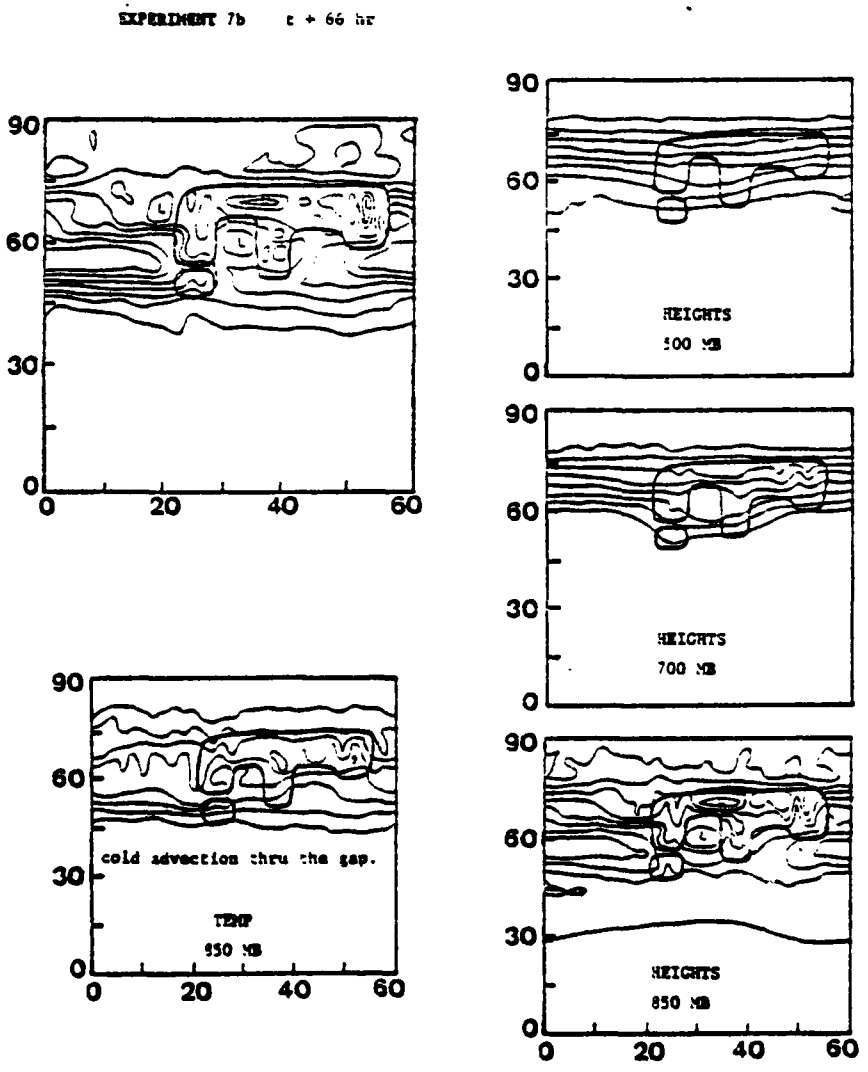

Figure 67. Heights at 850, 700, 500 mb; 850 mb Temperature Field; and Surface Pressure for Experiment 7b at t+66h

fluctuations suggest the possibility of internal gravity waves. However, as discussed in previous experiments, this was probably due to lack of resolution. In the Alaska case, it appears that a weak low-level circulation is present over Cook Inlet during lee cyclogenesis but a significant pressure fall is not noted at Anchorage. The results of this experiment are consistent with this observation.

The low over the area representing Cook Inlet developed at t+48h (Figure 65) and weakened over the eastern mountain at t+76h. This is a 28h transition time. Throughout this time, much noise was evident along the northern range. Also, a developing disturbance, formed by the sheared-off trough along the northern ridge, was able to enter the west boundary again at t+30h (Figure 61). A secondary development appeared farther south (Figure 65). However, their effects did not appear to contribute to the overall development, except to possible enhance the low-level advection over the windward side of the mountain.

The following sequence of upper-level features was observed during the time of cyclogenesis. At t+48h (Figure 64), the low over the mountain intensified, and increased the westerly flow and possible the cold advection through the gap. At this time, the 700 mb trough had just become superposed over the 850 mb closed low, and the upper-level difluence ahead of the 500 mb trough was superposed. By t+54h, there was a low over the area representing Cook Inlet (the deepest low) and a low over the mountain associated with the superposed trough aloft (Figure 65). Upper-level divergence was evident over the area (Figure 66). After t+60h, the vertically stacked low and trough system over the mountain moved eastward (Figure 67) as cold air evidently pushed through

the gap and the only low remaining was the one over the inlet, which is now vertical with closed contours through the 500 mb level. The low then continues eastward and weakens as the upper trough continues eastward, apparently unimpeded by the 2000m terrain below. The low fills as it moves up the windward side of the central north-south range, since the warm advection ahead of the low diminishes and the cold advection from the west dominates. In the Alaska lee cyclogenesis case, the low appears to move northeastward along the thickness lines. This does not occur in experiment 7b since the thermal pattern is not as intense nor of sufficient amplitude to attain the same trajectory of the low. However, the low did apparently follow the mean low-level thickness pattern.

Experiment 7c began with initial conditions from t_0=0 of the control run with no superposed perturbation. The mountain was raised to its maximum height of 3000m in 12h.

The results showed a similar development to that in experiment 7b, only weaker. There was very little development through t_0+36h. At t_0+36h (Figure 68), closed contours at the 850 mb level were observed over the western ridge. However, this low was not as intense as in experiment 7b. The trough at the 700 mb level was also weaker than in experiment 7b. A weak front had formed and extended westward from the windward slope. This front was much weaker than in experiment 7b. The cold front at t_0+36h was moving southward in response to the northerly winds ahead of the high to the west. It should be noted that by t_0+36h, the temperature of the air over the area representing Cook Inlet was

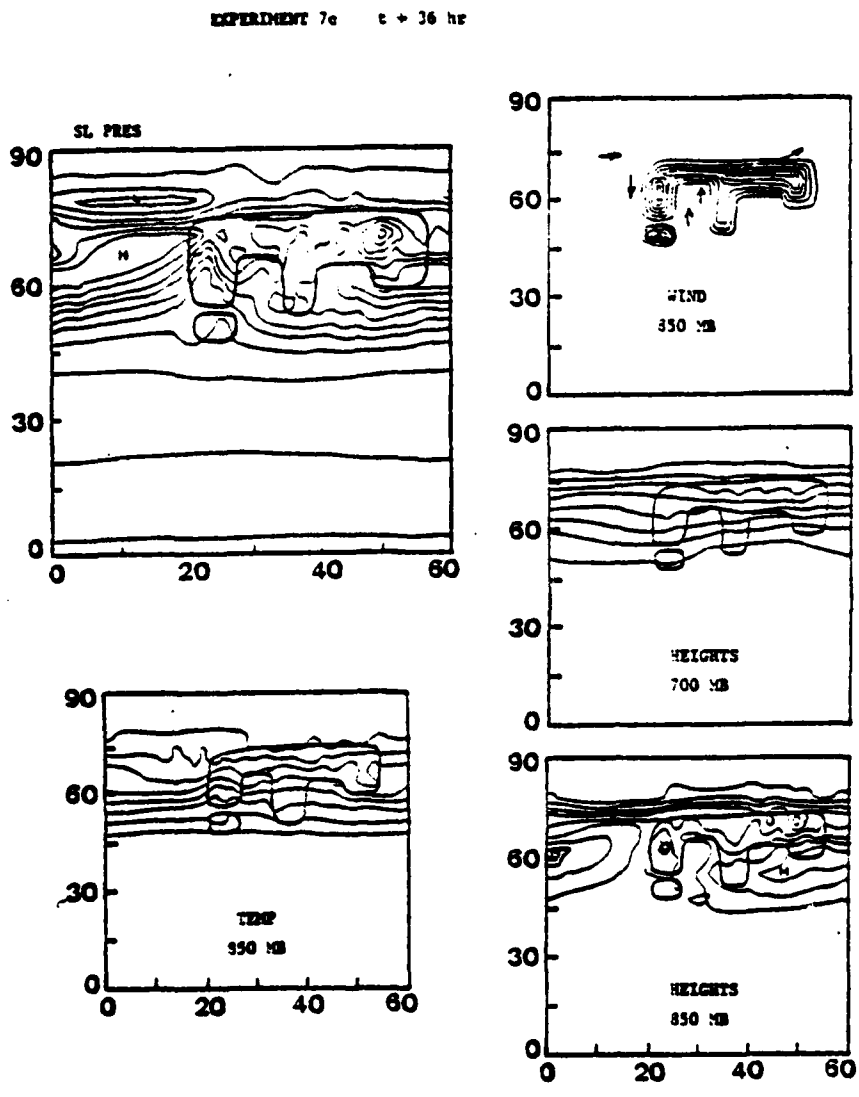

Figure 68. 850 and 700 mb Heights; 850 mb Temperature and Wind Vectors; and Surface Pressure at t+36h for Experiment 7b

much warmer in experiment 7b that in 7c, and the front to the west was stronger in 7b.

By t_o+48h, a weak cyclonic circulation can be seen in the wind field in the lee of the mountain at the 850 mb level (Figure 69). The front west of the mountain pushed southward west of the gap, in response to stronger northerly winds west of hte 850 mb low over the western ridge. No clear development can be seen in the surface pressure field. A pressure versus time plot could not be constructed, because there were no closed contours in the surface pressure pattern in the lee of the west ridge. A weak "inverted" trough moved eastward with the upper-level trough, but no "central" pressure could be distinguished. This week inverted trough is also evident in Alaska lee cyclogenesis cases.

From t_o+42h through t_o+54h, the 850 mb low becomes more organized (although weak) and flow through the gap can be seen at t_o+54h (Figure 70). The differential advection associated with the low-level wind field suggested a weak baroclinic conversion process. There was also divergence alfot associated with the upper trough moving slowly eastward over the area. The northerly wind to the west of the gap became stronger and the air flowed southward rather than through the gap at t_o+60h (Figure 71). The low in the lee then began to fill.

The vertical tilt of the system appeared negligible after t_o+42h. A slight increase in amplitude was noted through t_o+72h as the weak cyclone that formed, with maximum amplitude at the 850 mb level as in the Alaska case, moved eastward along a path similar to that in experiment 7b. The negligible intensity of the low over the mountain through

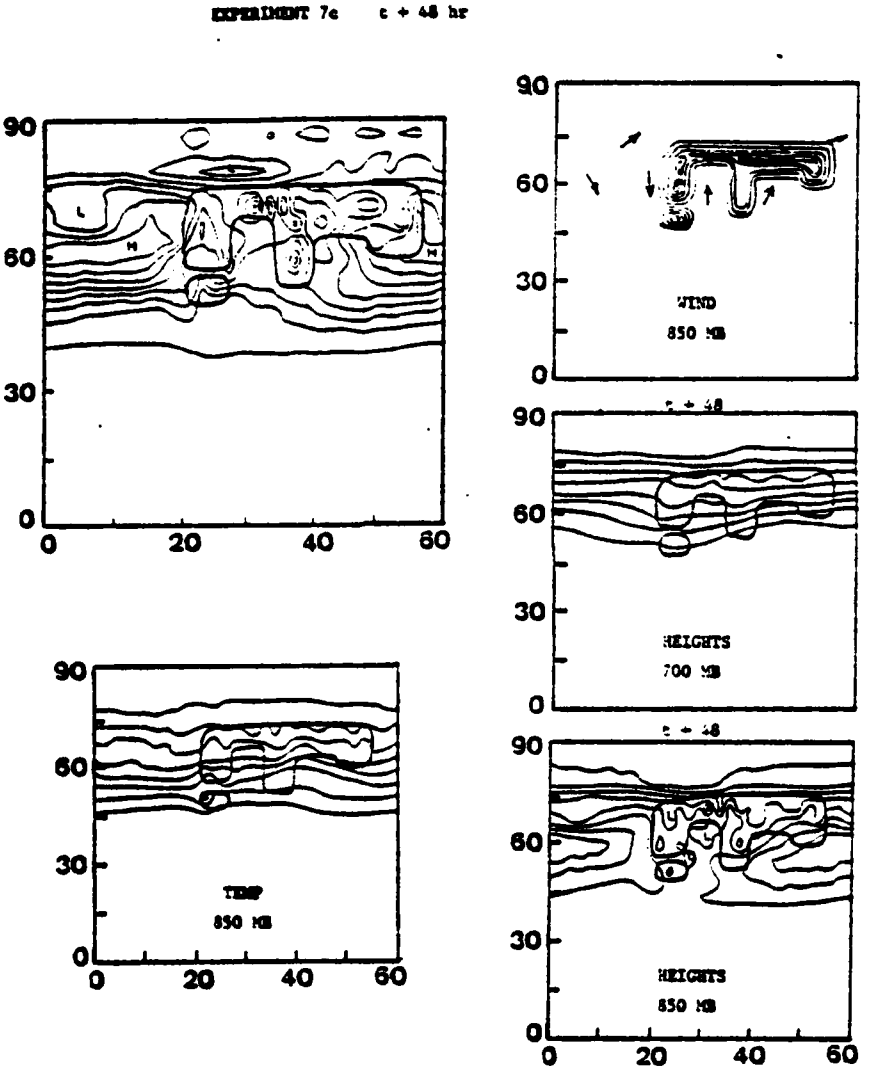

Figure 69. 850 and 700 mb Heights; 850 mb Temperature and Wind Vectors; and Surface Pressure at t+48h for Experiment 7b

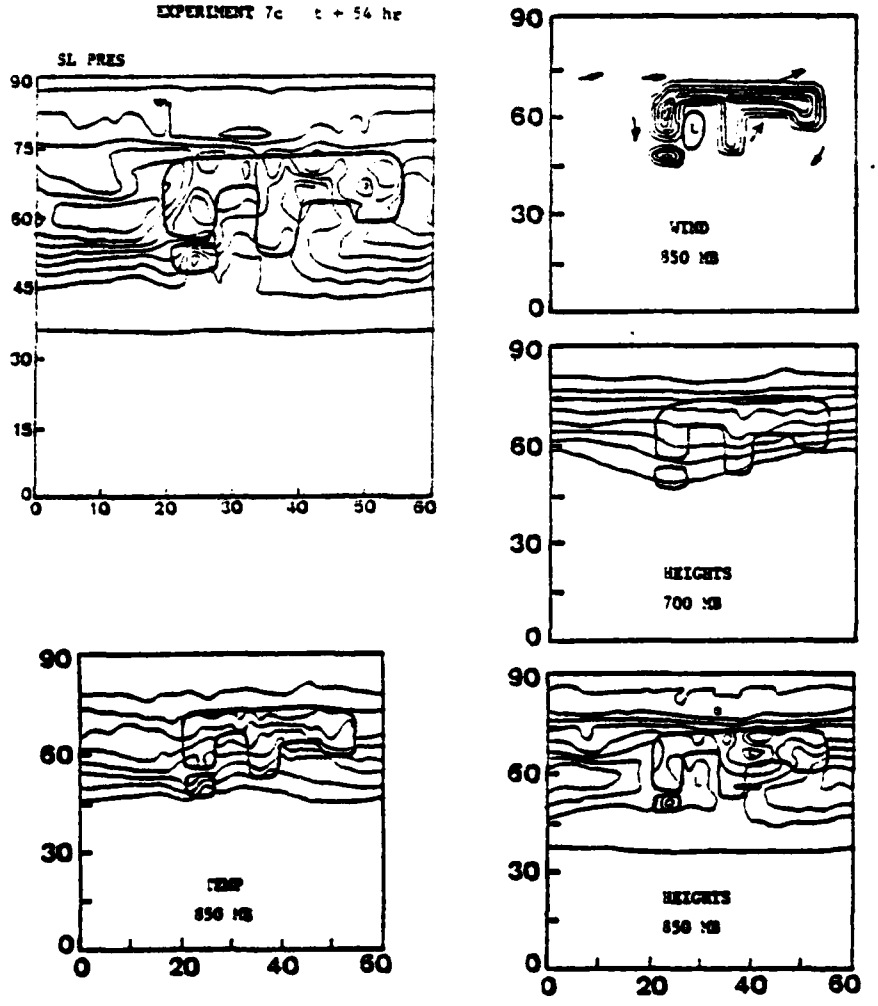

Figure 70. 850 and 700 mb Heights; 850 mb Temperature and Wind Vectors; and Surface Pressure at t+54h for Experiment 7b

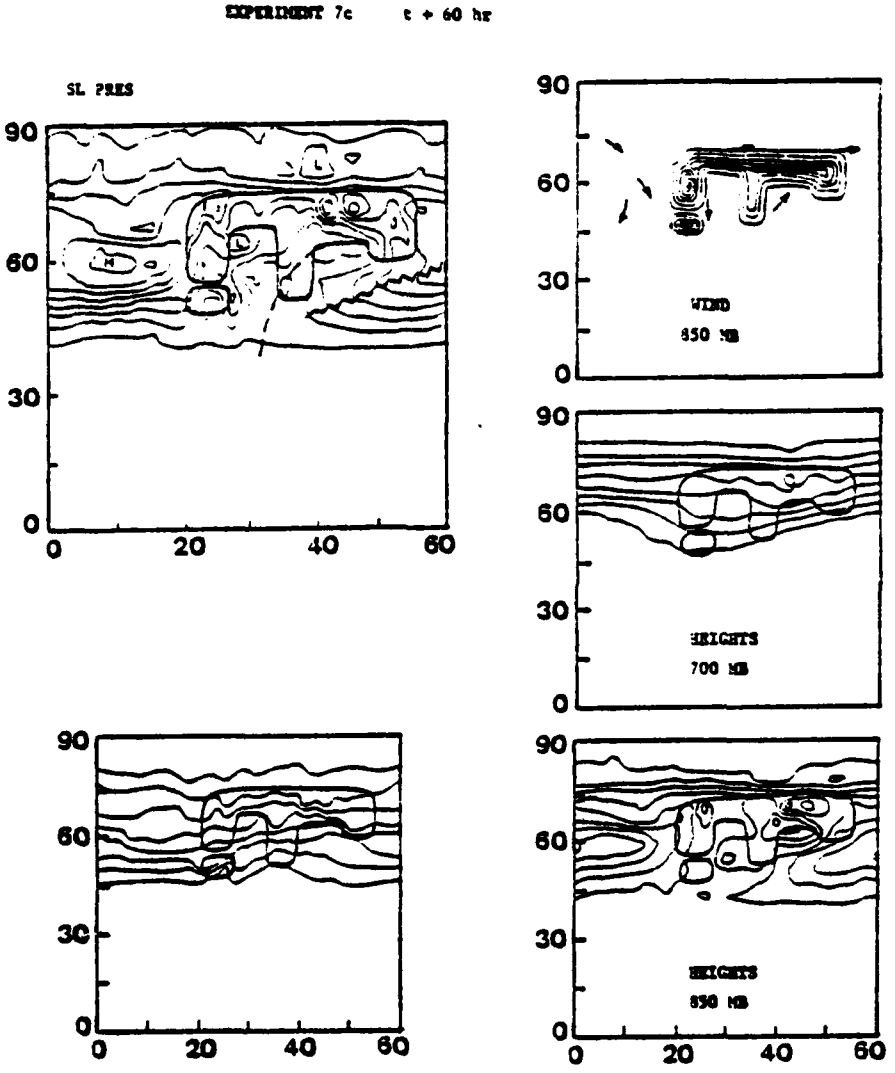

Figure 71. 850 and 700 mb Heights; 850 mb Temperature and Wind Vectors; and Surface Pressure at t+60h for Experiment 7b

t_o+48h appeared to be the reason for the lack of development (i.e. no strong differential advection for a stronger baroclinic conversion process). No closed contours occurred above the 840 mb level.

As in previous experiments, a weak, local baroclinic conversion process appears to occur, at least at the 850 mb level, in the lee of the mountain. However, a low in the surface pressure field is not apparent as in the results of experiment 7b. Further, the development that did occur was evidently forced by the mountain since there was no initial perturbation. Due to the short time scale of the development, strong mountain forcing is suggested as the primary mechanism.

VII. CONCLUSIONS

The influence of several different mountains on a westerly, baroclinic flow, and on an amplifying disturbance within that flow, were investigated. The motivation was to isolate mechanisms that might be involved in an apparently topographically-induced cyclogenesis in the lee of the Alaska Range. It was found that the model appeared to simulate various mechanisms that are present in observed cases of cyclogenesis in the lee of the Rockies, Alps, and Greenland.

Experiments using mountains of finite north-suth extent (experiments 1 through 3) caused an initially amplifying disturbance to develop a cyclone in the lee that deepened at a rate faster than in the cases with no mountains. However, the overall deepening and intensity of the cycline was greater if the cyclone was allowed to evolve naturally with the mountains removed. A mountain with a maximum height of 3000m reduced the eastward movement of the disturbance more than a 1500m mountain. These mountains also produced lee development, although slower and weaker, when they interacted with the mean flow without an initial amplifying disturbance. This suggests that the presence of the north-south mountain strongly contributed to the baroclinic energy conversion. In general, the presence of the mountains appeared to cause a local energy conversion process that was "tuned" to the specific mountain complex and reduced the efficiency of the baroclinic conversion over the whole domain. This is in close agreement with the findings of Tibaldi, et al. (1980) for the Alps.

Experiments with the "horseshoe-shaped" mountains also appeared to cause a local development of a low in the lee of the western ridge at the expense of the development over the whole domain. The 3000m mountain was seen to be more effective in maintaining the lee development locally compared to the 1500m mountain. The results suggested that a disturbance moving over, or forming in the lee of, this type of mountain, would be "trapped" within the horseshoe, and then move slowly eastward. Otherwise, the low would develop normally, during an unimpeded eastward movement, as in the control run. Similar results were obtained when the mountain was made to interact with the mean flow without the initial disturbance. The mountain, therefore, played a significant role in determining the location where the development took place and on the subsequent movement of the disturbance.

It is interesting to note that this "horseshoe-shaped" mountain closely resembles the orography surrounding the northern Gulf of Alaska. The results suggest that the shape and height of the mountain complex are responsible for the "trapping" of strong mature lows that develop over Alaska, and possible those that move northward over the Gulf of Alaska. These lows are often observed to be quasi-stationary or drifting slowly eastward along the north Gulf coast. Present operational numerical weather prediction models include a rather poor approximation of this mountain range and do not always predict this trapping effect.

The results of experiment 5, with a narrower area within the horseshoe, and with a gap to the west, showed a development (baroclinic conversion) similar to the one in experiment 4 (larger area within the horseshow and no gap to the west). The experiment using 2° north-south

resolution, rather than 4° as in the other experiments, resulted in: 1) stronger and more obvious flow through the gap; 2) closed contours at the 500 mb level; and 3) a short-wave trough that rotated north over the area representing Cook Inlet. This suggests that, to simulate features on these scales, it is desirable to increase the resolution in the model. However, since the model was configured with no friction, diffusion, or smoothing, the growth of small-scale ($2\Delta x$) waves would increase. The figures presented in this paper show that some method of minimizing the growth of these waves is desirable.

The sequence of events that occurred in experiment 5 resembled features that are present during the apparent cyclogenesis in the lee of the Alaska Range. Briefly, these are: 1) a quasi-stationary synoptic pattern; 2) warm advection due to southerly flow east of the area in the lee; 3) a strong trough at 850 mb over the western ridge; 4) cold advection eastward through the gap resulting in a negative Laplacian of thickness in the low-levels east of the gap; 5) difluence (or divergence) aloft moving eastward over the area; and 6) an apparent low-level baroclinic conversion (weak and small-scale). The low than moved along the mean low-level isotherms. The depression within the horseshoe filled as cold air advection over the area became dominant and the trough aloft moved eastward. Therefore, it appears that the configuration of the mountain complex itself has a significant effect on the resulting disturbance, especially in light of the role that the gap played in the baroclinic conversion process.

The smaller-scale "horseshoe-shaped" mountain used in experiment 6 had less of an effect on retarding the eastward moving amplifying disturbance compared to the larger complex of experiment 5. However, the horseshoe-shape and the presence of the gap caused a local development within the horseshoe area. An apparent baroclinic conversion occurred in the lee, and was accompanied by flow through the gap beneath the upper trough. The higher mountain altered the development seen in the control run in a manner similar to experiment 5.

Therefore, the results suggest that, on various scales, the evolution of the local disturbance and the effect on the baroclinic conversion over the whole domain is similar but of shorter duration for smaller mountains. Further, it appears that the horseshoe-shape, the presence of the gap, and mountain elevations above a critical height all contribute to a local development in the lee. It also appears that the presence of an amplifying disturbance in the initial stages only serves to enhance the development, since a weak but similar development occurs in experiments using only the mean flow.

The results of the last experiment (experiment 7) with the mountain most similar to the one in Alaska, showed the evolution of a disturbance in the lee in a manner similar to the sequence seen in experiments 5 and 6. However, in this experiment, the lee cycline remained weak at the surface and was more apparent at the 850 mb level.

The overall results of these mountain experiments suggest that a weak form of development in the lee of the Alaska Range is indeed possible. Further, the resulting surface development would likely remain weak and be more clearly identified in the 850 mb height and temperature

fields. The low would undergo a weak baroclinic conversion forced by a cold air injection from the gap and the passage of a trough with southerly flow ahead (to produce warm advection) and divergence aloft. The warm air advection over Cook Inlet prior to lee cyclogenesis is evidently produced by southerly flow along the west side of the ridge of high pressure situated along the north Gulf coast. The mountains to the west slow the progress of the upper trough, block cold advection into Cook Inlet, and thereby allow the initial depression to remain there. The horseshoe configuration then impedes the eastward movement of the depression, allows the weak local baroclinic conversion as the upper divergence becomes superposed, and causes the depression to follow the low-level isotherm pattern (thickness) arranged according to the shape of the surrounding topography. The slight negative Laplacian of thickness within the horseshoe area contributes to the maintenance of low-level cyclonic vorticity during the process.

As was mentioned above, the mountains apparently cause a local baroclinic conversion, in the baroclinic flow, regardless of the presence of an initial amplifying disturbance. This is important since it suggests that a migrating jet, encountering mountain complexes with characteristics similar to the mountains used in these experiments, can result in a local baroclinic conversion of some of its available potential energy. Further, if the mountain is too smoothed in numerical weather prediction models, developments in the wrong location and with incorrect intensities can result.

APPENDIX A

MODEL PRIMITIVE EQUATIONS

MOMENTUM

$$\frac{\partial}{\partial t}\left(\frac{\pi}{mn}u\right)+\frac{\partial}{\partial \xi}\left(\frac{\pi u}{n}u\right)+\frac{\partial}{\partial \eta}\left(\frac{\pi v}{m}u\right)+\frac{\partial}{\partial \sigma}\left(\frac{\pi\dot{\sigma}}{mn}u\right)-\left[\frac{f}{mn}+\left(v\frac{\partial}{\partial \xi}\frac{1}{n}-u\frac{\partial}{\partial \eta}\frac{1}{m}\right)\right]$$

$$+\frac{\pi}{n}\left[\frac{\partial \Phi}{\partial \xi}+\sigma\alpha\frac{\partial \pi}{\partial \xi}\right]=0,$$

$$\frac{\partial}{\partial t}\left(\frac{\pi}{mn}v\right)+\frac{\partial}{\partial \xi}\left(\frac{\pi u}{n}v\right)+\frac{\partial}{\partial \eta}\left(\frac{\pi v}{m}v\right)+\frac{\partial}{\partial \sigma}\left(\frac{\pi\dot{\sigma}}{mn}v\right)+\left[\frac{f}{mn}+\left(v\frac{\partial}{\partial \xi}\frac{1}{n}-u\frac{\partial}{\partial \eta}\frac{1}{m}\right)\right]$$

$$+\frac{\pi}{m}\left[\frac{\partial \Phi}{\partial \eta}+\sigma\alpha\frac{\partial \pi}{\partial \eta}\right]=0,$$

FIRST LAW OF THERMODYNAMICS

$$\frac{\partial}{\partial t}\left(\frac{\pi}{mn}Cp\ T\right)+\frac{\partial}{\partial \xi}\left(\frac{\pi u}{n}Cp\ T\right)+\frac{\partial}{\partial \eta}\left(\frac{\pi v}{m}Cp\ T\right)+\left(\frac{p}{p_o}\right)^{K}\frac{\partial}{\partial \sigma}\left(\frac{\pi\dot{\sigma}}{mn}Cp\ \theta\right)=$$

$$\pi\sigma\alpha\left[\frac{\partial}{\partial t}\left(\frac{\pi}{mn}\right)+\frac{u}{n}\frac{\partial \pi}{\partial \xi}+\frac{v}{m}\frac{\partial \pi}{\partial \eta}\right]$$

CONTINUITY

$$\frac{\partial}{\partial t}\left(\frac{\pi}{mn}\right) + \frac{\partial}{\partial \xi}\left(\pi \frac{u}{n}\right) + \frac{\partial}{\partial \eta}\left(\pi \frac{v}{m}\right) + \frac{\partial}{\partial \sigma}\left(\frac{\pi \dot{\sigma}}{mn}\right) = 0$$

EQUATION OF STATE

$$p\alpha = RT$$

HYDROSTATIC EQUATION

$$\frac{\partial \Phi}{\partial \sigma} = -\pi\alpha$$

where,

$$\frac{1}{m} = a \cos \phi$$

$$\frac{1}{n} = a$$

and

ϕ = latitude

LIST OF REFERENCES

1. Arkawa, A. and M. Suarez, 1982: Vertical Differencing of the Primitive Equations in Sigma-Coordinates. Submitted to Mon. Wea. Rev.

2. Arkawa, A. and Y. Mintz, 1974: The UCLA General Circulation Model. Workshop Notes, I-VIII, Department of Meteorology, UCLA.

3. Bleck, R., 1977: Numerical Simulation of Lee Cyclogenesis in the Gulf of Genoa. Mon. Wea. Rev., 105, 428-445.

4. Bonner, W. D., 1961: Development Processes Associated with the Formation and Movement of an Alberta Cyclone. University of Chicago, Tech. Rep. No. 4, Contr. Nr. 2121(10), NR 082 161.

5. Bretherton, F. P., 1975: Recent Developments in Dynamical Oceanography, Quart. J.R. Met. Soc., 101, 705-721.

6. Buzzi, A., and S. Tibaldi, 1978: Cyclogenesis in the Lee of the Alps: A Case Study. Quart. J. R. Met. Soc., 104, 271-287.

7. Chung Y. -S., 1977: An Observational Study of the Influence of Large-Scale Mountains on Air Flow and Lee Cyclogenesis. Arch. Met. Geoph. Biokl., Ser. A, 26, 109-126.

8. Chung, Y. -S., K. Hage, and E. Reinelt, 1976: On Lee Cyclogenesis and Airflow in the Canadian Rocky Mountains and the East Asian Mountains. Mon. Wea. Rev., 104, 879-891.

9. Chung, Y. -S., and E. R. Reinelt, 1973: On Cyclogenesis in the Lee of the Canadian Rocky Mountains. Arch. Met. Geoph. Biokl., Ser. A, 22, 205-226.

10. Egger, J., 1972: Numerical Experiments on the Cyclogenesis in the Gulf of Genoa. Beitr. Phys. Atmos., 45, 320-346.

11. Egger, J., 1974: Numerical Experiments on Lee Cyclogenesis. Mon. Wea. Rev., 102, 847-860.

12. Elias, W. T., 1973: Numerical Experiments with a Five-Level Global Atmospheric Prediction Model Using a Staggered, Spherical, Sigma Coordinate System. Master's Thesis, Naval Postgraduate School, Monterey, California, 65 pp.

13. Finch, D., and J. Walker, 1979: Snowfall at Anchorage, Alaska Associated with Cold Advection. NOAA Technical Memorandum NWS AR-25, 39 pp.

14. Haltiner, G. J. and F. L. Martin, 1957: Dynamical and Physical Meteorology, McGraw-Hill, 52-53.

15. Haltiner, G. J. and R. T. Williams, 1980: Numerical Prediction and Dynamic Meteorology. John Wiley & Sons, Inc. 477 pp.

16. Hayes, J. L. and R. T. Williams, 1977: Numerical Simulation of Air Flow Over Mountains. Naval Postgraduate School Technical Report NPS-63Wu7741, 68 pp.

17. Hess, S. L. and H. Wagner, 1948: Atmospheric Waves in Northwestern United States. J. Meteor. 5, 1-19.

18. Huppert, H. E. and K. Bryan, 1976: Topographically Generated Eddies. Deep-Sea Research, 23, 655-679.

19. McClain, E. P., 1960: Some Effects of the Western Cordillera of North America on Cyclone Activity. J. Meteor. 17, 104-115.

20. Macklin, S. A, R. W. Lindsay, and R. M. Reynolds, 1980: Observations of Mosescale Winds in an Orographically-Dominated Estuary: Cook Inlet, Alaska. Reprints: Second Conference on Coastal Meteorology (Los Angeles, California), AMS, Boston, 176-180.

21. McCollough, J. M., 1974: Initialization of a 5-Level Global Atmospheric General Circulation Model Using a Staggered, Spherical, Sigma Coordinate System. Master's Thesis, Naval Postgraduate School, Monterey, California, 96 pp.

22. Merkine, L., 1975: Steady Finite-Amplitude Baroclinic Flow Over Long Topography in a Rotating Stratified Atmosphere. J. Atmos. Sci., 32, 1881-1893.

23. Monaco, A. V. and R. T. Williams, 1975: An Atmospheric Global Prediction Model Using a Modified Arakawa Differencing Scheme. Naval Postgraduate School Report NPS-51Wu75041, 86 pp.

24. Newton, C. W., 1956: Mechanisms of Circulation Change During a Lee Cyclogenesis. J. Meteor., 13, 528-539.

25. Petterssen, S., 1956: Weather Analysis and Forecasting. Vol. 1, 2nd ed. McGraw-Hill, Chaps. 3, 12, 13, and 16.

26. Phillips, N. A., 1957: A Coordinate System Having Some Special Advantages for Numerical Forecasting. J. Meteor., 14, 184-185.

27. Radinovic, D., 1965: On Forecasting of Cyclogenesis in the West Mediterranean and Other Areas Bounded by Mountain Ranges by Baroclinic Model. Arch. Met. Geoph. Biokl., Ser. A, 14, 279-299.

28. Robinson, A. R. and J. McWilliams, 1974: Baroclinic Instability in the Open Ocean. Journal of Physical Oceanography, 4, 281-294.

29. Schallert, W. L., 1962: An Investigation of Colorado Cyclones. Sci. Report No. 7, Contract AF 19 (604)-7230, Dept. of Meteorology, University of Chicago, 68 pp.

30. Schultz, R. S., 1976: Personal Communication.

31. Tibaldi, S., A. Buzzi, and P. Malguzzi, 1980: Orographically Induced Cyclogenesis: Analysis of Numerical Experiments, Mon. Wea. Rev., 108, 1302-1314.

32. Trevisan, A., 1976: Numerical Experiments on the Influence of Topography on Cyclone Formation with an Isentropic Primitive Equation Model. J. Atmos. Sci., 33, 768-780.

33. Williams, R. T., J. Hayes, F. Winninghoff, and O. Haney, 1981: Numerical Simulation of Air Flow Over and Around a Long Mountain Range. Preprints: Fifth Conference on Numerical Weather Prediction (Monterey, California), AMS, Boston, 137-138.

INITIAL DISTRIBUTION LIST

		No. Copies
1.	Defense Technical Information Center Cameron Station Alexandria, Virginia 22314	2
2.	Library, Code 0142 Naval Postgraduate School Monterey, California 93940	2
3.	Dr. R. T. Williams, Code 63Wu Department of Meteorology Naval Postgraduate School Monterey, California 93940	8
4.	Director Naval Oceanography and Meteorology National Space Technology Laboratories Bay St. Louis, Mississippi 39520	1
5.	Officer in Charge Navy Environmental Prediction Research Facility Monterey, California 93940	1
6.	Commanding Officer Fleet Numerical Oceanographic Central Monterey, California 93940	1
7.	Naval Oceanographic Office Library, Code 3330 Washington, D.C. 20373	1
8.	AFCRL Research Library ATTN: Nancy Davis/Stop 29 L. G. Hanscom Field Bedford, Massachusetts 01730	1
9.	Commander, Air Weather Service Military Airlift Command United States Air Force Scott Air Force Base, Illinois 62226	1
10.	Dr. A. Arakawa Department of Meteorology University of California Los Angeles, California 90024	1

11. Mr. Jeffrey P. Walker — 6
6810 Rovenna Street
Anchorage, Alaska 99502

12. Captain John L. Hayes, Code 63 — 1
Naval Postgraduate School
Monterey, California 93940

13. Atmospheric Sciences Library — 1
National Oceanic and Atmospheric Administration
Silver Spring, Maryland 20910

14. Dr. John Brown — 1
National Meteorological Center/NOAA
World Weather Building
Washington, D.C. 20233

15. Dr. C.-P. Chang, Code 63Cj — 1
Department of Meteorology
Naval Postgraduate School
Monterey, California 93940

16. Dr. R. L. Elsberry, Code 63Es — 1
Department of Meteorology
Naval Postgraduate School
Monterey, California 93940

17. Dr. R. L. Haney, Code 63Hy — 1
Department of Meteorology
Naval Postgraduate School
Monterey, California 93940

18. CDR D. Hinsman — 1
NEPRF
Monterey, California 93940

19. Dr. J. Holton — 1
Department of Atmospheric Sciences
University of Washington
Seattle, Washington 98105

20. Dr. B. J. Hoskins — 1
Department of Geophysics
University of Reading
Reading, United Kingdom

21. Dr. J. Young — 1
Department of Meteorology
University of Wisconsin
Madison, Wisconsin 53706

22. Dr. A. Kasahara — 1
National Center for Atmospheric Research
P. O. Box 3000
Boulder, Colorado 80303

23. Dr. M. G. Wurtele — 1
Department of Meteorology
University of California
Los Angeles, California 90024

24. Dr. E. N. Lorenz — 1
Department of Meteorology
Massachusetts Institute of Technology
Cambridge, Massachusetts 02139

25. Dr. R. Madala — 1
Code 7750
Naval Research Laboratories
Washington, D. C. 20390

26. Meteorology Library, Code 63 — 1
Naval Postgraduate School
Monterey, California 93940

27. National Center for Atmospheric Research — 1
Box 1470
Boulder, Colorado 80302

28. Director, Naval Research Laboratory — 1
ATTN: Technical Services Information Center
Washington, D.C. 20390

29. Dr. E. C. Nickerson — 1
NOAA, Atmospheric Physics & Chemistry Laboratory
Boulder, Colorado 80302

30. Department of Oceanography, Code 68 — 1
Naval Postgraduate School
Monterey, California 93940

31. Office of Naval Research — 1
Department of the Navy
Washington, D. C. 20360

32. Prof. N. A. Phillips — 1
National Meteorological Center/NOAA
World Weather Building
Washington, D. C. 20233

33. Dr. J. Smagorinsky, Director — 1
Geophysical Fluid Dynamics Laboratory
Princeton University
Princeton, New Jersey 08540

34. Dr. T. Rosmond — 1
Naval Environmental Prediction Research Facility
Monterey, Calfornia 93940

35. Dr. D. Williamson — 1
National Center for Atmospheric Research
P. O. Box 3000
Boulder, Colorado 80303

36. Dr. Y. Sasaki — 1
Department of Meteorology
University of Oklahoma
Norman, Oklahoma 73069

37. Prof. A. L. Schoenstadt — 1
Code 53 Zh
Naval Postgraduate School
Monterey, California 93940

38. Professor Fedor Mesinger — 1
Department of Meteorology
University of Belgrade
11001 Beograd, p.p. 550
Yugoslavia

39. Dr. M. J. P. Cullen — 2
Meteorological Office
Bracknell, Berks,
United Kingdom

40. Dr. R. L. Lee
Atmospheric and Geophysical Science Division — 1
University of California
P. O. Box 808
Livermore, California 94550

41. Dr. C. H. Wash — 1
Code 63
Naval Postgraduate School
Monterey, California 93940

42. Professor R. J. Renard — 1
Code 63
Naval Postgraduate School
Monterey, California 93940

43. Dr. Andrew Staniforth 1
Recherce en Prevision Numerique
We. Isle Office Tower, 5 ieme etage
2121 route Trans-Canada
Dorval, Quebec H9P1J3, Canada

44. Dr. A. Weinstein 1
Naval Environmental Prediction Research Facility
Monterey, California 94930

45. Dr. F. J. Winninghoff, Code 63 1
Naval Postgraduate School
Monterey, California 93940

46. Dr. R. T. Pierrehumbert 1
Geophysical Fluid Dynamics Lab/NOAA
P. O. Box 308
Princeton, New Jersey 08540

47. D. W. Blumen
Campus Box 391 1
University of Colorado
Boulder, Colorado 80309

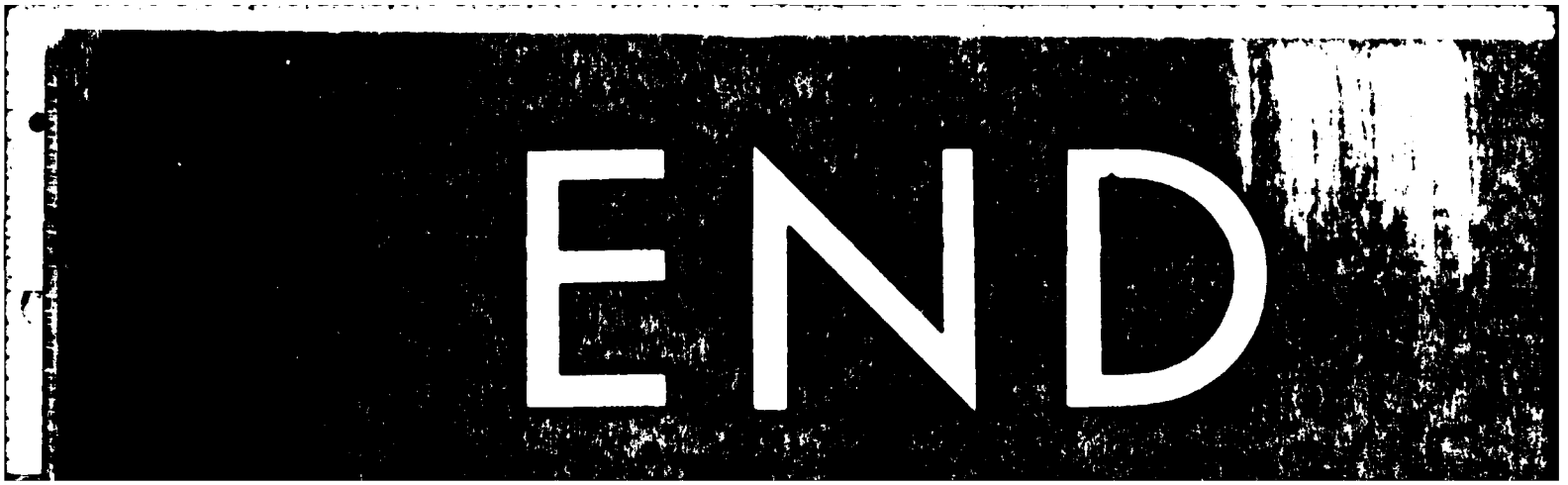
END